THE DYNAMICAL BEHAVIOR OF SOME WEAKLY ANISOTROPIC MAGNETIC SYSTEMS

W. M. DE JONG

THE DYNAMICAL BEHAVIOR OF SOME WEAKLY ANISOTROPIC MAGNETIC SYSTEMS

ISBN 90 6231 002 8

THE DYNAMICAL BEHAVIOR OF SOME WEAKLY ANISOTROPIC MAGNETIC SYSTEMS

PROEFSCHRIFT

ter verkrijging van de graad van Doctor in de Wiskunde en Natuurwetenschappen aan de Rijksuniversiteit te Leiden, op gezag van de Rector Magnificus Dr. A.E. Cohen, Hoogleraar in de Faculteit der Letteren, volgens besluit van het college van Dekanen te verdedigen op woensdag 10 september 1975 te klokke 15.15 uur.

door

WILLEM MELS DE JONG
geboren te Rotterdam in 1941

Dutch Efficiency Bureau - Pijnacker

PROMOTOREN: PROF.DR.IR. N.J. POULIS
PROF.DR. C.J. GORTER

Dit proefschrift is tot stand gekomen onder leiding van Dr. J.C. Verstelle .

Aan mijn moeder

Ter herinnering aan mijn vader

Aan Christine

CONTENTS

SURVEY

In this thesis we study, both experimentally and theoretically, the dynamical behavior of some weakly anisotropic magnetic systems. The basic property we investigate, is the time evolution of the average total magnetization of an isolated electron spin system. To this extent we performed relaxation and resonance experiments in the paramagnetic, critical and antiferromagnetic state of three different copper compounds.Two of these compounds, $CuCl_2.2H_2O$ and $LiCuCl_3.2H_2O$, are known to be magnetically high-dimensional while the third, $Cu(NH_3)_4SO_4.H_2O$, is one of the first known magnetic linear chain compounds.

At high temperatures we investigate the influence of antisymmetric Dzialoshinsky-Moriya exchange interaction on relaxation and resonance. Introduction of antisymmetric exchange in the copper compounds leads to a perfect agreement between experiment and theory. The interaction model, which contains only one adjustable exchange parameter, is further checked on the independent results obtained in the critical and antiferromagnetic state.

In the critical region near the Néel temperature our measurements show an anisotropic speeding-up of the relaxation process. Using such techniques as Random Phase Approximation, spatial Fourier transforms and dynamical scaling, we develop a theory on the critical relaxation and resonance in weakly anisotropic magnetic systems. It is shown that the dynamical properties of the magnetic system are strongly influenced by the magnetic anisotropy. By transforming this magnetic anisotropy into an anisotropy in the critical slowing-down of the spin fluctuations, we are able to derive a relatively simple expression for the relaxation time (and the resonance linewidth) in the critical region. The results of this theory, which is a generalization of the theory given by Huber (2)(12), are in very good agreement with experiment in both $CuCl_2.2H_2O$ and $LiCuCl_3.2H_2O$. In the linear chain CTS the same theory yields experimental evidence for a linear dependence of the inverse correlation length on the temperature.

Below the Néel temperature it is shown that in the easy-axis of orthorhombic antiferromagnets a low-frequency relaxation occurs. These relaxation measurements are shown to be a valuable tool in testing theories on spin-wave relaxation.

In the linear chain CTS special attention is paid to the long-time behavior of the correlation functions. The long-time tails of the relaxation memory functions are computed straightforwardly from the measurements. The results are compared with an adapted version of the theory of Hennessy et al.(79). Although most of the features are explained qualitatively, it is shown that the memory function shows less pronounced long-time behavior than should be expected theoretically. Experimental evidence is given for either important inaccuracy in the Random Phase Approximation or anisotropy in the two-spin correlation functions.

CHAPTER I

GENERAL INTRODUCTION TO THE THEORY

1.1 *Macroscopic theory of magnetic relaxation*

In this part of chapter I we will survey shortly the most important ideas of the macroscopic relaxation theory.

In magnetic relaxation or resonance the response of a magnetic system to an arbitrary magnetic field variation is studied. In the linear response approximation the response of the magnetization to such an arbitrary field variation $\Delta\vec{H}(t)$ is described by

$$\Delta\vec{M}(t,\vec{H}) = -\int_0^\infty \dot{\phi}(\tau,\vec{H}).\Delta\vec{H}(t-\tau)d\tau \qquad (1.1)$$

where $\phi(t,\vec{H})$ is the so-called relaxation tensor which describes the system's search for equilibrium. It is a second order tensor with elements $\phi_{\alpha\beta}(t,\vec{H})$. All these elements are real while all $\phi_{\alpha\alpha}(t,\vec{H})$ are even in time. In this equation not only the approximation of linearity but also the principle of causality has been included. Virtual instantaneous effects from diamagnetic origin have been neglected. In the often studied case of a negative field step $\Delta\vec{H}$ at time t = 0, eq. (1.1) reduces to

$$\Delta\vec{M}(t,\vec{H}) = \vec{M}(t,\vec{H}) - \vec{M}(0,\vec{H}) = \phi(t,\vec{H}).\Delta\vec{H} \qquad (1.2)$$

$\vec{M}(t,\vec{H})$ and $\vec{M}(0,\vec{H})$ are the magnetizations at time t and 0 respectively. As in this case the magnetic system is supposed to be in equilibrium for $t<0$, $\vec{M}(0,\vec{H})$ is equal to the static magnetization in field $\vec{H}$.

As all experimental field variations are continuous with continuous derivatives one may reduce eq. (1.1) by partial integration to the more manageable form

$$\Delta\vec{M}(t,\vec{H}) = -\phi(\infty,\vec{H}).\Delta\vec{H}(-\infty) + \phi(o,\vec{H}).\Delta\vec{H}(t) - \int_0^\infty \phi(\tau,\vec{H}).\Delta\dot{\vec{H}}(t-\tau)d\tau \qquad (1.3)$$

As $\phi(t,\vec{H})$ is bounded for all t and $\Delta\vec{H}(-\infty) = 0$ we have

$$\Delta\vec{M}(t,\vec{H}) = \phi(0,\vec{H}).\Delta\vec{H}(t) - \int_0^\infty \phi(\tau,\vec{H}).\Delta\dot{\vec{H}}(t-\tau)d\tau \qquad (1.4)$$

As we suppose the magnetic system to return to some sort of equilibrium for $t\to\infty$, $\phi(\infty,\vec{H}) = \lim_{t\to\infty}\phi(t,\vec{H})$ exists but its value needs not to be equal to zero. As we are, at this moment, only interested in the time dependent part of $\phi(t,\vec{H})$, we introduce another relaxation tensor $\Phi(t,\vec{H})$ defined by

$$\Phi(t,\vec{H}) = \phi(t,\vec{H}) - \phi(\infty,\vec{H}) \tag{1.5}$$

Substitution of eq. (1.5) in (1.4) yields

$$\Delta\vec{M}(t,\vec{H}) = \Phi(o,\vec{H}).\Delta\vec{H}(t) - \int_0^\infty \Phi(\tau,\vec{H}).\Delta\dot{\vec{H}}(t-\tau)d\tau \tag{1.6}$$

In our experiments the response of a system to a periodic field variation is studied. This periodic field variation is of the form

$$\Delta\vec{H}(t) = \Delta\vec{H}\cos\omega t = \mathrm{Re}\ \Delta\vec{H}\ e^{i\omega t} \tag{1.7}$$

Substituting this in eq. (1.6) and using that $\Phi(t,\vec{H})$ is a real tensor, one gets

$$\Delta\vec{M}(t,\vec{H}) = \mathrm{Re}\{(\Phi(o,\vec{H}) - i\omega\int_0^\infty \Phi(\tau,\vec{H})e^{-i\omega\tau}d\tau).\Delta\vec{H}\ e^{i\omega t}\} \tag{1.8}$$

1.1.1 *Frequency dependent susceptibility tensor*

We define the field and frequency dependent susceptibility tensor $\chi(\omega,\vec{H})$ by

$$\Delta\vec{M}(t,\vec{H}) = \mathrm{Re}\{\chi\ (\omega,\vec{H}).\Delta\vec{H}\ e^{i\omega t}\} \tag{1.9}$$

Comparing this with eq. (1.8) one finds

$$\chi(\omega,\vec{H}) = \Phi(o,\vec{H}) - i\omega\int_0^\infty \Phi(\tau,\vec{H})\ e^{-i\omega\tau}d\tau \tag{1.10}$$

The susceptibility tensor, which is a complex second order tensor, can be split up in a real and an imaginary part.

$$\chi(\omega,\vec{H}) = \chi'(\omega,\vec{H}) - i\chi''(\omega,\vec{H}) \tag{1.11}$$

Substituting eq. (1.11) in (1.10) and using once again that $\Phi(t,\vec{H})$ is a real tensor, one gets

$$\chi'(\omega,\vec{H}) = \Phi(o,\vec{H}) - \omega\int_0^\infty \Phi(\tau,\vec{H})\ \sin\omega\tau d\tau \tag{1.12}$$

$$\chi''(\omega,\vec{H}) = \omega\int_0^\infty \Phi(\tau,\vec{H}) \cos\omega\tau \, d\tau \tag{1.13}$$

$$\chi(o,\vec{H}) = \chi'(o,\vec{H}) = \Phi(o,\vec{H}) \tag{1.14}$$

The fact that both the real part $\chi'(\omega,\vec{H})$ and the imaginary part $\chi''(\omega,\vec{H})$ can be expressed in the same relaxation tensor $\Phi(t,\vec{H})$ indicates that there might be a more direct relation between $\chi'(\omega,\vec{H})$ and $\chi''(\omega,\vec{H})$. One has for the diagonal elements

$$\chi'_{\alpha\alpha}(\omega,\vec{H}) - \chi'_{\alpha\alpha}(\infty,\vec{H}) = \frac{2}{\pi}\int_0^\infty \frac{\omega_1\chi''_{\alpha\alpha}(\omega_1,\vec{H}) - \omega\chi''_{\alpha\alpha}(\omega,\vec{H})}{\omega_1^2 - \omega^2} d\omega_1 \tag{1.15}$$

$$\chi''_{\alpha\alpha}(\omega,\vec{H}) = -\frac{2\omega}{\pi}\int_0^\infty \frac{\chi'_{\alpha\alpha}(\omega_1,\vec{H}) - \chi'_{\alpha\alpha}(\omega,\vec{H})}{\omega_1^2 - \omega^2} d\omega_1 \tag{1.16}$$

These are the well-known Kramers-Kronig relations. Substituting $\omega = 0$ in eq. (1.15) one gets

$$\chi'_{\alpha\alpha}(o,\vec{H}) - \chi'_{\alpha\alpha}(\infty,\vec{H}) = \frac{2}{\pi}\int_0^\infty \frac{\chi''(\omega,\vec{H})}{\omega} d\omega \tag{1.17}$$

$\chi'_{\alpha\alpha}(\omega,\vec{H})$ is generally called the dispersion while $\chi''_{\alpha\alpha}(\omega,\vec{H})$ is related to the energy absorption by the sample out of the alternating magnetic field. During one period of the oscillating field, this absorption equals

$$-\int_0^{\frac{2\pi}{\omega}} \Delta\vec{M}(t,\vec{H}).d\Delta\vec{H}(t) = \pi \, \Delta\vec{H}. \, \chi''(\omega,\vec{H}).\Delta\vec{H} \tag{1.18}$$

1.1.2 *Memory function and memory spectrum*

In most magnetic systems the relaxation tensor $\Phi(t,\vec{H})$ is decaying at microscopically very long times. By using integro-differential equality (1.19), each of the diagonal elements $\Phi_{\alpha\alpha}(t,\vec{H})$ of the relaxation tensor can be transformed into a corresponding function $G_\alpha(t,\vec{H})$, the so-called memory function or kernel, which is usually decaying at microscopic times. As it will be shown in section 1.2, one finds by using this function a link between the microscopic and macroscopic dynamical properties of the electron spin system.

$$\frac{\partial\Phi_{\alpha\alpha}(t,\vec{H})}{\partial t} = -\int_0^t G_\alpha(\tau,\vec{H}) \, \Phi_{\alpha\alpha}(t-\tau,\vec{H}) d\tau \tag{1.19}$$

The elements $G_\alpha(t,\vec{H})$ are even in time.

$$G_\alpha(t,\vec{H}) = G_\alpha(-t,\vec{H}) \qquad \alpha = x, y \text{ or } z \tag{1.20}$$

Assuming that both the Fourier transform and the Laplace transform of the memory function exist, one has for the Fourier transform

$$\tilde{G}_\alpha(\omega,\vec{H}) = \frac{1}{2\pi} \int_{-\infty}^{+\infty} e^{-i\omega t}\, G_\alpha(t,\vec{H})\,dt \tag{1.21}$$

$$G_\alpha(t,\vec{H}) = \int_{-\infty}^{+\infty} e^{i\omega t}\, \tilde{G}_\alpha(\omega,\vec{H})\,d\omega \tag{1.22}$$

and for the Laplace transform

$$\hat{G}_\alpha(i\omega,\vec{H}) = \int_0^\infty e^{-i\omega t}\, G_\alpha(t,\vec{H})\,dt \tag{1.23}$$

The Fourier transform of the memory function is sometimes called the memory spectrum. By definition both the susceptibility tensor and the memory function have been expressed in the same relaxation tensor. The direct relation between $\chi_{\alpha\alpha}(\omega,\vec{H})$ and $G_\alpha(t,\vec{H})$ is given by

$$\hat{G}_\alpha(i\omega,\vec{H}) = -i\omega \frac{\chi_{\alpha\alpha}(\omega,\vec{H})}{\chi_{\alpha\alpha}(\omega,\vec{H}) - \chi_{\alpha\alpha}(o,\vec{H})} \tag{1.24}$$

Using further $\mathrm{Re}\ \hat{G}(i\omega,\vec{H}) = \pi\tilde{G}(\omega,\vec{H})$ one gets

$$\pi\tilde{G}_\alpha(\omega,\vec{H}) = \frac{\omega\chi''_{\alpha\alpha}(\omega,\vec{H})\ \chi_{\alpha\alpha}(o,\vec{H})}{(\chi'_{\alpha\alpha}(\omega,\vec{H}) - \chi_{\alpha\alpha}(o,\vec{H}))^2 + (\chi''_{\alpha\alpha}(\omega,\vec{H}))^2} \tag{1.25}$$

Once again virtual instantaneous effects have been omitted.

1.1.3 *Relaxation time and memory function*

Suppose that the memory function $G_\alpha(t,\vec{H})$ goes to zero at times small compared with the characteristic times which govern the time evolution of $\Phi_{\alpha\alpha}(t,\vec{H})$. In that case one has

$$\frac{\partial\Phi_{\alpha\alpha}(t,\vec{H})}{\partial t} = -\int_0^t G_\alpha(t',\vec{H})\ \Phi_{\alpha\alpha}(t-t',\vec{H})\,dt' \simeq -\Phi_{\alpha\alpha}(t,\vec{H}) \int_0^t G_\alpha(t',\vec{H})\,dt' \tag{1.26}$$

At sufficiently large times the solution of eq. (1.26) is then given by

$$\Phi_{\alpha\alpha}(t,\vec{H}) = \Phi_{\alpha\alpha}(o,\vec{H})e^{-t/\tau_\alpha(\vec{H})} \tag{1.27}$$

with

$$\tau_\alpha^{-1}(\vec{H}) = \int_o^\infty G_\alpha(t',\vec{H})dt' \tag{1.28}$$

Substituting eq. (1.27) in (1.12) and (1.13) one gets

$$\frac{\chi'_{\alpha\alpha}(\omega,\vec{H})}{\chi_{\alpha\alpha}(o,\vec{H})} = \frac{1}{1+\omega^2\tau_\alpha^2(\vec{H})} \tag{1.29}$$

$$\frac{\chi''_{\alpha\alpha}(\omega,\vec{H})}{\chi_{\alpha\alpha}(o,\vec{H})} = \frac{\omega\tau_\alpha(\vec{H})}{1+\omega^2\tau_\alpha^2(\vec{H})} \tag{1.30}$$

which are the well-known Lorentzian expressions for single relaxation processes. The case of a sufficiently narrow memory function $G_\alpha(t,\vec{H})$ is normally encountered in three-dimensional magnetic systems with large secular interactions. In low-dimensional systems diffusivity leads to important long-time behavior which, in most cases, impedes an approximation as shown in eq. (1.26).

1.2 *Microscopic expression for the memory function*

The time evolution of the α-th component of the average total magnetization is given by

$$M_\alpha(t) = e^{\frac{i}{\hbar}\mathcal{H}t} M_\alpha e^{-\frac{i}{\hbar}\mathcal{H}t} \equiv e^{iLt}M_\alpha \tag{1.31}$$

$$\dot{M}_\alpha(t) = \frac{i}{\hbar}[\mathcal{H},M_\alpha(t)] \equiv iL\,M_\alpha(t) \tag{1.32}$$

where $\mathcal{H}$ is the Hamiltonian of the magnetic system and L the quantum mechanical Liouville operator. Although the above mentioned operators are all dependent on the static field we will not state this explicitely. Furthermore one has

$$e^{iLt_1} M_\alpha(t) = M_\alpha(t+t_1) \tag{1.33}$$

For a description of the relaxation process of $M_\alpha(t)$ one should look for the correlation between $M_\alpha(0)$ and $M_\alpha(t)$ at arbitrary times t. The magnetic system is supposed to be in equilibrium at times $t< 0$. To study the correlations we introduce a correlation function $(A,B(t))$, which will be defined by

$$(A,B(t)) = \int_0^\beta < e^{\lambda\mathcal{H}} A\, e^{-\lambda\mathcal{H}} B(t) > d\lambda \qquad (1.34)$$

where $\beta = 1/k_B T$, T is the temperature of the bath with which the magnetic system is supposed to be in equilibrium just before the perturbation. The brackets denote an ensemble average defined by

$$<A> = \frac{\mathrm{Tr}\, e^{-\beta\mathcal{H}} A}{\mathrm{Tr}\, e^{-\beta\mathcal{H}}} \qquad (1.35)$$

Using the Kubo formalism (1) one obtains for the elements of the relaxation tensor $\phi(t,\vec{H})$

$$\phi_{\alpha\beta}(t,\vec{H}) = \int_0^\beta < e^{\lambda\mathcal{H}} M_\beta e^{-\lambda\mathcal{H}} M_\alpha(t) > d\lambda \qquad (1.36)$$

The indices α and β denote the Cartesian coordinates x, y or z.
Using definition (1.34) one gets

$$\phi_{\alpha\beta}(t,\vec{H}) = (M_\beta, M_\alpha(t)) \qquad (1.37)$$

1.2.1 *Projection technique*

The relaxation tensor $\phi(t,\vec{H})$ contains a time independent part which is not directly involved in the time evolution of the average total magnetization. This part, which is equal to $\phi(\infty,\vec{H})$, can be eliminated by the Zwanzig projection operator technique. Let the projection operator P_A in the operator space be defined by

$$P_A B = \frac{(A,B)}{(A,A)} A \qquad (1.38)$$

Let further I be the identity operator and let

$$\mathcal{H}' = (1-P_I)\mathcal{H} = \mathcal{H} - <\mathcal{H}> I \qquad (1.39)$$

The brackets being defined by eq. (1.35). Let furthermore

$$\mu_\alpha = (1-P_I-P_{\mathcal{H}'})\, M_\alpha \qquad (1.40)$$

It can be proved that the part of M_α, which gave rise to a non-zero limit value of $\phi(t,\vec{H})$ for $t\to\infty$, is equal to $(P_I+P_{\mathcal{H}'})M_\alpha$ So, by taking μ_α instead of M_α, one eliminates the part which plays no direct role in the time evolution of the magnetic system. in fact, μ_α is the time dependent part of the magnetization M_α, the constant part being eliminated by the projection technique.

One has

$$\phi_{\alpha\beta}(t,\vec{H}) = (M_\beta, M_\alpha(t)) \tag{1.37}$$

$$\phi_{\alpha\beta}(t,\vec{H}) = (\mu_\beta, \mu_\alpha(t)) \tag{1.41}$$

Using eq. (1.41) and the integro-differential equality one derives for the memory function

$$G_\alpha(t,\vec{H}) = \frac{((L\mu_\alpha)^\dagger, e^{i(1-P_\mu)Lt}\, L\mu_\alpha)}{(\mu_\alpha,\mu_\alpha)} \tag{1.42}$$

where P_μ is found by substituting (1.40) in (1.38). Eq. (1.42) is the most general microscopic expression for the memory function $G_\alpha(t,\vec{H})$. It contains all the information relevant to the time evolution of the magnetic system. The Hamiltonian of the magnetic electron spin system can be split up as follows

$$\mathcal{H} = \mathcal{H}_{\text{zeeman}} + \mathcal{H}_{\text{interaction}} \tag{1.43}$$

The Zeeman term is given by eq. (2.2) of chapter 2. For the interaction part one has

$$\mathcal{H}_{\text{interaction}} = \mathcal{H}_{\text{secular}} + \mathcal{H}_{\text{non-secular}} \tag{1.44}$$

The secular part, denoted from now on as $\mathcal{H}_{\text{sec}}$, is that part of the interaction Hamiltonian that commutes with $\mathcal{H}_{\text{zeeman}}$ while the non-secular $\mathcal{H}_{\text{nsec}}$ is the non commuting part. In analogy one has for the Liouville operator

$$L = L_z + L_{\text{sec}} + L_{\text{nsec}} \tag{1.45}$$

Substitution of eq. (1.45) in (1.42) yields an expression which in fact is very complicated, so one tries to introduce some simplifications. The most widely used simplification is found in the so-called weak-coupling limit. The basic assumption of the weak-coupling approximation is that, in a magnetic system with large secular interactions, one can safely put in the exponent of eq. (1.42)

$$(1-P_\mu)L_z + (1-P_\mu)L_{\text{sec}} + (1-P_\mu)L_{\text{nsec}} \simeq L_z + L_{\text{sec}} \tag{1.46}$$

It is impossible to say exactly what kind of information is lost by this approximation. At high temperatures, the physical consequence of the approxi-

mation is the occurrence of only four lines in the memory spectrum which moreover shift rigidly with the external static field.
In the weak-coupling approximation one has for the memory function

$$G_\alpha(t,\vec{H}) = \frac{((L\mu_\alpha)^\dagger,\ e^{iL_z t + iL_{sec} t} L\mu_\alpha)}{(\mu_\alpha,\mu_\alpha)} \qquad (1.47)$$

Combination of eq. (1.47) with (1.28) yields a microscopic expression for the relaxation time in the weak-coupling limit.

CHAPTER 2

SPIN-SPIN RELAXATION IN DIFFERENT TEMPERATURE REGIMES

2.1 *Introduction*

In this chapter we will derive expressions for the electron spin-spin relaxation times and resonance linewidths in the different temperature regions. The expressions valid at high temperatures have been given by many authors. The only new point here is that antisymmetric exchange, of which we will show the dominant role in Cu-compounds, has been included. The derivation of the relaxation times in the critical region (near the Néel temperature) is new although extensive use has been made of the ideas of Huber (2) and of the scaling arguments of Riedel (3). In the antiferromagnetic state the approach is new in so far that the magnetic parallel-field relaxation process in the easy-axis has been ascribed to spin-wave relaxation. A survey of the results of the dynamical spin-wave theory is given.

Before we start the calculation in the different temperature regimes we will specify our magnetic Hamiltonian.

2.2 *A choice for the magnetic Hamiltonian*

As the characteristic times at which the electron spin system goes to its internal equilibrium are normally much smaller than the spin-lattice relaxation times, one is allowed to suppose the spin system to be isolated during its search for internal equilibrium. In that case the spin-spin relaxation process is governed by the interactions between the spins only. So our Hamiltonian only includes magnetic spin-spin interactions terms. In general one has

$$\mathcal{H} = \mathcal{H}_z + \mathcal{H}_{dd} + \mathcal{H}_{ex} + \mathcal{H}_{hfs} + \mathcal{H}_{el} \qquad (2.1)$$

which consists of, in this order, the Zeeman, dipolar, exchange, hyperfine and electric field part. As we only study compounds where the effective spin value equals $\frac{1}{2}$, the electric field does not influence the energetic situation, so $\mathcal{H}_{el} = 0$. We further neglect $\mathcal{H}_{hfs}$ as in the copper compounds, studied in this thesis, both secular and non-secular hyperfine contributions are small compared with those of the other interactions. This implies that we exclude very narrow hyperfine contributions to the memory spectrum. This is justified by

our measurements where no strongly field dependent relaxation times have been found. For the remaining Hamiltonian we have

$$\mathcal{H}_z = g\mu_B \vec{H} . \sum_i \vec{S}_i \tag{2.2}$$

$$\mathcal{H}_{dd} = \tfrac{1}{2} g^2 \mu_B^2 \sum_{i \neq j} r_{ij}^{-3} \{ (\vec{S}_i . \vec{S}_j) - 3 r_{ij}^{-2} (\vec{S}_i . \vec{r}_{ij})(\vec{S}_j . \vec{r}_{ij}) \} \tag{2.3}$$

$$\mathcal{H}_{ex} = - \sum_{i \neq j} \vec{S}_i . \bar{\bar{J}}_{ij} . \vec{S}_j + \vec{D}_{ij} . (\vec{S}_i \times \vec{S}_j) \tag{2.4}$$

where $\bar{\bar{J}}_{ij}$ is a symmetric exchange tensor between spins i and j. In the case of isotropic exchange interaction this tensor reduces to the well-known Heisenberg scalar J_{ij}. The second part of the exchange Hamiltonian represents the antisymmetric Dzialoshinsky-Moriya exchange interaction. From eqs. (2.2)-(2.4) it is clear that we neglected the (supposedly small) anisotropy of the g-value in the Zeeman and dipolar part of the Hamiltonian. The g-value anisotropy is however implicitely included in the antisymmetric exchange where it is of extreme importance.

$$\vec{D}_{ij} = -\vec{D}_{ji} \tag{2.5}$$

The axial vectors $\vec{D}_{ij}$ are restricted by the symmetry elements of the crystal structure. This restriction is easily determined by using the thumb rule

$$(\overline{\mathcal{T}} D_\beta)_{ij} = D_\beta (\overline{\mathcal{T}} ij) \tag{2.6}$$

where $\mathcal{T}$ denotes a symmetry transformation while β denotes an arbitrary Cartesian component of the axial vector. For example, in the case of an inversion center halfway ions i and j one has

$$\left.\begin{array}{l} \mathcal{T} D_\beta = D_\beta \\ \mathcal{T} ij = ji \end{array}\right\} \qquad D_{\beta ij} = D_{\beta ji} \tag{2.7}$$

Combination of eq. (2.7) with (2.5) leads then to $D_{\beta ij} = 0$ for all three β. It is clear that the symmetry elements of the whole crystal structure should be used and not those of the magnetic ions only.

Antisymmetric exchange was first introduced by Dzialoshinsky (4) to explain the weak ferromagnetism of α-Fe_2O_3. Moriya (5) gave a theoretical microscopic foundation for the second order case of this exchange interaction. It was found that antisymmetric exchange has its origin in some residual spin-orbit coupling.

An interesting point is that antisymmetric exchange, in some cases, leads to a canting of the electron spins in the antiferromagnetic state. The criterion for this canting is

$$\sum_j D_{\beta ij} \neq 0 \qquad (2.8)$$

When the sum is equal to zero for all components β, no canting will result. Measurements of both static and dynamical phenomena in the antiferromagnetic state normally only reveal the canting part of the antisymmetric exchange. As we will see later, in paramagnetic relaxation or resonance all components of the antisymmetric exchange contribute to the relaxation process, so these measurements allow one to investigate antisymmetric exchange in all its features.

An exact numerical calculation of the non-zero components D_β is practically impossible. Moriya (5) estimated $D_{\beta ij} = (\Delta\bar{g}/\bar{g})J_{ij}$ with $\bar{g} = \bar{g} - 2$. This is an order larger than what has to be expected for the pseudo-dipolar form of anisotropic symmetric exchange which is contained in the first bilinear part of eq. (2.4). We will now make a crucial assumption. The Dzialoshinsky-Moriya interaction is due to a left over from the spin-orbit coupling, which also manifests itself in the g-value. We assume now that the spin-orbit coupling manifests itself in the same way in the antisymmetric components D_β as it did in the g-values. This leads then to

$$D_{\beta ij} = \alpha(g_\beta - 2)J_{ij} \qquad (2.9)$$

where α is a numerical constant which is independent of the direction and which is expected to be in the order of unity. We expect this assumption to hold in systems with effective g-values only slightly different from the free electron value g = 2.0023. The index β denotes now the principal axes of the effective g-tensor. As we will show in this thesis, assumption (2.9) is perfectly confirmed by our relaxation measurements on $CuCl_2 \cdot 2H_2O$ and $LiCuCl_3 \cdot 2H_2O$. Rutten (6) applicated our assumption to the two-dimensional planar compound $Cu(C_2H_5NH_3)_2Cl_4$ and also in this case a confirmation of (2.9) was found.

2.3 *Spin-spin relaxation at high temperatures*

The relaxation time $\tau_z(\vec{H})$ is given by

$$\tau_z(\vec{H})^{-1} = \int_0^\infty G_z(t,\vec{H})dt = \pi \tilde{G}_z(o,\vec{H}) \tag{2.10}$$

z is the direction of both static and rf field. By using eq. (2.10) we restrict ourselves to the case of sufficiently narrow memory functions. The linear chain case where the memory functions are expected to show relevant long-time behavior will be treated in chapter 7.4.

The memory function $G_z(t,\vec{H})$ is given by

$$G_z(t,\vec{H}) = \frac{((L\mu_z)^+,\ e^{iL_z t + iL_{sec} t} L\mu_z)}{(\mu_z,\mu_z)} \tag{2.11}$$

In the high-temperature and weak-coupling limit $G_z(t,\vec{H})$ can be written as

$$G_z(t,\vec{H}) = \sum_k G_{zk}(t,\vec{H}) \qquad k = \pm 1, \pm 2 \tag{2.12}$$

with

$$G_{zk}(t,\vec{H}) = \frac{\langle\langle \mathcal{H}^2 \rangle\rangle}{\langle\langle \mathcal{H}^2_{sec} \rangle\rangle} e^{ik\omega_\ell t} G_{zk}(t,o) \tag{2.13}$$

$\mathcal{H}$ is the full spin Hamiltonian, $\mathcal{H}_{sec}$ the secular part of the interaction Hamiltonian and ω_ℓ the Larmor frequency. Furthermore one has

$$\langle\langle A \rangle\rangle = \frac{\mathrm{Tr}\ A}{\mathrm{Tr}\ 1} \tag{2.14}$$

The factor $\langle\langle \mathcal{H}^2 \rangle\rangle / \langle\langle \mathcal{H}^2_{sec} \rangle\rangle$ has first been introduced by Tjon (7).
Terwiel and Mazur (8) have shown that this factor is related to the non-zero limit value of the relaxation function $\phi(t,\vec{H})$ for $t \to \infty$.
One has $(\mu_z,\mu_z) = (\langle\langle \mathcal{H}^2_{sec} \rangle\rangle / \langle\langle \mathcal{H}^2 \rangle\rangle)(M_z,M_z)$

Substituting eq. (2.13) in (2.10) one gets

$$\tau_z(\vec{H})^{-1} = \frac{\langle\langle \mathcal{H}^2 \rangle\rangle}{\langle\langle \mathcal{H}^2_{sec} \rangle\rangle} \pi \sum_k G_{zk}(-k\omega_\ell, o) \tag{2.15}$$

where

$$G_{zk}(-k\omega_\ell, o) = \frac{1}{2\pi} \int_{-\infty}^{+\infty} e^{ik\omega_\ell t} G_{zk}(t,o) \tag{2.16}$$

For $G_{zk}(t,o)$ one has in the high-temperature and weak-coupling limit

$$G_{zk}(t,o) = \frac{k^2}{\hbar^2} \frac{<<\mathcal{H}_{-k}\, e^{\frac{i\mathcal{H}_{sec}t}{\hbar}}\, \mathcal{H}_k\, e^{-\frac{i\mathcal{H}_{sec}t}{\hbar}} >>}{<<S_z^2>>} \tag{2.17}$$

where $S_z = \sum_i S_{zi}$. Use has been made of $M_z = g\mu_B S_z$. The $\mathcal{H}_k$ are defined by

$$[S_z, \mathcal{H}_k] = -k\mathcal{H}_k \tag{2.18}$$

$$\mathcal{H}_{nsec} = \mathcal{H}_{-2} + \mathcal{H}_{-1} + \mathcal{H}_1 + \mathcal{H}_2 \tag{2.19}$$

For an explicit expression for the relaxation times, one has to know the shape of the memory spectrum. The exact shape of the functions $G_{zk}(t,o)$ or $\tilde{G}_{zk}(\omega,o)$, however, is still unknown although, for some models, much progress has been made in recent years. Making some realistic assumption about the shape of the memory function, one is however able to calculate explicitely the relaxation times in many cases. The n^{th}-moment of the memory spectrum is given by

$$<\omega^n>_k = \int_{-\infty}^{+\infty} \omega^n\, \tilde{G}_{zk}(\omega,o)d\omega = i^{-n}\left(\frac{d^n}{dt^n} G_{zk}(t,o)\right)_{t=o} \tag{2.20}$$

By inspection of eq. (2.17), one finds the odd moments to be equal to zero. Furthermore one has

$$<\omega^o>_k = \frac{k^2}{\hbar^2} \frac{<<\mathcal{H}_{-k}\, \mathcal{H}_k>>}{<<S_z^2>>} \tag{2.21}$$

$$<\omega^2>_k = \frac{k^2}{\hbar^4} \frac{<<[\mathcal{H}_{sec},\mathcal{H}_k][\mathcal{H}_{-k},\mathcal{H}_{sec}]>>}{<<S_z^2>>} \tag{2.22}$$

It is usually assumed now that the memory spectrum is a sum of Gaussian lines with moments given by eqs. (2.21) and (2.22). In that case the partial memory spectrum functions $\tilde{G}_{zk}(\omega,0)$ are given by

$$\tilde{G}_{zk}(\omega,o) = -\frac{k^2}{\hbar\sqrt{2\pi}} \frac{1}{<<S_z^2>>} \frac{<<\mathcal{H}_k\mathcal{H}_{-k}>>^{3/2}}{<<[\mathcal{H}_{sec},\mathcal{H}_k][\mathcal{H}_{-k},\mathcal{H}_{sec}]>>^{1/2}} \exp -\frac{\hbar^2}{2} \frac{<<\mathcal{H}_k\mathcal{H}_{-k}>>\,\omega^2}{<<[\mathcal{H}_{sec},\mathcal{H}_k][\mathcal{H}_{-k},\mathcal{H}_{sec}]>>} \tag{2.23}$$

Due to the fact that $\tilde{G}_{zk}(\omega,0)$ is even in ω, eq. (2.15) reduces to

$$\tau_z(\vec{H})^{-1} = \frac{<<\mathcal{H}^2>>}{<<\mathcal{H}_{sec}^2>>} 2\pi \{\tilde{G}_{z1}(\omega_\ell,o) + \tilde{G}_{z2}(2\omega_\ell,o)\} \tag{2.24}$$

Combination of eqs. (2.23) and (2.24) yields an explicit, microscopic expression for the relaxation time of the average total magnetization.

Using this result one easily finds an expression for the low-frequency paramagnetic resonance linewidth. Verbeek et al. (19) have shown that the full resonance linewidth at half maximum is given by

$$(\Delta H_{1/2})_\alpha = \frac{\hbar}{g_\alpha \mu_B} \left(\frac{1}{\tau_\beta(0)} + \frac{1}{\tau_\gamma(0)}\right) \qquad (2.24a)$$

The indices α, β and γ denote the three magnetic axes. So, the low-frequency field linewidth is given by the average value of the zero-field relaxation times in the plane perpendicular to the static field direction. Combination of eqs. (2.23), (2.24) and (2.24a) yields a microscopic expression for the resonance linewidth.

2.3.1 *Note on the Gaussian assumption for the memory spectrum*

In this note we restrict ourselves to three-dimensional compounds where long-time behavior of the spin correlation functions is relatively unimportant. It is shown in chapter 2.4 that the memory function, which is in fact a sum of four-spin correlation functions, can be reduced, using some decoupling scheme, to products of two-spin correlation functions. By further transforming to the wavevector space one can in a simple way describe all distance dependent correlation functions in terms of wavevector $\vec{q}$. Theoretical calculations of Blume and Hubbard (9) have shown that in the Heisenberg cubic lattice the two-spin correlation functions with small q behave diffusively, those with intermediate q are Gaussian-like while those with large q (border of the Brillouin zone) have an oscillatory character.
It depends now on the part of the Brillouin zone from where the most important contributions to the total memory function come, whether the Gaussian assumption is realistic or not. It is to be expected that in directions where no pathological preference exists for either small or large q-values, the real shape of the memory function is very well approximated by a sum of four Gaussians. It should be noted that the above stated is only valid for three-dimensional compounds. In the linear chain or planar compound the memory function normally deviates strongly from the Gaussian. We will discuss this more amply in section 7.4.

2.3.2 *Expressions for* $\langle\langle \mathcal{H}_k \mathcal{H}_{-k} \rangle\rangle$ *and* $\langle\langle [\mathcal{H}_{sec}, \mathcal{H}_k][\mathcal{H}_{-k}, \mathcal{H}_{sec}] \rangle\rangle$

Explicit calculation yields

$$\frac{\langle\langle \mathcal{H}^2 \rangle\rangle}{\langle\langle \mathcal{H}^2_{sec} \rangle\rangle} = 1 + 2\,\frac{H^2}{H_i^2} \tag{2.25}$$

H is the static field and H_i an internal field given by

$$H_i^2 = \frac{2}{k_B C}\{\langle\langle \mathcal{H}^2_{dd} \rangle\rangle + \langle\langle \mathcal{H}^2_{ex} \rangle\rangle + 2\langle\langle \mathcal{H}_{dd}\mathcal{H}_{ex} \rangle\rangle\} \tag{2.26}$$

C is the Curie constant and k_B the Boltzman constant. For exchange interactions much larger than the dipolar interaction, one has

$$H_i^2 = \frac{2}{k_B C}\ \langle\langle \mathcal{H}^2_{ex} \rangle\rangle = \frac{4S(S+1)}{g^2\mu_B^2} \sum_j J_{ij}^{xx\,2} + J_{ij}^{yy\,2} + J_{ij}^{zz\,2} \tag{2.27}$$

In the expressions for $\tilde{G}_{zK}(\omega,0)$ one further has

$$\langle\langle S_z^2 \rangle\rangle = \frac{1}{3}\,S(S+1) \tag{2.28}$$

For a bilinear Hamiltonian, such as given by eqs. (2.1)-(2.4), one has

$$\mathcal{H}_{sec} = \sum_{i\neq j} C_{ij}^{oo}\, S_{zi} S_{zj} + C_{ij}^{+-}\, S_{+i} S_{-j} \tag{2.29}$$

$$\mathcal{H}_{\pm 1} = \sum_{i\neq j} C_{ij}^{\pm o}\, S_{\pm i}\, S_{zj} \tag{2.30}$$

$$\mathcal{H}_{\pm 2} = \sum_{i\neq j} C_{ij}^{\pm\pm}\, S_{\pm i}\, S_{\pm j} \tag{2.31}$$

The factors C_{ij} are given by

$$C_{ij}^{oo} = -J_{ij}^{zz} + \tfrac{1}{2}g^2\mu_B^2\, r_{ij}^{-3}\,(1-3\cos^2\theta_{ij}) \tag{2.32}$$

$$C_{ij}^{+-} = -\tfrac{1}{2}(J_{ij}^{xx} + J_{ij}^{yy}) - iD_{zij} - \tfrac{1}{4}g^2\mu_B^2\, r_{ij}^{-3}(1-3\cos^2\theta_{ij}) \tag{2.33}$$

$$C_{ij}^{\pm o} = D_{yij} \pm iD_{xij} - \frac{3}{2}g^2\mu_B^2\, r_{ij}^{-3} \sin\theta_{ij}\cos\theta_{ij}\, e^{\mp i\phi_{ij}} \tag{2.34}$$

$$C_{ij}^{\pm\pm} = \tfrac{1}{4}(J_{ij}^{yy} - J_{ij}^{xx}) - \frac{3}{8}g^2\mu_B^2 r_{ij}^{-3} \sin^2\theta_{ij}\, e^{\mp 2i\phi_{ij}} \tag{2.35}$$

r_{ij}, θ_{ij} and ϕ_{ij} are the usual spherical coordinates of $\vec{r}_{ij}$ in the Cartesian

reference system (x, y, z). It has been assumed that the principal axes of the exchange tensors coincide with the magnetic axes (x, y, z). z is the direction of both static and rf field. In the case of large exchange interactions and small anisotropy, C_{ij}^{oo} and C_{ij}^{+-} reduce to

$$C_{ij}^{oo} \simeq C_{ij}^{+-} \simeq -J_{ij} \tag{2.36}$$

with

$$J_{ij} = \frac{1}{3}\,(J_{ij}^{xx} + J_{ij}^{yy} + J_{ij}^{zz}) \tag{2.37}$$

We see that, in that case, antisymmetric exchange is only influencing $\hat{G}_{z1}(\omega,0)$ while anisotropic symmetric exchange only influences $\hat{G}_{z2}(\omega,0)$.
The calculation of $<<\mathcal{H}_k\mathcal{H}_{-k}>>$ and $<<[\mathcal{H}_{sec},\mathcal{H}_k][\mathcal{H}_{-k},\mathcal{H}_{sec}]>>$ is laboreous. We have

$$<<\mathcal{H}_k\mathcal{H}_{-k}>> = <<\mathcal{H}_k\mathcal{H}_{-k}>>_{is} + \Delta<<\mathcal{H}_k\mathcal{H}_{-k}>> \tag{2.38}$$

$$<<[\mathcal{H}_{sec},\mathcal{H}_k][\mathcal{H}_{-k},\mathcal{H}_{sec}]>> = <<[\mathcal{H}_{sec},\mathcal{H}_k][\mathcal{H}_{-k},\mathcal{H}_{sec}]>>_{is} + \Delta<<[\mathcal{H}_{sec},\mathcal{H}_k][\mathcal{H}_{-k},\mathcal{H}_{sec}]>> \tag{2.39}$$

The index is denotes the normalized traces for isotropic exchange interaction and (anisotropic) dipolar interaction only. The prefix Δ denotes the change in these traces when adding antisymmetric and anisotropic symmetric exchange interaction to the interaction Hamiltonian. Explicit expressions for $<<\mathcal{H}_k\mathcal{H}_{-k}>>_{is}$ and $<<[\mathcal{H}_{sec},\mathcal{H}_k][\mathcal{H}_{-k},\mathcal{H}_{sec}]>>_{is}$ will not be given here as these are easily found elsewhere, see e.g. references (10) and (11). For large exchange interactions (compared with the non-secular interactions) and small anisotropy, we calculate for the spin $S = \frac{1}{2}$ case.

$$\Delta<<\mathcal{H}_1\mathcal{H}_{-1}>> = \frac{1}{8}\sum_{i\neq j} D_{xij}^2 + D_{yij}^2 \tag{2.40}$$

$$\begin{aligned}\Delta<<[\mathcal{H}_{sec},\mathcal{H}_1][\mathcal{H}_{-1},\mathcal{H}_{sec}]>> = {} & \sum_{i\neq j} \tfrac{1}{2}(D_{xij}^2 + D_{yij}^2)J_{ij}^2 \\ & + \tfrac{1}{4}\sum_{i,j,l\neq} 2J_{ij}^2(D_{xjl}^2+D_{yjl}^2) - 3J_{ij}J_{jl}(D_{xij}D_{xjl}+D_{yij}D_{yjl}) \\ & - J_{ij}J_{il}(D_{xjl}^2+D_{yjl}^2) - 2J_{ij}^2(D_{xil}D_{xjl}+D_{yil}D_{yjl}) \\ & + 2J_{ij}J_{jl}(D_{xil}D_{xjl}+D_{yil}D_{yjl})\end{aligned} \tag{2.41}$$

$$\Delta<<\mathcal{H}_2\mathcal{H}_{-2}>> = \frac{1}{32}\sum_{i\neq j}(J_{ij}^{yy}-J_{ij}^{xx})^2 - 3(J_{ij}^{yy}-J_{ij}^{xx})g^2\mu_B^2\, r_{ij}^{-3}\sin^2\Theta_{ij}\cos 2\phi_{ij} \tag{2.42}$$

$$\Delta<<[\mathcal{H}_{sec},\mathcal{H}_2][\mathcal{H}_{-2},\mathcal{H}_{sec}]>> = \frac{1}{16}\sum_{i,j,l\neq}$$

$$(J_{jl}^{yy}-J_{jl}^{xx})\{(J_{jl}^{yy}-J_{jl}^{xx})-3g^2\mu_B^2\, r_{jl}^{-3}\sin^2\theta_{jl}\cos 2\phi_{jl}\}(J_{ij}^2+J_{il}J_{ij}+J_{il}^2)$$

$$-(J_{jl}^{yy}-J_{jl}^{xx})\{(J_{ij}^{yy}-J_{ij}^{xx})-3g^2\mu_B^2\, r_{ij}^{-3}\sin^2\theta_{ij}\cos 2\phi_{ij}\}$$

$$.(J_{il}J_{ij}+J_{jl}J_{il}+2J_{il}^2-J_{ij}J_{jl}) \qquad (2.43)$$

D denotes the components of the antisymmetric exchange vector (see eq. 2.9). Using these expressions and eqs. (2.23) and (2.24), one is able to calculate numerically the field dependent high-temperature relaxation times in the three magnetic axes. In the case of large antisymmetric or anisotropic symmetric interactions (compared with the dipolar interactions), one may neglect the traces denoted with *is*. In that special case the calculation of the relaxation times is very simple.
The resonance linewidths are found by substituting the calculated relaxation times in eq. (2.24a).

2.4 *Spin-spin relaxation near the Néel temperature*

Near the Néel temperature the critical slowing down of the spin fluctuations strongly influences the dynamical behavior of the magnetic system.
Using dynamical scaling assumptions and a factorization of the spin correlation functions we will derive relatively simple expressions for the zero-field spin-spin relaxation times in weakly anisotropic, magnetic systems. Although we restrict ourselves to antiferromagnets, the basic ideas of the theory also apply to ferromagnets. Our theory is an extension of the theory given by Huber (2)(12)

In the weak-coupling and low-field limit the relaxation time τ of $M_z(t)$ is given by (cf. eqs. (1.47) and (2.10))

$$\tau^{-1} = \chi_{oz}^{-1}\int_0^\infty((LM_z)^\dagger,\, e^{iL_z t+\, iL_{sec}\, t}\, LM_z)dt \qquad (2.44)$$

where χ_{oz} is the zero-field static susceptibility in the z-direction. In (2.44) we used that at low fields $\chi_{oz} = (M_z,M_z) \simeq (\mu_z,\mu_z)$.

The Liouville operator L is defined by

$$LM_z \equiv \frac{1}{\hbar}[\mathcal{H}, M_z] = \frac{1}{\hbar}[\mathcal{H}_{nsec}, M_z] \tag{2.45}$$

We shall further use the notation

$$A(t) = e^{\frac{i\mathcal{H}_o t}{\hbar}} A\, e^{-\frac{i\mathcal{H}_o t}{\hbar}} \tag{2.46}$$

$$\mathcal{H}_o = \mathcal{H}_z + \mathcal{H}_{sec} \tag{2.47}$$

Of the possible non-secular interactions we will take into account dipolar and antisymmetric Dzialoshinsky-Moriya interaction. Of course any other interaction could be included but in the copper compounds we study, dipolar and antisymmetric interaction are the major sources of non-secular contribution. Eq. (2.3) can also be written as

$$\mathcal{H}_{dd} = \tfrac{1}{2} g^2 \mu_B^2 \sum_{i \neq j} \sum_{\alpha,\beta} U^{ij}_{\alpha\beta} S^{\alpha}_i S^{\beta}_j \tag{2.48}$$

with $\alpha,\beta = x, y, z$, the coordinates in the Cartesian reference system.

$$U^{ij}_{\alpha\beta} = (r^2_{ij}\delta_{\alpha\beta} - 3(\vec{r}_{ij})_\alpha (\vec{r}_{ij})_\beta) r^{-5}_{ij} \tag{2.49}$$

δ denotes the usual Kronecker symbol. For the antisymmetric exchange

$$\vec{D}_{ij}.(\vec{S}_i x \vec{S}_j) = D^{ij}_x (S^y_i S^z_j - S^z_i S^y_j) + D^{ij}_y (S^z_i S^x_j - S^x_i S^z_j) + D^{ij}_z (S^x_i S^y_j - S^y_i S^x_j) \tag{2.50}$$

with the condition that $D^{ij}_\alpha = - D^{ji}_\alpha$. The part with D^{ij}_z is fully secular and plays no role in LM_z.

Substituting eqs. (2.48) and (2.50) in (2.44) and (2.45) one finds $((LM_z)^\dagger, LM_z(t))$ as a sum of four-spin correlation functions. For an uniform description of all these correlation functions one usually transforms to the wavevector space. This spatial Fourier transformation will be defined by

$$U^{ij}_{\alpha\beta} = N^{-1} \sum_q e^{i\vec{q}.\vec{r}_{ij}} U(\vec{q})_{\alpha\beta} \tag{2.51}$$

$$D^{ij}_\alpha = N^{-1} \sum_q e^{i\vec{q}.\vec{r}_{ij}} D(\vec{q})_\alpha \tag{2.52}$$

$$S^\alpha_j = N^{-1} \sum_q e^{i\vec{q}.\vec{r}_{ij}} S^\alpha(\vec{q}) \tag{2.53}$$

Four-spin correlation functions, here expressed in $\vec{q}$ instead of in $\vec{r}_{ij}$, are extremely difficult to work with.

To evade much of the difficulty, we factorize the correlation functions by using a dynamical Random Phase Approximation, defined by

$$(S^{\alpha}_{q_1}\, S^{\beta}_{q_2}, S^{\gamma}_{q_3}(t) S^{\delta}_{q_4}(t)) \xrightarrow{\text{DRPA}}$$

$$k_B T(\delta_{\alpha\gamma}\delta_{\beta\delta}\delta_{q_1,-q_3}\delta_{q_2,-q_4} + \delta_{\alpha\delta}\delta_{\beta\gamma}\delta_{q_1,-q_4}\delta_{q_2,-q_3})(S^{\alpha}_{-q_1}, S^{\alpha}_{q_1}(t))(S^{\beta}_{-q_2}, S^{\beta}_{q_2}(t)) \tag{2.54}$$

The Kronecker delta should not be confused with the index δ which denotes a Cartesian coordinate. It is impossible to say whether by this decoupling important information is lost. We will assume that the two-spin correlation functions still contain all information relevant to the dynamical behavior of the magnetic system.

Using the DRPA one derives for the integrand in expression (2.44)

$$\begin{aligned}((LM_z)^{\dagger}, LM_z(t)) = \frac{g^6 \mu_B^6 k_B T}{\hbar^2 N^2} \sum_q \\ |U_{xx}(q) - U_{yy}(q)|^2 (S^x_{-q}, S^x_q(t))(S^y_{-q}, S^y_q(t)) + \\ +2|U_{xy}(q)|^2 \{(S^x_{-q}, S^x_q(t))^2 + (S^y_{-q}, S^y_q(t))^2\} + \\ +\{|U_{xz}(q)|^2 + \frac{4}{g^4 \mu_B^4} |D_y(q)|^2\}(S^y_{-q}, S^y_q(t))(S^z_{-q}, S^z_{-q}(t)) + \\ +\{|U_{yz}(q)|^2 + \frac{4}{g^4 \mu_B^4} |D_x(q)|^2\}(S^x_{-q}, S^x_q(t))(S^z_{-q}, S^z_q(t))\end{aligned} \tag{2.55}$$

Although the vector symbol has been omitted, q still stands for the wavevector $\vec{q}$. The q-sum is taken over the total Brillouin zone. In the simple case of isotropy in the two-spin correlation functions and when omitting the contribution due to antisymmetric exchange, eq. (2.55) reduces to the expression given by Huber (2). Substitution of eq. (2.55) in (2.44) gives a formal expression for the low-field relaxation time.

The basic feature of all dynamical critical phenomena is the critical slowing down of the spin fluctuations. This slowing down, which arises from the progressive correlation between the electron spins, makes itself mostly felt in the two-spin correlation functions with q-values near the wavevector $\vec{q}_o$ of the ordered state. Both the time surface and the start value of each of these correlation functions drastically increases when nearing the Néel temperature. To determine the wavevector $\vec{q}_o$ the antiferromagnetic spin structure should be known in so far that the magnetic spins can be labeled in sublattices.

The vector $\vec{q}_o$ is then the vector that maximizes $(S^{\alpha}_{-q}, S^{\alpha}_{q})$ with S^{α}_{q} given by

$$S^{\alpha}_{q} = \sum_{j} e^{-i\vec{q}.\vec{r}_{ij}} S^{\alpha}_{j} \tag{2.56}$$

For a two-sublattice antiferromagnet this implies that for spins i and j in the same sublattice $\vec{q}_o.\vec{r}_{ij} = 0$ and for spins in different sublattices $\vec{q}_o.\vec{r}_{ij} = (2n + 1)\pi$.

The progressive correlation between the spin fluctuations can be described by a parameter ξ usually called the correlation length. This parameter ξ sets the length scale of the critical spin fluctuations. It is obvious that the relaxations rate Γ, which sets the time scale of the fluctuations, will be strongly influenced by the progressive correlation between the spins. The functional relation between length and time scale is given by the so-called scaling function Ω. In an antiferromagnet one has (3)

$$\Gamma(\Delta q, \kappa) = \kappa^{3/2} \; \Omega(\Delta q / \kappa) \tag{2.57}$$

$$\kappa = \xi^{-1} \tag{2.58}$$

with $\Delta\vec{q} = \vec{q} - \vec{q}_o$. Eq. (2.57) is a direct result of dynamical scaling assumptions by which some homogeneity conditions are forced on the scaling function. The dynamical scaling theory for isotropic magnetic systems has been given by Halperin and Hohenberg (13) and can be seen as an extension of the static Widom-Kadanoff scaling theory (14)(15). Eq. (2.57) is valid in the so-called hydrodynamic region defined by $|\Delta\vec{q}| \lesssim \kappa$.
The scaling function Ω reflects the symmetry of the magnetic system. Riedel (3) has shown that in anisotropic magnetic systems with uniaxial symmetry, the anisotropy can be described by a second length which is finite at the Néel temperature. This is in agreement with the neutron scattering data of Schulhof et al. (16) on the uniaxial compound MnF_2. In their experiments it was found that only the staggered susceptibility parallel to the easy-axis was divergent at the Néel point, the perpendicular staggered susceptibilities remained finite.

We assume now that in anisotropic systems where the small magnetic anisotropy is not necessarily uniaxial, the critical fluctuations can, in first order, still satisfactorily be described by two correlation lengths.

Let $\kappa_{//}$ be the inverse correlation length parallel to the easy-axis and $\kappa_{\perp}$ the inverse correlation length perpendicular to the easy-axis. One has then

$$\kappa_{//}(T_N) = 0 \qquad , \kappa_{\perp}(T_N) = \kappa_{\Delta} \tag{2.59}$$

The value for κ_{Δ} is related to the anisotropy of the magnetic system. An analysis of the data of Schulhof et al. shows that $\kappa_{\perp}$ can, in good approximation, be described by

$$\kappa_{\perp}^2(T) = \kappa_{//}^2(T) + \kappa_{\Delta}^2 \tag{2.60}$$

The anisotropy in the correlation length introduces an anisotropy in the two-spin correlation functions of eq. (2.55). We assume now that the anisotropy in the two-spin correlation functions wholly stems from this anisotropy in the correlation length. This implies that the correlation functions are supposed to be isotropic at high temperatures.
Assuming further that the long-time behavior of the correlation functions is exponential in the hydrodynamic region, one has

$$(S^{\alpha}_{-\Delta q-q_o}, S^{\alpha}_{\Delta q+q_o}(t)) = (S^{\alpha}_{-\Delta q-q_o}, S^{\alpha}_{\Delta q+q_o}) e^{-\Gamma_{\alpha}(\Delta q,\kappa)t} \tag{2.62}$$

where α denotes the Cartesian components. The relaxation rate $\Gamma_{\alpha}(\Delta q,\kappa)$ of the spin fluctuations near the wavevector $\vec{q}_o$ is given by

$$\Gamma_{\alpha}(\Delta q,\kappa) = \kappa_{\alpha}^{3/2}\, \Omega(\Delta q/\kappa_{\alpha}) \tag{2.63}$$

Eq. (2.63) states that the relaxation rate Γ_{α} of the spin fluctuations in the α-direction only depends on the correlation length in that direction. This, in fact, is an approximation as the relaxation rate may also slightly depend on the correlation lengths in the other directions (3). Expression (2.63) however represents in a reasonable good approximation the basic correlation length dependence of the relaxation rates.

In general the scaling function Ω is not symmetrical in the components of $\Delta\vec{q}$ Expansion of the scaling function up to the second degree yields

$$\Omega(\Delta q/\kappa_{\alpha}) \simeq B_o\left(1+\sum_{\beta,\beta'}\left(\frac{\partial^2 \Omega}{\partial \Delta q_{\beta}\partial \Delta q_{\beta'}}\right)_{\Delta q=o} \frac{\Delta q_{\beta}\Delta q_{\beta'}}{\kappa_{\alpha}^2}\right) \tag{2.63a}$$

which by a simple linear transformation $\Delta\vec{q} \rightarrow \Delta\vec{q}^{\,*}$ which is governed by the crystal symmetry, can be written as

$$\Omega(\Delta q^*/\kappa_\alpha) \simeq B_o(1+c\frac{\Delta q^{*2}}{\kappa_\alpha^2}) \tag{2.64}$$

an expression which is symmetrical in the components of $\Delta\vec{q}^*$. For simplicity the prime will henceforth be omitted, it should thus be reminded that below $\Delta\vec{q}$ stands for $\Delta\vec{q}^*$.

The scaling function (2.64) has been verified by neutron scattering experiments (16) on the uniaxial compound MnF_2. The numerical constant c depends on the crystal symmetry and is normally in the order of unity. As our final results will only be weakly dependent on c, we will take this constant equal to unity.

In that case one has

$$\Gamma_\alpha(\Delta q,\kappa) = \kappa_\alpha^{3/2} B_o(1+\frac{\Delta q^2}{\kappa_\alpha^2}) \tag{2.65}$$

For the wavevector dependence of the staggered susceptibility we shall use the so-called Ornstein-Zernike form,

$$(S^\alpha_{-\Delta q-q_o}, S^\alpha_{\Delta q+q_o}) = \frac{(S^\alpha_{-q_o}, S^\alpha_{q_o})\kappa_\alpha^2}{\kappa_\alpha^2 + \Delta q^2} \tag{2.66}$$

The Ornstein-Zernike form is valid for the case where η, the critical exponent which describes the temperature dependence of the numerator in eq. (2.66), is equal to zero. The approximation of $\eta = 0$ is justified by the fact that η is expected to be very small, e.g. $\eta \simeq 0.04$ for the three-dimensional isotropic Heisenberg system (17).

As we supposed the two-spin correlation functions to be isotropic at temperatures for which $\kappa_{//} >> \kappa_\Delta$, one gets, using the fact that the small critical exponent η is independent of the direction, for temperatures sufficiently near T_N

$$(S^{//}_{-q_o}, S^{//}_{q_o})\kappa^2_{//} = (S^\perp_{-q_o}, S^\perp_{q_o})\kappa^2_\perp \simeq (S^\perp_{-q_o}, S^\perp_{q_o})_{T=T_N}\kappa^2_\Delta \tag{2.67}$$

The inverse correlation length in the direction parallel to the easy-axis is, for temperatures sufficiently near the Néel temperature, given by

$$\kappa_{//}(T) = \kappa_o(\frac{T-T_N}{T_N})^\nu = \kappa_o \epsilon^\nu \tag{2.68}$$

κ_o is a constant, the critical exponent ν is related to the critical exponent γ of the parallel staggered susceptibility. For $\eta = 0$ one has

$$\gamma = 2\nu \tag{2.69}$$

The temperature dependence of the perpendicular inverse correlation length is found by substituting eq. (2.68) in (2.60).

We will now turn our attention once again to the relaxation time of the average total magnetization $M_z(t)$, given by eq. (2.44). The q-sum in eq. (2.55) can in good approximation be split up into a critical part, which contains all the contributions from the hydrodynamical region around $\vec{q}_o$, and a non-critical part which shows a much less pronounced temperature dependence.

$$\frac{1}{\tau} = (\Delta\frac{1}{\tau})_{\text{critical}} + (\Delta\frac{1}{\tau})_{\text{non-critical}} \tag{2.70}$$

Assuming that the coefficients U and D in eq. (2.55) are not singular at $\vec{q}_o$, one has, for temperatures sufficiently near T_N, in good approximation

$$\begin{aligned}(\Delta\frac{1}{\tau})_{\text{crit.}} = \frac{g^6\mu_B^6 k_B T}{\hbar^2 \chi_o N} \{ & |U_{xx}(q_o)-U_{yy}(q_o)|^2 F'_{xy} + 2|U_{xy}(q_o)|^2 (F'_{xx}+F'_{yy}) \\ & + \{|U_{xz}(q_o)|^2 + \frac{4}{g^4\mu_B^4} |D_y(q_o)|^2\} F'_{yz} \\ & + \{|U_{yz}(q_o)|^2 + \frac{4}{g^4\mu_B^4} |D_x(q_o)|^2 \} F'_{xz}\}\end{aligned} \tag{2.71}$$

with

$$F'_{\alpha\beta} = N^{-1} \sum_{\Delta q} \int_o^\infty (S^\alpha_{-\Delta q - q_o}, S^\alpha_{\Delta q + q_o}(t))(S^\beta_{-\Delta q - q_o}, S^\beta_{\Delta q + q_o}(t))dt \tag{2.72}$$

The $\Delta\vec{q}$-sum includes all the hydrodynamical modes. Using eqs. (2.62), (2.65), (2.66) and (2.68) one gets

$$F'_{\alpha\beta} = \frac{(S^{//}_{-q_o}, S^{//}_{q_o})^2 \kappa_{//}^4 \kappa_o^{-5/2} V}{2\pi^2 B_o} \in^{-\frac{5}{2}\nu} F_{\alpha\beta} \tag{2.73}$$

where V is a reduced volume per spin. This reduced volume is equal to the real volume per spin multiplied by a factor which describes the deviation of the lattice from the cubic lattice. This factor is related to the transformation $\Delta\vec{q} \to \Delta\vec{q}^*$ and is normally in the order of unity. $F_{\alpha\beta}$ is given by

$$F_{\alpha\beta} = \frac{2\pi^2}{NV} \sum_{\Delta q} \frac{\kappa_{//}^{5/2}}{(\kappa_\alpha^2+\Delta q^2)(\kappa_\beta^2+\Delta q^2)[\kappa_\alpha^{-\frac{1}{2}}(\kappa_\alpha^2+\Delta q^2)+\kappa_\beta^{-\frac{1}{2}}(\kappa_\beta^2+\Delta q^2)]} \tag{2.74}$$

The functions $F_{\alpha\beta}$ are only dependent on $\kappa_\Delta/\kappa_{//}$ and are easily computed by transforming the $\Delta\vec{q}$-sum into an integral. Care should be taken to include all hydrodynamic modes. The numerical results are given in Fig. 1. The interesting point is that the values for $F_{\alpha\beta}$ are not restricted to one case but can be applied to all antiferromagnets as long as our assumptions hold.

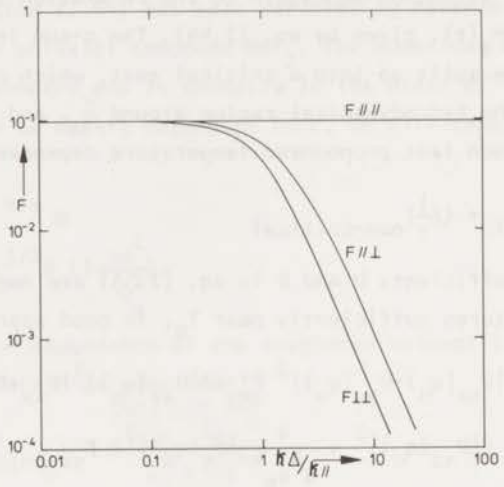

Fig. 1 *The dependence of* $F_{\alpha\beta}$ *(defined by eq. (2.74)) on* $\kappa_\Delta/\kappa_{//}$

For small $\kappa_\Delta/\kappa_{//}$: $F_{//\,//} = F_{//\perp} = F_{\perp\perp} = 0.09817$

For large $\kappa_\Delta/\kappa_{//}$: $F_{//\,//} = 0.09817$

$$F_{//\perp} = 0.3861\ (\kappa_\Delta/\kappa_{//})^{-2.5}$$

$$F_{\perp\perp} = 0.0981\ (\kappa_\Delta/\kappa_{//})^{-2.5}$$

The critical part of the relaxation time is thus given by

$$\left(\Delta\frac{1}{\tau}\right)_{crit.} = A\,\frac{TN}{\chi_o}\in^{-\frac{5}{2}\nu}\{|U_{xx}(q_o)-U_{yy}(q_o)|^2\,F_{xy}+2|U_{xy}(q_o)|^2(F_{xx}+F_{yy})$$
$$+\{|U_{xz}(q_o)|^2+\frac{4}{g^4\mu_B^4}|D_y(q_o)|^2\}F_{yz}$$
$$+\{|U_{yz}(q_o)|^2+\frac{4}{g^4\mu_B^4}|D_x(q_o)|^2\,F_{xz}\} \qquad (2.75)$$

with

$$A = \frac{g^6\mu_B^6 k_B}{2\pi^2\hbar^2N^2}\,(S^{//}_{-q_o},S^{//}_{q_o})^2\,\kappa_{//}^4\,V\,B_o^{-1}\,\kappa_o^{-5/2} \qquad (2.76)$$

It should be noted that A is a calibration factor which is independent of the temperature and the direction.

For an explicit calculation of the critical part of the relaxation time the only problem left now is to determine the exact value of $\kappa_\Delta/\kappa_{//}$ at a given temperature. We have (cf. eq. (2.68))

$$\kappa_{//} = \kappa_o \epsilon^\nu \tag{2.77}$$

Let a reduced temperature $\epsilon_\Delta(\kappa_\Delta)$ be defined by

$$\kappa_\Delta \equiv \kappa_o \epsilon_\Delta^\nu \tag{2.78}$$

The value for κ_Δ and thus for ϵ_Δ depends on the magnetic anisotropy of the system.

Making a molecular field approach we estimate, using the fact that the anisotropy finally turns the electrons spins towards the easy-axis, that in a three-dimensional orthorhombic antiferromagnet

$$\epsilon_\Delta \simeq \frac{H_{A1} + H_{A2}}{H_E} \tag{2.79}$$

where H_{A1} and H_{A2} are the orthorhombic anisotropy fields. H_E is the exchange field.

For MnF_2, where $H_{A1} = H_{A2} = H_A$, this yields $\epsilon_\Delta = 0.031$ which should be compared with experimental value $\epsilon_\Delta = 0.033$ found by Schulhof et al. (16) (see also ref. (3)) from their neutron scattering data. Combining eqs. (2.77)-(2.79) one gets

$$\frac{\kappa_\Delta}{\kappa_{//}} \simeq \left(\frac{H_{A1} + H_{A2}}{H_E}\right)^\nu \epsilon^{-\nu} \tag{2.80}$$

We further approximate the non-critical part of the relaxation time by

$$\left(\Delta\frac{1}{\tau}\right)_{\text{non-critical}} = \left(\frac{1}{\tau}\right)_{T\to\infty} \tag{2.81}$$

In compounds (such as $RbMnF_3$) where due to symmetry reasons the critical part of the relaxation time is equal to zero, only a very weak dependence of the relaxation time on the temperature, even very near T_N, is found (18). This is also the case in MnF_2 in the direction parallel to the easy-axis (19).

All this supports the approximation (2.81).

Using eqs. (2.70), (2.75), (2.80) and (2.81) and the values for $F_{\alpha\beta}$ from Fig. 1, one is able to calculate the relaxation time τ over the total temperature region above the Néel temperature. Stating this we have implicitly used that where the theory for the critical part of the relaxation time looses its accuracy, the deviations will not be important any more as at higher temperatures the non-critical part determines nearly completely the relaxation process. The value for A, defined by eq. (2.76), is very difficult to calculate for non-cubic systems. Such drastic approximations have to be made that comparison of a theoretical value with an experimental value cannot be conclusive in any way. The value for A may therefore be inferred from experiment by adapting the theory to experiment at a given temperature in a given direction. This is a loss of generality but as A is only a calibration factor, the temperature dependence of the relaxation times and the relative differences between the relaxation times in the different axes still allow a thorough check on the theory.

2.4.1 *Note on the value for* ν

The critical exponent ν is related to γ by eq. (2.69).
For a three-dimensional isotropic Heisenberg system high-temperature series expansions (20) have shown that $\gamma = 1.43$. The critical exponents have been found (21) to be independent of the lattice anisotropy (different strength of interaction in different directions). Only in extreme cases where a large lattice anisotropy implies a change in dimensionality the critical exponents are influenced by the lattice anisotropy. For a magnetic anisotropy in the interaction parameters the case is completely different. It is believed (22) (23) that the introduction of a very small magnetic anisotropy in the isotropic three-dimensional Heisenberg system changes the exponent γ discontinueosly from the Heisenberg to the Ising or XY value, dependent on the kind of anisotropy one introduces. Although the dependence on the anisotropy may turn out not to be singular at the isotropic Heisenberg case, the critical exponent γ certainly is very sensitive to small anisotropy variations. This point is demonstrated by the experimental fact that for the highly isotropic $RbMnF_3$ one has $\nu = 0.72$ (24), while for the weakly anisotropic MnF_2 (1.5% anisotropy) one has $\nu = 0.63$ (16), a value which is very near the Ising value.

The absolute magnitude of the shift in γ due to magnetic anisotropy is however small and the relaxation process will be much more influenced by the cut-off effect in the correlation length than by the dependence of γ (and thus of ν) on the magnetic anisotropy.

2.4.2 *Some final remarks*

In studying the critical temperature dependence of an arbitrary property there is a strong tendency to look for a critical exponent. Also the temperature dependence of dynamical phenomena, such as relaxation and resonance, are normally rather well described by a power-law dependence although, in most cases, near the Néel temperature some deviation occurs. This deviation is usually attributed to an inaccuracy in the measurements.
For the critical exponents derived from relaxation and resonance experiments very different values are found. Even the exponent is sometimes found to be dependent on the direction. All this seems to be in contradiction with the so-called universality principle which states that the critical point exponents should only be dependent on drastic changes in dimensionality and range of interaction and not on the specific lattice and interaction parameters of the compound studied.
The generalization of the theory of Huber (2)(12) presented in this chapter gives a full explanation of this apparent contradiction. It is shown that the magnetic anisotropy strongly influences the dynamical critical behavior. It depends now on a combination of crystal symmetry and anisotropy in the critical slowing-down of the spin fluctuations which critical temperature dependence will be found. It is shown that in the anisotropic system the total critical temperature dependence cannot be described by a single critical exponent, although in some temperature region some power-law dependence may exist.
In this thesis it will be shown that the results of this theory are in perfect agreement with experiment in three different magnetic compounds.

2.5 *Relaxation in the antiferromagnetic state*

In studying antiferromagnetic relaxation one has to differentiate between the temperature region near the Néel temperature where critical fluctuations are

important and the temperature region far below T_N where the relaxation process is governed by the regular spin-wave fluctuations. The relaxation process in antiferromagnets can be complicated by the simultaneous occurrence of different spin-wave scattering processes. Before going into detail on the theoretical results we will discuss and compare shortly the different experimental ways of measuring antiferromagnetic relaxation. We will restrict ourselves to the easy-axis case where the static field is parallel to the easy-axis. The most important experimental methods are antiferromagnetic resonance, neutron scattering, parallel pumping and direct relaxation measurements.

2.5.1 *Antiferromagnetic resonance*

The wavevector dependent spin-wave spectrum of an orthorhombic antiferromagnet, at T = 0 and with the static field H parallel to the easy-axis, is given by

$$\left(\frac{\omega_{1,2\,k}}{\gamma}\right)^2 = (H_E + H_{A1})(H_E + H_{A2}) + H^2 - (H_E\gamma_k)^2 \pm \{(2H_E + H_{A1} + H_{A2})^2H^2 + (H_{A2} - H_{A1})^2(H_E\gamma_k)^2 - 4H^2(H_E\gamma_k)^2\}^{\frac{1}{2}} \tag{2.82}$$

H_E is the exchange field, H_{A1} and H_{A2} are the orthorhombic anisotropy fields. ω_{1k} and ω_{2k} are the spin-wave frequencies at wavevector $\vec{k}$.

$$\gamma = g\mu_B\hbar^{-1} \tag{2.83}$$

$$\gamma = \exp(i\vec{k}.\vec{r}_{nn}) \tag{2.84}$$

where $\vec{r}_{nn}$ is the vector which points to one of the nearest neighbors.
The orthorhombic anisotropy introduces an energy gap in the spin-wave spectrum which persists at zero field. The wavevector and field dependence of the spin-wave spectrum is given in Fig. 2. At non-zero temperature the whole spectrum is shifted to lower frequencies. For low temperatures the spin-wave gap remains unchanged but as $T \to T_N$ the spin-wave gap is believed to approach zero with a certain power of the correlation length.
The usual resonance situation is now that at a fixed frequency ($k \simeq 0$) one increases the static field till the resonance conditions are satisfied. By varying the static field around the resonance field one measures the field linewidth of the antiferromagnetic resonance lines. See Fig. 2.

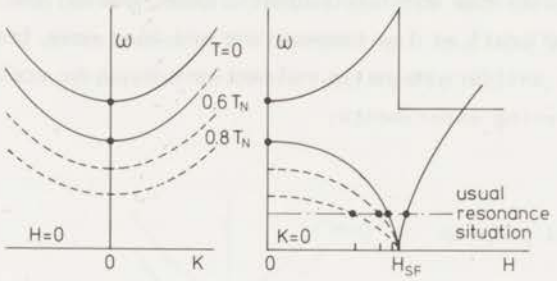

Fig. 2 *The spin-wave resonance frequencies of an orthorhombic antiferromagnet at T = 0. The static field is parallel to the easy-axis. The broken lines give the temperature dependence of the low branch at increasing temperatures.*

There are several reasons why AFMR is not always a good method to determine the relaxation rate of the magnetic system. From Fig. 2 it is easy to see that with increasing temperature the low-branch resonance field at fixed frequency decreases (H_{SF} is only weakly temperature dependent). When comparing the experimental temperature dependence of the resonance linewidth with theoretical results, one has to eliminate first the intrinsic field dependence of the relaxation process. This is very difficult and therefore omitted more than once.

Suppose further that the relaxation process is due to several decay processes with different decay times. In direct relaxation measurements this is easily detected but in the resonance field-linewidth these processes broaden simultaneously and thus are difficult to distinguish, especially in the case of asymmetrical lines. Furthermore it is an important experimental fact that the relaxation of the uniform precession is very sensitive to crystal imperfections, such as cracks, which give rise to a temperature independent residual linewidth. This broadening effect is difficultly accounted for theoretically, one has to measure at sufficiently low temperatures to determine this residual linewidth.

2.5.2 *Neutron scattering*

Neutron scattering is usually one of the best experimental methods to probe spin dynamics. In the antiferromagnetic case however the decay rates turn out to be very small at low temperature and long wave lengths. For this reason the $k \simeq 0$ antiferromagnetic relaxation cannot be accurately observed by neutron scattering experiments.

2.5.3 *Parallel pumping*

Parallel pumping is based on a non-linear parametric excitation of spin-waves. The static and rf field are both parallel to the easy-axis. Under certain conditions a large rf field excites so many spin-waves of a certain wavevector k that the growth rate exceeds the decay rate. In that case instability of the particular spin-waves occurs which manifests itself as a sudden increase of the rf field absorption by the sample. This spin-wave instability was first observed by Schlömann et al. (25) in a ferromagnetic compound in 1960. There is more than one way to create spin-wave instability but in an orthorhombic antiferromagnet, at frequencies lower than the zero-field low-branch spin-wave frequency, only one process is important. In that process a photon of the rf field creates two magnons in the low spin-wave branch. Due to energy and wavevector conservation and the symmetry of the spin-wave spectrum, these two magnons have opposite wavevectors and equal energy. This implies that

$$\omega_{1k} = \omega/2 \tag{2.85}$$

ω_{1k} is the k-dependent frequency of the low-branch, ω is the frequency of the rf field. The excitation process leads to instability above a rf threshold field h_{thr} given (26) by

$$h_{thr}(k) = \frac{\omega_{1k}}{\gamma^4} \frac{\omega_{2k}^2 - \omega_{1k}^2}{H(H_{A2}-H_{A1})(2H_E+H_{A1}+H_{A2})} \Gamma(k) \tag{2.86}$$

$\Gamma(k)$ is the decay rate of the spin-waves with wavevector k. The low and high-branch frequencies, ω_{2k} and ω_{1k}, are given by eq. (2.82). This equation is only valid for sufficiently low temperatures. At higher temperatures a more general expression for ω_{1k} and ω_{2k} should be used.

The usual situation is that at H = 0 the condition $\omega_{1k} = \omega/2$ is not satisfied. If however one increases the static field H, the low branch is shifted to lower frequencies and at a certain field the condition $\omega_{1k} = \omega/2$ is satisfied for k = 0. So, if one increases the static field the first spin-waves to become unstable are the k = 0 waves. When still increasing H the condition will be satisfied for $k \neq 0$. The situation is visualized in Fig. 3.

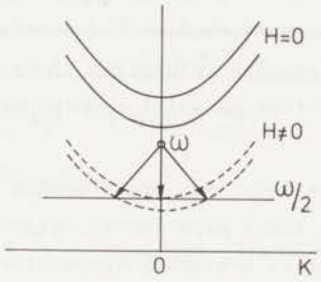

Fig. 3 *Creation of two spin-waves of half measuring frequency at non-zero static field. The dotted lines represent the low branch at two values of the external static field.*

So by merely changing the static field one can select spin-waves of a certain wavevector k. By measuring the threshold rf field the relaxation rate of the particular spin-waves can be determined.

A negative aspect of this most promising method is that, if the rf field is applied for some time, the sample will heat up considerably. Furthermore it is difficult to measure at low static fields where very high frequencies or very high rf powers are necessary to create spin-wave instability. Finally it should be noted that the accuracy for the relaxation rates depends on the accuracy with which the molecular fields H_E, H_{A1} and H_{A2} are known.

2.5.4 *Direct relaxation measurements*

It has been reported by some authors that when one orients both static and rf field parallel to the easy-axis, apart from spin-wave instabilities at large

rf powers, no absorption will be detected. As it has already been pointed out by Verbeek (19a), the non-zero value for the static susceptibility in the easy-axis implies that somewhere in the frequency region a decay process should occur which relaxates the susceptibility towards zero. In this thesis it will be shown that, in at least two antiferromagnets of different structure, an absorption corresponding to a single relaxation process is found in the case where both static and rf field are parallel to the easy-axis. Such an absorption was also detected by Verbeek (19a) in MnF_2.
The discrepancy between both results can be explained by the fact that the earlier experiments have been performed at frequencies much higher than the typical relaxation frequencies. The relaxation times we find are in excellent agreement with those derived from parallel pumping experiments for $k = 0$.

In our opinion regular relaxation times measurements in antiferromagnets below T_N are most promising as there experiments determine directly the $k \simeq 0$ decay process of the spin-waves at arbitrary temperatures and fields. In contrast to the other experimental methods the temperature and field region are not limited.

2.5.5 *Theoretical results for the k=0 decay process*

At temperatures well below the ordering temperature the dynamical properties of antiferromagnets can be described in terms of spin-wave excitations. The validity of such a description depends upon the product of the spin-wave frequency and the spin-wave lifetime being much greater than one. In the compounds we study this will be the case at nearly all temperatures and static fields outside the critical regions near T_N and the spin-flop field. At intermediate temperatures, outside the linear spin-wave regime, the decay process arises mainly from scattering of spin-waves by thermally excited spin fluctuations. Many authors have derived expressions for the k-dependent spin-wave decay rates in the different temperature regimes. Apart from the fact that some of these results do not apply to our $k \simeq 0$ case, it has been shown by Harris et al. (27) that some of the results are in mathematical error. In nearly all studies the possible field dependence of the decay rates is not taken into account, so these results only apply to vanishingly small fields.
Apart from the two-magnon imperfection scattering which is especially important to the relaxation of the uniform precession (i.e. uniform resonance) the relaxation process is governed by multiple-magnon and magnon-phonon processes.

The various theoretical results for the k = 0 relaxation rate $\Gamma(\equiv 1/\tau)$ are given in table 1. For the symbols in table 1 we have

$$\omega_A = g\mu_B \hbar^{-1} H_A$$

$$\omega_E = g\mu_B \hbar^{-1} H_E = 2zJS\hbar^{-1}$$

$$T_{AE} = \hbar k_B^{-1} (2\omega_A \omega_E)^{\frac{1}{2}}$$

z = number of nearest neighbors

table 1

author	ref.	Γ (k = 0)	region
Genkin	(28)	$64\omega_A^2 \omega_E^{-2} k_B \hbar^{-1}\ T \exp(-T_{AE}/T)$	$T \ll T_{AE}$
Urushadze	(29)	$2\omega_A^2 \omega_E^{-2} k_B \hbar^{-1} T$	$T \gg T_{AE}$
Kawasaki	(30)	$8.5\ 10^{-4} z^2 S^{-2} \omega_A \omega_E^{-1} k_B \hbar^{-1} T \exp(-T_{AE}/T)$	$T \ll T_{AE}$
		$8.5\ 10^{-4} z^2 S^{-2} \omega_A^{\frac{1}{2}} \omega_E^{-3/2} k_B^2 \hbar^{-2} T^2$	$T \gg T_{AE}$
Harris	(31)	$2.919\ S^{-2} \omega_A^{3/2} \omega_E^{-5/2} k_B^2 \hbar^{-2} T^2 \exp(-T_{AE}/T)$	$T \ll T_{AE}$
		$1.548\ S^{-2} \omega_A \omega_E^{-3} k_B^3 \hbar^{-3} T^3$	$T \gg T_{AE}$

All the results given in table 1 are valid for antiferromagnets with axial anisotropy at infinitely small static fields and $T \ll T_N$.
Harris et al. (27) recently published more detailed results but these contain unknown numerical constants. Their results (31) in table 1 are from an investigation of the damping in the lowest Born approximation using the Dyson-Maleev formalism, which for small S they believe to be a better formalism than the Holstein-Primakoff one.

In the critical region below T_N the relaxation process is complicated and, apart from the results of dynamical scaling, relatively little is known theoretically. The transverse fluctuations of the magnetization show well-defined spin-wave excitations while the longitudinal fluctuations are diffusive. As the temperature dependences of the damping constants of the spin-wave excitations and of the longitudinal diffusion constant are still unknown, no comparison of our experimental results with numerical calculations could be made. On the other hand the situation is too complex to derive these temperature dependences from our measurements.

CHAPTER 3

EXPERIMENTAL TECHNIQUE

3.1 *Equipment*

For the relaxation and resonance experiments described and discussed in this thesis we used a calorimetric method.
The sample is placed inside a quartz sample holder which is connected, by a quartz capillary, with a pressure transducer outside the cryostat. See Fig. 4. The sample holder and capillary are filled to a certain pressure with helium gas.
The static field is supplied by a water-cooled Newport (4 inch type A) magnet outside the cryostat while the rf field is supplied by a coaxial Lecher system inside the cryostat. The Lecher system has been described by Van der Molen (10). The static field magnet and the sample can be rotated independently about the same axis over more than 270°. In that way, both relaxation (static field parallel to the rf field) and resonance (static field perpendicular to the rf field) measurements can be performed in nearly all directions of the crystal plane perpendicular to the rotation axis.

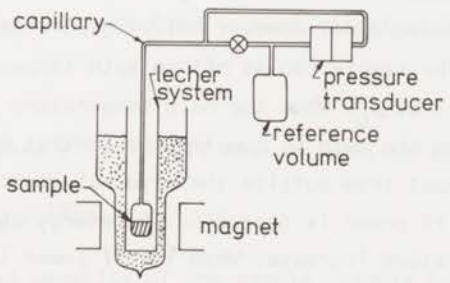

Fig. 4 *Calorimetric system*

Due to the rf energy absorption by the sample the temperature of the sample and sample holder increases, which reflects itself in a pressure increase of the helium gas inside the closed calorimetric system. The pressure increase is detected by a pressure transducer (S.E. 150/20") and converted into an electronic signal which is written on a recorder.

During the measurements the sample is isolated from the bath. The static field is measured using a Hall probe (Siemens FC 34) just outside the cryostat while the rf power is detected by measuring the rf voltage at a given point of the Lecher system. The rf power is supplied by a high-power oscillator (Airmec type 304), push-pull amplifier and (for the highest frequencies) a tripler. The frequency and static field ranges are given by ν = 4 - 540 MHz and H = 0 - 8 kOe respectively.

3.2 *Calorimetric system*

The calorimetric system can be represented by a volume V_ℓ at low temperature T_0 and a volume V_h at room temperature T_h, see Fig. 5.

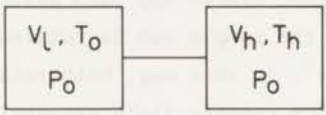

Fig. 5 *Schematic representation of the calorimetric system.*

In equilibrium the pressure of the helium gas is the same throughout the system. At the start of each measurement contact helium gas is let in between the sample holder and the bath. The sample cooles off to bath temperature T_0 and the pressure in the system will be p_0. When the bath temperature has been reached the sample is isolated from the bath by pumping the contact helium gas out.
Due to a small heat input from outside the cryostat the temperature begins to rise slowly. When the rf power is turned on the energy absorption by the sample gives a steeper temperature increase. When the rf power is turned off the temperature increase returns to its former value. A typical run is given in Fig. 6.

For the schematic model of Fig. 5, the relation between the pressure increase Δp and the temperature increase ΔT of the volume V_ℓ is given by

$$\frac{\Delta T}{T_o} = \frac{\Omega(T_1)\Omega(T_2)}{\Omega(T_o)} \frac{\Delta p}{p_o} \qquad (3.1)$$

with

$$\Omega(T) = 1 + \frac{V_h T}{V_\ell T_h} \tag{3.2}$$

T_1 and T_2 are given in Fig. 6, T_0 is the bath temperature and p_0 is the pressure of the calorimeter gas at bath temperature.

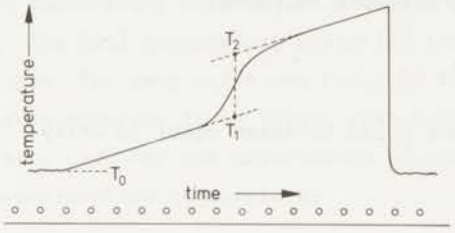

Fig. 6 *A typical example of the temperature increase due to rf absorption in the sample. The curve, which in fact represents a pressure increase, has been transformed into a temperature increase by using eq. (3.1).*

By checking eq. (3.1) in different situations, we found that the schematic model given in Fig. 5 was appropriate for the real calorimetric system.

$$\Delta T = T_2 - T_1 \tag{3.3}$$

The temperature increase dT due to rf absorption (see eq. (1.18)) is given by

$$C(T)dT = \pi\nu h_o^2 g_z \chi''(T)dt \tag{3.4}$$

$C(T)$ is the total heat capacity of the sample, sample holder and helium gas in volume V_ℓ. ν is the rf frequency, h_o the rf field in the sample and g_z the weight of the sample. χ'' is given per unit weight.
When $T_2 - T_1$ is sufficiently small one has

$$\chi''(\overline{T}) = C(\overline{T}) \frac{\Omega^2(\overline{T})}{\Omega(T_o)} \frac{T_o}{\pi\nu h_o^2 g_z p_o} \frac{\Delta p}{t} \tag{3.5}$$

$\overline{T} = (T_1 + T_2)/2$ while further $C(\overline{T})$ is given by

$$C(\overline{T}) = C_{sh}(\overline{T}) + C_s(\overline{T}) + \gamma C_{He}(\overline{T}) \tag{3.6}$$

$C_{sh}(\overline{T})$ is the heat capacity of the sample holder, $C_s(\overline{T})$ of the sample and $C_{He}(\overline{T})$ of the helium gas.

$$C_{He}(\overline{T}) = \frac{3}{2}\frac{p_o}{T_o} V_\ell \tag{3.7}$$

γ is a correction factor for the work performed by the gas which is transported from V_ℓ to V_h when the pressure increases.

$$\gamma = \frac{1}{3}(2\Omega(T_o) + 1) \tag{3.8}$$

In nearly all situations γ can be taken equal to unity.

3.3 *Calibration*

The static field has been calibrated by using proton resonance while at the lowest fields also a rotating coil Gauss meter has been used. The magnet showed a remanent field of about 100 Oe which could easily be compensated for by a small reverse current. The Hall probe showed itself to be sufficiently linear in our field region up to 8 kOe. The rest voltage at zero field was about 0.20 mV (at 200 mA current) and corresponded to a fictitious field of about 7 Oe. This rest voltage was easily compensated for.

The rf field h_o has been calibrated by using the magnetic properties of a well-known compound (powdered $CuCl_2.2H_2O$). Verstelle (32) has found that the frequency dependence of χ'' at zero field for the powdered sample was very well described by a Lorentzian. Using this we could calibrate our rf field h_o as a function of frequency and rf power. In our measurements on the single crystal of $CuCl_2.2H_2O$ we found the frequency dependence of χ'' to be Lorentzian in all magnetic axes.

We then recalibrated the rf field on the single crystal. This calibration should be a few percent better than the calibration on the powdered sample as there the frequency dependence of χ'' cannot be exactly Lorentzian.

3.4 *Accuracy of the temperature measurement*

The accuracy of our temperature measurement depends strongly on the ideality of the helium gas in the calorimetric system and on the validity of the model given in Fig. 5. We found the real system to be very well described by the schematic model of two volumes.

The ideality of the helium gas only plays a role at low temperatures below 5 K. The pressure p_0 within the system was always taken much smaller than the helium bath pressure at the given temperature. The accuracy was checked by measuring the value of the Néel temperature of $CuCl_2.2H_2O$ starting from different initial bath temperatures T_0. The Néel temperature presented itself as a sharp kink in the temperature increase. The same value was found in every case. We estimate the relative temperature accuracy to be better than 0.005 K at He temperatures. The calorimetric method, used for the experiments of this thesis, allows measuring at accurately predetermined temperatures.

CHAPTER 4

INTRODUCTION TO $CuCl_2.2H_2O$

4.1 *General introduction*

$CuCl_2.2H_2O$ was for a long time one of the most thoroughly investigated antiferromagnets. Nuclear magnetic resonance experiments by Poulis and Hardeman (34) as early as 1952 showed that this compound exhibited an antiferromagnetic phase transition just above He-temperatures. The easy-axis of the antiferromagnetic arangement was found to be the a-axis. Further investigations by the Leiden group, using the nmr technique, revealed many of the now well-known antiferromagnetic features, such as the occurrence of a threshold field. It was found that these features could be explained by the molecular field model initially proposed by Néel (35) and extended by Gorter and Haantjes (35a). In later years also much attention was paid to antiferromagnetic resonance as it was believed that this would yield additional information. In general the static resonance behavior, e.g. the dependence of the resonance fields on frequency and temperature, could be rather well explained by sophisticated molecular field theories such as introduced by Ubbink (36), Nagamiya (37) and Yosida (38). Later experiments showed the occurrence of some unexplained new resonance lines which are probably related to the degree of collinearity of the electron spins in the antiferromagnetic state.
Specific heat measurements by Friedberg (39) showed a sharp λ-like maximum at a transition temperature which within experimental error was the same as that found from resonance experiments. The entropy change in passing from the totally ordered to the totally disordered state was found to be in good agreement with an effective spin value $S = \frac{1}{2}$, the same value also derived from susceptibility measurements by Van den Handel et al. (40). As about one third of the total entropy change occurred above T_N it was clear that a considerable degree of short range order existed above the transition. This relatively large short range order was confirmed by the susceptibility measurements by Van der Marel (41) et al. who found a broad maximum in the uniform susceptibility above the Néel point.

Of the investigations on the dynamical behavior of the magnetic system are worth mentioning the relaxation experiments in antiferromagnetic resonance by Yamazaki and Date (42), the parallel pumping experiments by Yamazaki (26) and the EPR

linewidth measurements in the critical region by Zimmermann et al. (43), experiments to which we shall direct our attention later.

In spite of all these experiments still relatively little is known about the real dynamical behavior of the electron spin system.
As $CuCl_2.2H_2O$ might be an important test case to the dynamical theories at both high and low temperatures, we performed relaxation and resonance experiments in the paramagnetic, critical and antiferromagnetic state.

4.2 *Crystal structure*

The crystal structure of $CuCl_2.2H_2O$ is well known and found to be orthorhombic with spacegroup P_{bmn}. The lattice parameters are a = 7.38, b = 8.04 and c = 3.72 Å. There are two copper ions in the chemical unit cell at positions (0,0,0) and $(\frac{1}{2},\frac{1}{2},0)$. Each copper ion is surrounded by four chlorine ions and two water molecules together forming an octahedron. The copper ions are subject to an orthorhombic crystalline field which has different orientations for the corner and base-center ions. The principle axes of the field coincide with the body diagonals of the surrounding octahedron. One of the principal axes is parallel to the b-axis while the other two are rotated about the b-axis away from the a and c axes respectively by an angle of -38^o for the corner ions and $+38^o$ for the base-center ions. The crystal structure is shown in Fig. 7.

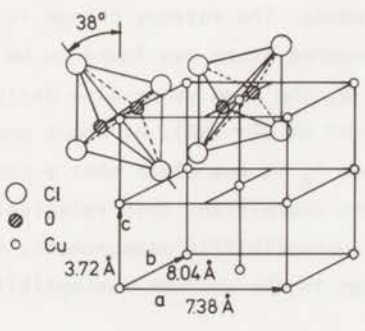

Fig. 7 *The crystal structure of* $CuCl_2.2H_2O$

The single crystals used in our experiments were grown from a solution of $CuCl_2.2H_2O$ in water to which some alcohol was added (43a). Single crystals of up to two grams were obtained in this way. Determination of the crystal axes is very simple by observing the crystal angles while the exhibition of pleochroism (blue-green) allows one to check on the orientation found. The direction of maximum growth is the c-axis. For the experiments we used several single crystals of different shape and weight while special attention was paid to assure the absence of macroscopic imperfections such as cracks and inclusions.

4.3 *Magnetic interactions in $CuCl_2.2H_2O$*

As most magnetic interactions can be at least qualitatively determined by studying the static spin structure near or in the antiferromagnetic state, we will discuss the antiferromagnetic spin configuration and the magnetic interactions together.

By examining their nuclear magnetic resonance data, Poulis and Hardeman (34) found that below T = 4.33 K $CuCl_2.2H_2O$ behaved as an orthorhombic antiferromagnet with the a-axis as the first easy direction. To explain their data they proposed a spin configuration, shown in Fig. 8, where the electron spins within an a-b plane were parallel to each other but antiparallel to the spins in adjacent a-b planes. This configuration, which was the most simple but not the only possible , was later confirmed by the neutron diffraction experiments of Shirane et al. (44).

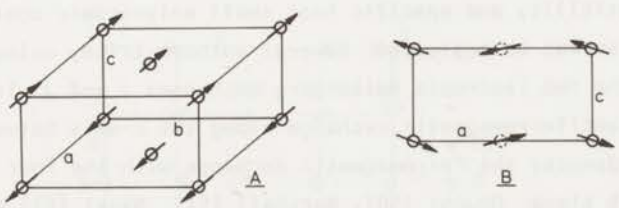

Fig. 8 *A antiferromagnetic spin structure introduced by Poulis and Hardeman (34).*
B spin canting in the a-c plane due to antisymmetric exchange

The most simple interaction model which leads to such a spin structure includes an antiferromagnetic Heisenberg interaction along the c-axis between nearest neighbors and a ferromagnetic Heisenberg interaction between next-nearest neighbors in the a-b plane. Calculations by Van Dalen (45) of the overlap of orbitals using the MO-LCAO approach proved this model to be realistic from a theoretical point of view. While these isotropic Heisenberg interactions determine the relative orientation of the spins, it is the anisotropic part of the total interaction which determines the favoring of a certain direction as the easy-axis.

Moriya and Yosida (46) showed that dipolar interaction alone could not explain the experimentally determined orthorhombic anisotropy constants. Further calculation in which also anisotropic symmetric exchange was included in the way suggested by Van Vleck (47)(48) did not significantly improve the results.

One of the previous authors, Moriya (5), suggested in 1960 $CuCl_2.2H_2O$ as an example in which antisymmetric exchange interaction could occur. One of the important features of this interaction is that, if allowed by crystal symmetry, it cants the electron spins in the antiferromagnetic state. In $CuCl_2.2H_2O$ this canting should be in the a-c plane, see Fig. 8. Application of eqs. (2.6), (2.8) and (2.9) to $CuCl_2.2H_2O$ shows that only a small part of the antisymmetric exchange contributes to the spin canting, so this canting will be small (about 1^o) and difficult to detect experimentally. The neutron diffraction experiments by Umebayashi (49) on $CuCl_2.2D_2O$ revealed some canting but no exclusive proof could be given that antisymmetric exchange was at the origin.

We will now give a more detailed discussion of the magnetic interactions in $CuCl_2.2H_2O$. We assume that the effective Hamiltonian of the isolated spin system is given by eqs. (2.2)-(2.4). For a description of static phenomena such as uniform susceptibility and specific heat small anisotropic contributions to the spin Hamiltonian can be neglected. Several authors tried, using different methods, to determine the two isotropic Heisenberg exchanges J and J' in $CuCl_2.2H_2O$. J denotes the antiferromagnetic exchange along the c-axis between nearest neighbors while J' denotes the ferromagnetic exchange with the four next-nearest neighbors in the a-b plane. Oguchi (50), Marshall (51), Nagai (52) and Hewson et al. (53) started from both the observed broad maximum in the uniform susceptibility just above the Néel temperature and the value for the Néel temperature itself while Friedberg (39) and Clay and Stavely (54) evaluated the magnetic contribution to the specific heat. Van Dalen (45) gave a theoretical calculation of the exchange constants while De Jongh (55) estimated the constants from the saturation field below the Néel temperature.

There is not much agreement between the various results. The value for J/k_B varies from 3.5 to 11 K while the ratio J'/J varies from 0.05 to 0.5. For further calculation we selected the J-value of Clay and Stavely (54) as we believe that magnetic specific heat calculations are more reliable than molecular field approximations and theoretical calculations of the orbital overlap. Of the values for the ratio J'/J the value 0.131 found by Hewson et al. (53) seems to be the most reliable. Using this value for the ratio, one finds

$$J = -5.45\ 10^{-16}\ \text{erg}, \qquad J' = 0.71\ 10^{-16}\ \text{erg} \tag{4.1}$$

It should be stressed that a different choice for the exchange parameters does not qualitatively alter the conclusions to be made in the discussion of the relaxation and resonance process in $CuCl_2.2H_2O$.

As we study dynamical phenomena even relatively small anisotropic exchange contributions can be extremely important. In our spin Hamiltonian we include both anisotropic symmetric exchange and antisymmetric exchange. Van Vleck (47) suggested a way to calculate the anisotropic symmetric exchange which is of a pseudo-dipolar form. The calculation is difficult and crude assumptions have to be made to get a numerical result. Ryabchenko and Shul'man (56) tried to determine a symmetric anisotropy from the moments of the EPR lines in $CuCl_2.2H_2O$. They found two sets of values which were in bad agreement with each other. As was shown by Buluggiu (57) the usual method of determining the moments is sometimes inaccurate and may lead to remarkable errors.
The antisymmetric exchange Hamiltonian is given by the second part of eq. (2.4). We shall evaluate the symmetry restrictions on the axial vector $\vec{D}_{ij}$.
The symmetry elements of $CuCl_2.2H_2O$ are given in Fig. 9.

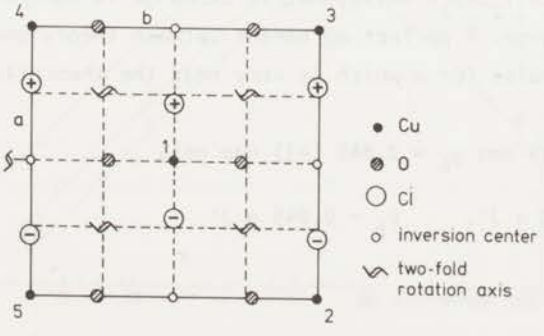

Fig. 9 *The symmetry elements of $CuCl_2.2H_2O$. The figures which denote the copper ions are used in the text.*

There are inversion centers halfway all crystal axes. The inversion center halfway the c-axis eliminates an antisymmetric component in J while the two-fold rotation axis halfway the corner and base-center ions restricts the antisymmetric component of J' to the a-b plane. After applying all symmetry elements one gets

nearest neighbors i and j along the c-axis

$$\vec{D}_{ij} = 0$$

next-nearest neighbors i and j in the a-b plane

$$D_{aij} \neq 0$$

$$D_{bij} \neq 0$$

$$D_{cij} = 0$$

$$D_{a12} = D_{a14} = - D_{a13} = - D_{a15}$$

$$D_{b12} = D_{b13} = D_{b14} = D_{b15}$$

The meaning of the numerical indices 1-5 are given in Fig. 9.
D_{a12} and D_{b12} will be denoted from now on as D_a and D_b. The exact calculation of the numerical values for D_a and D_b is extremely difficult. No experimental values are known. Joenk (58) estimated D_b after comparing the theoretical expressions for both the g-tensor and the D-vector and found after several quantitative approximations

$$D_b \simeq (g_b - 2)J' \qquad (4.2)$$

The result (4.2) is consistent with eq. (2.9). Comparing (4.2) with (2.9) one finds the numerical constant α to be equal to about 1.

In the discussion of the relaxation times and resonance linewidths it will be shown that in $CuCl_2.2H_2O$ antisymmetric exchange is dominant over anisotropic symmetric exchange. A perfect agreement between theory and experiment will be found using a value for α which is very near the theoretical estimate of $\alpha = 1$.

Using $g_a = 2.189$ and $g_b = 2.045$ (43) one gets

$$D_a = 0.189\ \alpha\ J', \qquad D_b = 0.045\ \alpha\ J' \qquad (4.3)$$

CHAPTER 5

RELAXATION AND RESONANCE EXPERIMENTS ON $CuCl_2.2H_2O$

5.1 *Paramagnetic relaxation at high temperatures*

In this part of chapter 5 we present and discuss our experimental high-temperature relaxation data on $CuCl_2.2H_2O$. For these relaxation data we measured the rf absorption while the static and rf field were oriented mutually parallel. This in contrast with the resonance experiments where static and rf field are perpendicular to each other. The relaxation experiments were performed in the temperature region from T = 2 K up to 77 K. At all temperatures we found the relaxation process to be very well described by a single relaxation time. As these relaxation times are temperature independent from about 6 K upwards, we suppose this region to coincide with the so-called high-temperature region. When studying relaxation or resonance processes in this temperature region appropriate simplifications of the dynamical theory can be made.
At hydrogen temperatures the experiments were performed on two single crystals of different shape and weight (0.1 and 0.5 gram). We could not detect any difference in χ''/χ_o, at the same temperature and static field, outside the experimental error of a few percent. In Fig. 10 the frequency dependence of the normalized zero-field absorption χ''/χ_o is plotted. The Lorentzian forms with maxima of 0.5 indicate a process which is governed by a single relaxation time.

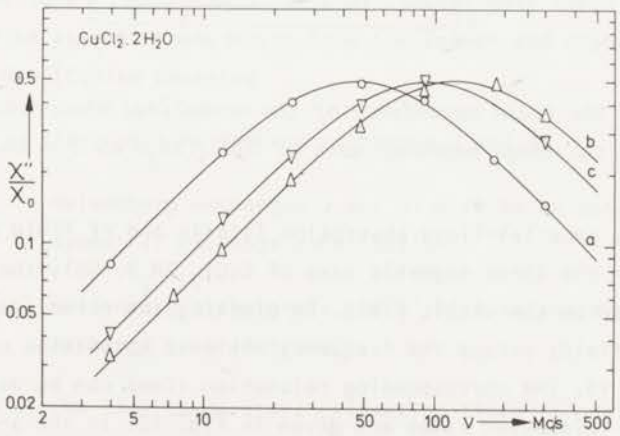

Fig. 10 *The frequency dependence of the normalized, zero-field absorption in the three magnetic axes of* $CuCl_2.2H_2O$ *at T = 20.4 K.*

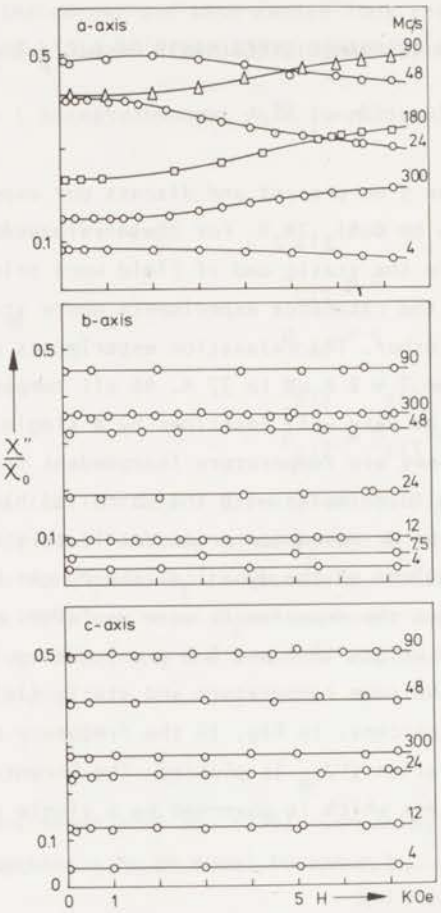

Fig. 11 *The field dependence of the normalized absorption in the three magnetic axes of* $CuCl_2.2H_2O$ *at* $T = 20.4$ *K.*

In Fig. 11 the parallel-field absorption (static and rf field mutually parallel) is plotted for the three magnetic axes of $CuCl_2.2H_2O$. Only the a-axis shows some dependence on the static field. By plotting the normalized absorption, at a given static field, versus the frequency one gets Lorentzian curves such as given in Fig. 10. The corresponding relaxation times can be determined by using $\tau = \omega_{top}^{-1}$. The relaxation times are given in Fig. 12. In the a-axis the relaxation process is weakly speeding up with increasing static field while in the b and c axes the process is field independent up to 8 kOe.

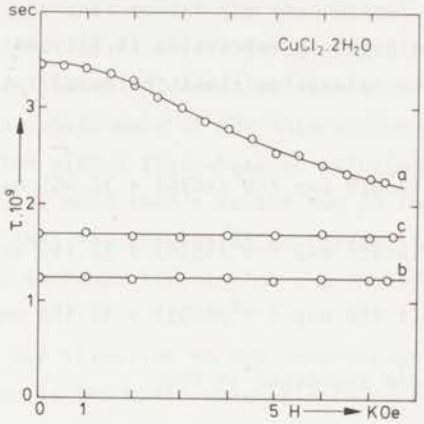

Fig. 12 *The field dependence of the relaxation time in the three magnetic axes of* $CuCl_2.2H_2O$ *at* $T = 20.4$ *K.*

5.1.1 *Discussion*

In this discussion we shall, by comparing the experimental high-temperature results with theoretical calculations, try to extract information about the magnetic interactions in $CuCl_2.2H_2O$. We shall investigate three interaction models. It will be assumed that, apart from the Zeeman and dipolar contribution, the spin Hamiltonian contains

model 1 — isotropic Heisenberg exchanges J and J'.

model 2 — Heisenberg exchanges J and J' with an anisotropic symmetric exchange contribution.

model 3 — Heisenberg exchanges J and J' with an antisymmetric exchange contribution.

The calculation of the high-temperature relaxation times is outlined in chapter 2.3. For this calculation we will make the usual assumption that the memory spectrum is a sum of Gaussian-like lines centered at $\omega = 0$ at zero static field. It will be shown in the discussion of the field effect in the a-axis that this

Gaussian shape assumption is realistic in the b and c axes while in the a-axis some finestructure has to be expected which gives us an explanation of the weak field dependence.

Using the exchange values given in expression (4.1), one finds after a laboreous calculation that the relaxation times for model 1 are given by (see eqs. (2.23) and (2.24))

$$\tau_a^{-1} = (1 + H^2/2295)(2.928 \exp(-H^2/4876) + 32.455 \exp(-H^2/1775))10^7 \text{ sec}^{-1}$$

$$\tau_b^{-1} = (1 + H^2/2295)(2.951 \exp(-H^2/4938) + 32.140 \exp(-H^2/1766))10^7 \text{ sec}^{-1}$$

$$\tau_c^{-1} = (1 + H^2/2295)(1.158 \exp(-H^2/6893) + 12.183 \exp(-H^2/982))10^7 \text{ sec}^{-1}$$

where H is the static field expressed in kOe.

The field dependences are negligibly small in the field region of up to 8 kOe. Omitting the small field dependence, one gets for the low-field relaxation times

$$\tau_a = 2.83\ 10^{-9} \text{ sec}, \qquad \tau_b = 2.85\ 10^{-9} \text{ sec}, \qquad \tau_c = 7.50\ 10^{-9} \text{ sec}$$

which should be compared with the experimental values of

$$\bar{\tau}_a = 2.6\ 10^{-9} \text{ sec}, \qquad \tau_b = 1.23\ 10^{-9} \text{ sec}, \qquad \tau_c = 1.69\ 10^{-9} \text{ sec}$$

One notes a rather large discrepancy between the theoretical and experimental values. It should be stressed now that another choice for the isotropic Heisenberg exchanges (see chapter 4.3) does not significantly reduce this discrepancy as a change in the isotropic exchange only shifts all relaxation times with the same factor. It can further be shown that a different value for the ratio J'/J does not significantly reduce the discrepancy either. This leads us to the conclusion that the results of an interaction model which contains only dipolar and isotropic exchange interactions are in disagreement with experiment in $CuCl_2.2H_2O$.

We will now start a calculation of the relaxation times using the interaction model 2 which contains anisotropic symmetric exchange. The influence of anisotropic symmetric exchange on the relaxation process can be calculated by using eqs. (2.37), (2.42) and (2.43). As the ratio J'/J is rather small one may rule out the possibility of an important contribution to the relaxation process from a symmetric anisotropy in the next-nearest neighbor exchange J'.

A symmetric anisotropy in the nearest neighbor exchange J yields two adjustable parameters as the third is determined by eq. (2.37). The two adjustable parameters can be derived from the experimental values for the relaxation times in two different directions. At that moment the theoretical result for the relaxation time in the third direction is fixed. So by comparing the theoretical value for the relaxation time in the third direction with the experimental value, one gets information about the consistency of the interaction model 2.
A laboreous calculation yields that whatever adjustment one makes there always remains a discrepancy of more than a factor two in the third direction.
So our conclusion is that the results of an interaction model which contains anisotropic symmetric exchange interaction are in disagreement with experiment.

We will finally turn our attention to the interaction model 3 of which the antisymmetric exchange is the most remarkable feature. The influence of the antisymmetric exchange can be calculated by using eqs. (2.9), (2.40) and (2.41). There is only one adjustable parameter α which, as we saw in chapter 4.3, is theoretically expected to be nearly equal to unity.
Using the values for J and J' given by (4.1) and the D-values given by (4.3), one finds a perfect agreement with experiment for the value $\alpha = 0.90$.
One has theoretically for the low-field relaxation times (the field dependences being negligibly small in our field region).

$$\tau_a = 2.65\ 10^{-9}\ \text{sec}, \qquad \tau_b = 1.25\ 10^{-9}\ \text{sec}, \qquad \tau_c = 1.66\ 10^{-9}\ \text{sec}$$

These should be compared with the experimental values.

$$\bar{\tau}_a = 2.6\ 10^{-9}\ \text{sec}, \qquad \tau_b = 1.23\ 10^{-9}\ \text{sec}, \qquad \tau_c = 1.69\ 10^{-9}\ \text{sec}$$

The experimental value $\alpha = 0.90$ is very near the theoretical estimate $\alpha \simeq 1.0$ by Joenk (58). In the light of this very good agreement between theory and experiment we conclude that antisymmetric exchange and dipolar interaction are the most dominant sources of anisotropy in $CuCl_2.2H_2O$.
Strong additional proof will be found in the dynamical critical behavior of $CuCl_2.2H_2O$. Further, in the next section it will be shown that the weak field dependence in the c-axis is consistent with the occurence of antisymmetric exchange in $CuCl_2.2H_2O$.

5.1.2 *Discussion of the field dependence in the a-axis*

Because of the large secular interaction in $CuCl_2.2H_2O$ the field dependence of the relaxation process in fields up to 8 kOe should be negligibly small as long as the Gaussian shape assumption for the memory spectrum holds. The weak field dependence indicates that in the a-axis this assumption is not justified in detail. Using the important weak-coupling and high-temperature feature that the four lines of the memory spectrum shift rigidly with the static field, it can be shown that the field effect in the a-axis implies, whatever the partition of the effect over the four lines, a negative undershoot in the memory function $G_a(t)$. As an illustration we calculated, using eqs. (1.22) and (2.24), the memory functions from our experimental relaxation times assuming the field effect to occur in the first Larmor lines ($k = \pm 1$ in eq. (2.13)) of the a-axis. Further it has been assumed that the four lines of the memory spectrum are Gaussian for large ω. This last assumption is in agreement with the theoretical notion that all wavevector dependent two-spin correlation functions are Gaussian for short times (9). The memory functions are plotted in Fig. 13.

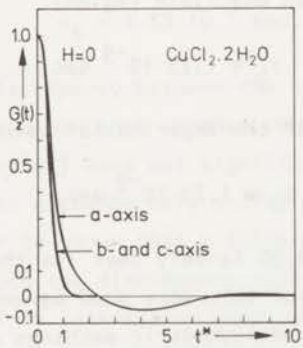

Fig. 13 *The experimentally determined memory functions $G_z(t)$ in the three magnetic axes at zero static field. The memory functions are normalized by the value at $t = 0$. The reduced time t^* is defined by $t^* = \frac{J}{\hbar} t$.*

To explain the negative undershoot in the memory function in the a-axis we will take a close look at the full expression (see eqs. (2.44) and (2.55)) for the memory function. $G_z(t)$ is a linear combination of four-spin correlation functions. Using a dynamical Random Phase Approximation and a transformation to the wavevector space we found eq. (2.55) which is a linear combination of wavevector dependent two-spin correlation functions. When all two-spin correlation functions are isotropic, $G_z(t)$ is semi-definite positive. So the negative undershoot in the a-axis necessarily indicates an inaccuracy in the Random Phase Approximation or an anisotropy in the two-spin correlation functions or both. As RPA and isotropy of the correlation functions are frequently used in theories on the dynamical properties of weakly anisotropic magnetic systems, this is an important experimental result.

Assuming the RPA to be sufficiently accurate one may wonder why the anisotropy of the two-spin correlation functions only manifests itself in the a-axis. The explanation can be found in the different sampling over the Brillouin zone. Restricting ourselves to the antisymmetric contribution to the q-dependent weight coefficients in eq. (2.55), we have

$$|D_a(q)|^2 = 16\, D_a^2 \sin^2 \tfrac{1}{2} q_a a \sin^2 \tfrac{1}{2} q_b b \qquad (5.1)$$

$$|D_b(q)|^2 = 16\, D_b^2 \cos^2 \tfrac{1}{2} q_a a \cos^2 \tfrac{1}{2} q_b b \qquad (5.2)$$

Using eqs. (2.55), (5.1) and (5.2) and the fact that $D_a^2 >> D_b^2$ (see eq. (4.3)) one easily calculates that in the b and c axes most contributions to the memory function come from intermediate q-values. In the a-axis however most contributions to the memory function come from low q-values ($\vec{q} \approx 0$) and high q-values (border of the Brillouin zone).
So the occurrence of the field effect in only the a-axis is consistent with an anisotropy in the two-spin correlation functions at low or high q-values. It should be noted that by the relaxation experiments described in this thesis, one measures directly $(S^{\alpha}_{-q}, S^{\alpha}_{q}(t))_{q=0}$ which is proportional to the relaxation function $\Phi_{\alpha\alpha}(t,H)$.

Our measurements indicate that these relaxation functions are slightly anisotropic but certainly not negative at relatively small times. So the field effect in the a-axis most probably indicates an anisotropy in the two-spin correlation functions at high q-values.
The fact that the Gaussian assumption for the memory functions in the b and c axes worked so well is not amazing as theoretical calculations by Blume and Hubbard (9) on the isotropic simple cubic lattice have shown that the two-spin correlation functions at intermediate q-values are Gaussian-like (see also section 2.3.1).

Recapitulating one has two possibilities:

If the two-spin correlation functions are isotropic at all $\vec{q}$ then our experiments give evidence that in $CuCl_2.2H_2O$ the RPA erroneously eliminates important contributions which lead to negative values of the memory functions (four-spin correlation functions) at relatively short times.

If the RPA is sufficiently accurate then our experiments give evidence for important anisotropy in the two-spin correlation functions, even at high temperatures. This anisotropy is attached to the correlation functions at low q-values ($\vec{q} \approx 0$) and/or high q-values (border of the Brillouin zone), of which the anisotropy at low q-values is less probable.

5.2 *Paramagnetic resonance at high temperatures in $CuCl_2.2H_2O$*

Recently Tjon and Verbeek (59) derived a general expression for the field dependence of the paramagnetic resonance absorption. They started from a low-field expansion in the Laplace transform of the memory function and found that, at low frequencies and small static fields, even in the exchange narrowed case the paramagnetic resonance lines were not exactly Lorentzian. The Lorentzian form is approached at increasing frequencies. To check on these theoretical results we performed some resonance experiments at hydrogen temperatures in the three magnetic axes of $CuCl_2.2H_2O$. Assuming that the relaxation processes in the three magnetic axes can be described by single relaxation times, Verbeek derived for the resonance absorption

$$\frac{\chi_\alpha''(\omega,H)}{\chi_{o\alpha}} = \frac{\frac{1}{\omega\tau_\alpha} + \eta_\beta^2 \frac{\tau_\gamma}{\omega(1+\omega^2\tau_\gamma^2)}}{[\eta_\beta^2 \frac{\tau_\gamma^2}{1+\omega^2\tau_\gamma^2} - 1]^2 + [\frac{1}{\omega\tau_\alpha} + \eta_\beta^2 \frac{\tau_\gamma}{\omega(1+\omega^2\tau_\gamma^2)}]^2} \qquad (5.3)$$

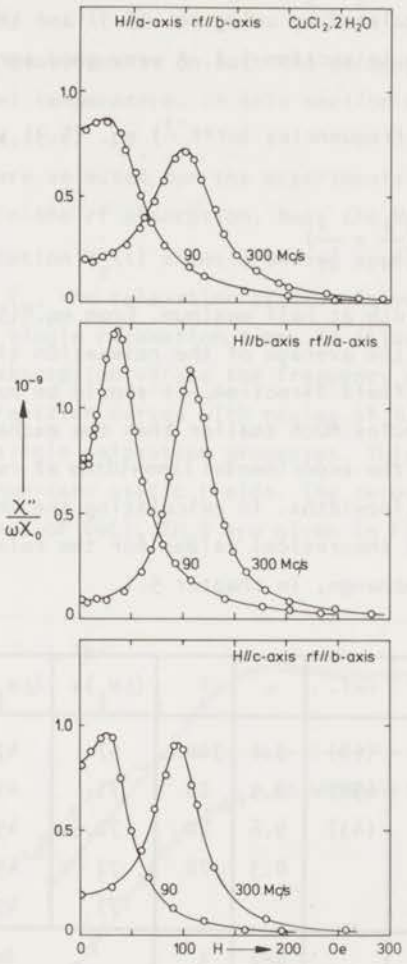

Fig. 14 *The paramagnetic resonance absorption in the three magnetic axes of $CuCl_2.2H_2O$ at T = 20.4 K. The solid lines are the theoretical curves calculated by using eq. (5.3) and our experimental zero-field relaxation times.*

$$\eta_\beta = g_\beta \mu_B \hbar^{-1} H \qquad (5.4)$$

where α, β and γ denote the three magnetic axes. The index α denotes the direction of the rf field, β the direction of the static field and γ the third direction perpendicular to α and β. τ is the zero-field relaxation time.

In Fig. 14 the resonance absorptions at different frequencies are given for the three magnetic axes of $CuCl_2.2H_2O$. The fully drawn lines correspond to the absorption values calculated by using eq. (5.3) and the experimental zero-field relaxation times given in section 5.1. A very good agreement between theory and experiment is found.

For sufficiently high frequencies ($\omega >> \tau_\gamma^{-1}$) eq. (5.3) takes a Lorentzian form with

$$(\Delta H_{\frac{1}{2}})_\beta = \frac{\hbar}{g_\beta \mu_B} \left(\frac{1}{\tau_\alpha} + \frac{1}{\tau_\gamma}\right) \qquad (5.5)$$

$\Delta H_{\frac{1}{2}}$ is the full linewidth at half maximum. From eq. (5.5) it is clear that the linewidth is given by the average of the relaxation times in the plane perpendicular to the static field direction. It should be noted that eq. (5.5) is only valid for frequencies much smaller than the exchange frequency.

In table 2 we compare the experimental linewidths at relatively high frequencies with the theoretical linewidths. In calculating the theoretical linewidths we used eq. (5.5) and the theoretical values for the relaxation times derived, using antisymmetric exchange, in chapter 5.1.

table 2

	ref.	ν	T	$(\Delta H_{\frac{1}{2}})_a$	$(\Delta H_{\frac{1}{2}})_b$	$(\Delta H_{\frac{1}{2}})_c$
Itoh	(60)	3.1	300	57	47	54
Ryabchenko	(56)	9.3	20	71	49	60
Zimmerman	(43)	9.6	20	72.5	49	62
Our exp.		0.3	20	72	49	56
theory				73	49	57
		GHz	K	Oe		

Once again the agreement is good.

5.3 *Relaxation in the critical region of $CuCl_2.2H_2O$*

We performed relaxation measurements on both the paramagnetic and the antiferromagnetic side of the Néel temperature. In this section we will restrict ourselves to the paramagnetic side.

Three single crystals were selected for the experiments. We could not detect any non-linear effects in the rf absorption. Near the Néel temperature the relaxation of the magnetization $M_z(t)$ shows a strong speeding-up. At all temperatures, even very near T_N, the relaxation process is very well described by a temperature dependent single relaxation time. To illustrate this we plot in Fig. 16 the zero-field absorption versus the frequency at different temperatures near the Néel point. Lorentzian curves with maxima of 0.5 χ_o are found which are characteristic for single relaxation processes. This single relaxation character is preserved at non-zero static fields. The zero-field relaxation times in the three magnetic axes of $CuCl_2.2H_2O$ are given in Fig. 15.

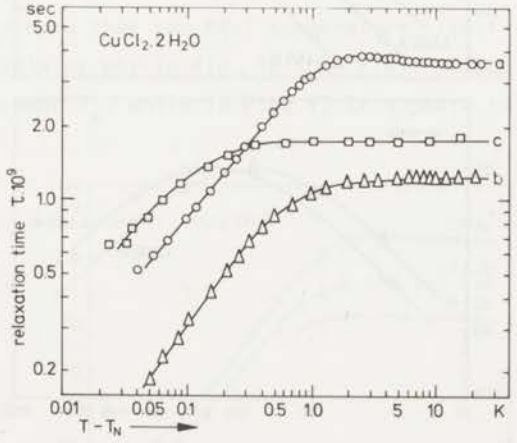

Fig. 15 *The temperature dependence of the zero-field relaxation time in the three magnetic axes of $CuCl_2.2H_2O$.*

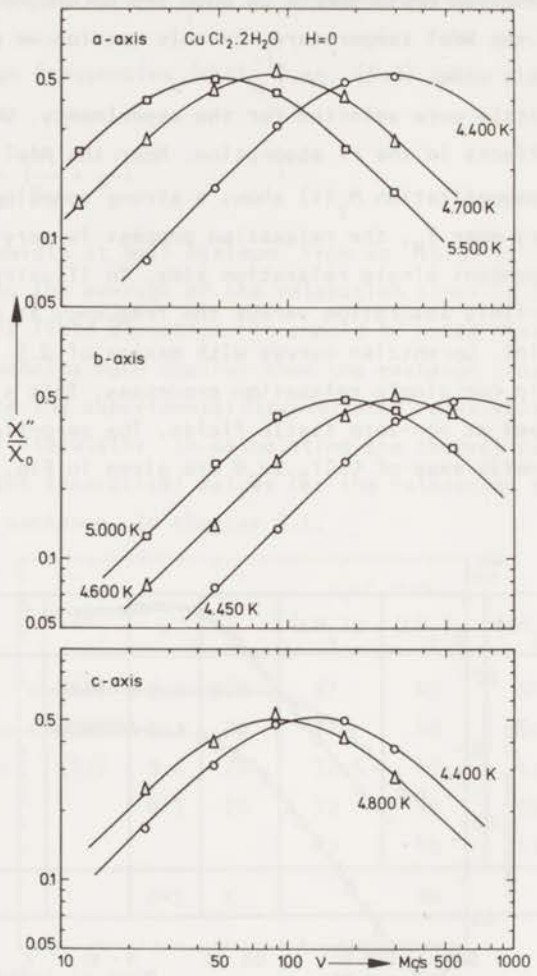

Fig. 16 *The frequency dependence of the zero-field absorption at different temperatures near the Néel point in the three magnetic axes of* $CuCl_2.2H_2O$.

The relaxation process remains independent of the static field in the b and c axes. The field dependence in the a-axis (see Figs. 11 and 12) appears to decrease at approaching the transition temperature, but has not vanished completely at as near as 0.05 K from T_N.
The field dependence of the relaxation time in the a-axis is given in Figs.17 and 18.

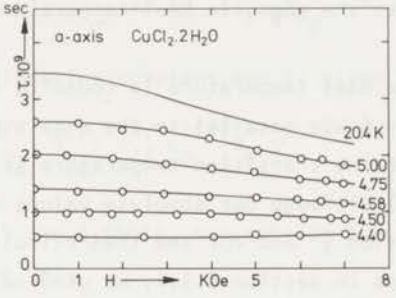

Fig. 17 *The field dependence of the relaxation time in the a-axis at different temperatures.*

It should be noted here that the Néel temperature itself is slightly field dependent which explains why in Fig. 18 some field effect is persisting at temperatures very near T_N, while in Fig. 17 it appears to vanish altogether.

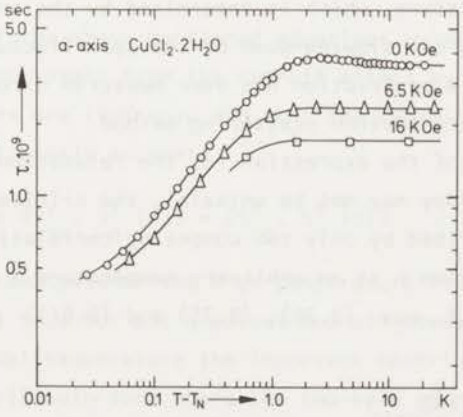

Fig. 18 *The temperature dependence of the relaxation time in the a-axis at different static fields parallel to the a-axis. The 16 kOe measurements are from Van Noort (61).*

The Néel temperature itself is easily observed with the calorimetric method. As the heat capacity of $CuCl_2.2H_2O$ decreases drastically just above the Néel temperature, the temperature increase of the calorimetric system, due to a certain constant heat input, will change sharply at the transition temperature. It is clear that the Néel temperature determined in that way is the transition temperature of the heat capacity. Within experimental error this temperature is found to coincide with the magnetic Néel temperature as determined from our measurements.

At zero static field the Néel temperature is found to be $T_N(0) = 4.35^6$ K while at a static field of H = 6 kOe parallel to the a-axis we found $T_N(6) = 4.34^2$ K. This field dependence of the transition temperature is the same as found by Poulis and Hardeman (62) although our absolute values are somewhat higher.

To normalize the absorption χ'' and for the theoretical calculation of the critical relaxation times in section 5.3.1, we used values for χ_o interpolated between the results of Van der Marel et al. (41) at He temperatures and those of Van den Handel et al. (40) at hydrogen temperatures.

5.3.1 *Discussion*

In section 2.4 we derived an expression for the relaxation time of the average total magnetization $M_z(t)$ in the critical region. The general idea is that below a certain temperature, which is determined by the anisotropy of the magnetic system, the critical slowing-down of the spin fluctuations is restricted to the easy-axis. Such a restriction has been measured directly by Schulhof et al. (16) in MnF_2 using the neutron scattering method.

In the derivation of the expression for the relaxation time we assumed that, although the anisotropy may not be uniaxial, the critical slowing-down is still satisfactorily described by only two competing correlation lengths $\kappa_{//}$ and $\kappa_{\perp}$. For the relaxation time τ at an arbitrary temperature T above the Néel temperature we derived (cf. eqs. (2.70), (2.75) and (2.81))

$$\frac{1}{\tau(T)} = \frac{1}{\tau(\infty)} + \left(\Delta\frac{1}{\tau}\right)_{crit.} \qquad (5.6)$$

with

$$\left(\Delta\frac{1}{\tau}\right)_{crit.} = A\,\frac{TN}{\chi_o}\,\epsilon^{-\frac{5}{2}\nu}\,\{|U_{xx}(q_o) - U_{yy}(q_o)|^2\,F_{xy} + 2|U_{xy}(q_o)|^2(F_{xx}+F_{yy})$$

$$+\{|U_{xz}(q_o)|^2 + \frac{4}{g^4\mu_B^4}|D_y(q_o)|^2\}F_{yz}$$

$$+\{|U_{yz}(q_o)|^2 + \frac{4}{g^4\mu_B^4}|D_x(q_o)|^2\}F_{xz}\} \qquad (5.7)$$

The factor A is a calibration constant and is given by

$$A = \frac{g^6\mu_B^6 k_B}{2\pi^2\hbar^2 N^2}\,(S^{//}_{-q_o}, S^{//}_{q_o})^2\kappa_{//}^4\,\kappa_o^{-5/2}B_o^{-1}V \qquad (5.8)$$

For the meaning of all the symbols, see section 2.4. In $CuCl_2.2H_2O$ the a-axis is the easy-axis so we get,

$$\begin{aligned} F_{aa} &= F_{// //} \\ F_{ab} = F_{ac} = F_{ca} = F_{ba} &= F_{//\perp} \\ F_{bb} = F_{cc} = F_{bc} = F_{cb} &= F_{\perp\perp} \end{aligned} \qquad (5.9)$$

These F - functions are given by eq. (2.74) of section 2.4. We will use the values calculated in chapter 2.4 and given in Fig. 1 of that chapter.

In the derivation of the above-mentioned equations we assumed that in the hydrodynamical region, apart from the cut-off effect by κ_Δ, the two-spin correlation functions are isotropic and that the dynamical Random Phase Approximation is sufficiently accurate,

$$(S^x_{-q}, S^x_q(t)) = (S^y_{-q}, S^y_q(t)) = (S^z_{-q}, S^z_q(t)) \qquad \text{for } \kappa_{//} >> \kappa_\Delta \qquad (5.10)$$

As we know from our analysis of the high-temperature field effect in the a-axis, this is probably not true for all q-values and all times t. One can only hope now that near the Néel temperature the important contributions to the q-sum come from parts of the Brillouin zone where the two-spin correlation functions are sufficiently isotropic or where the anisotropy is not significantly temperature dependent. In the neighborhood of T_N the most important contributions to the q-sum come from the $\vec{q}_0$ region where $\vec{q}_0$ is the wavevector for the staggered state. For $CuCl_2.2H_2O$ this vector is easily determined as (see section 2.4)

$$\vec{q}_0 = \pm\ (0,0,\pi/c) \tag{5.11}$$

In table 3 the calculation values for the q-dependent U and D coefficients of $CuCl_2.2H_2O$ are given for $\vec{q} = \vec{q}_0$.

table 3

axis	$U_{xx} - U_{yy}$	U_{xy}	U_{xz}	U_{yz}	D_x	D_y
a	132.8 E 21	0	0	0	$4D_b$	0
b	133.6 E 21	0	0	0	0	0
c	0.821 E 21	0	0	0	$4D_b$	0

The values for the coefficients are given in c.g.s. units and per ion.
The dipolar sums are extremely slowly converging and special care has to be taken to exclude important errors. The summation was directly performed over about 50.000 ions while the remainder was calculated by transforming the sum into an integral. Using eq. (5.7) and the D_b-value given by (4.3), one gets

$$(\Delta\frac{1}{\tau})_{crit.a} = A\,\frac{TN}{\chi_o}\,\epsilon^{-\frac{5}{2}\nu}\,(17630\ F_{\perp\perp} + 3340\ F_{//\perp})10^{42} \tag{5.12}$$

$$(\Delta\frac{1}{\tau})_{crit.b} = A\,\frac{TN}{\chi_o}\,\epsilon^{-\frac{5}{2}\nu}\,(17840\ F_{//\perp})10^{42} \tag{5.13}$$

$$(\Delta\frac{1}{\tau})_{crit.c} = A\,\frac{TN}{\chi_o}\,\epsilon^{-\frac{5}{2}\nu}\,(0.674\ F_{//\perp} + 3340\ F_{\perp\perp})10^{42} \tag{5.14}$$

From eq. (5.14) it is clear that in the c-axis the critical effect is nearly completely determined by the $F_{\perp\perp}$ term which is originating from antisymmetric exchange. The coefficient of the $F_{//\perp}$ term is so small that if there were no antisymmetric exchange the c-axis would not show any relevant critical behavior. So the experimental critical behavior in the c-axis is a direct and independent support for the occurrence of antisymmetric exchange in $CuCl_2.2H_2O$.
To get the values for the F-functions we transform the temperature into $\kappa_\Delta/\kappa_{//}$.
In section 2.4 we estimated (cf. eq. (2.80))

$$\frac{\kappa_\Delta}{\kappa_{//}} \simeq \left(\frac{H_{A1} + H_{A2}}{H_E}\right)^{\nu} \epsilon^{-\nu} \tag{5.15}$$

where H_E is the exchange field and H_{A1} and H_{A2} the orthorhombic anisotropy fields in the molecular field model. For the exchange field one has

$$g\mu_B H_E = 2zJS \tag{5.16}$$

Using for J the value derived from the heat capacity measurements of Clay and Staveley (54) (see eq. (4.1)), one finds H_E = 54.6 KOe. From antiferromagnetic resonance it is known that in $CuCl_2.2H_2O$ $H_{A1} \simeq 3H_{A2}$ while the spin-flop field at T = 0 is found to be H_{SF} = 6500 Oe. Using now that for small anisotropy one has

$$H_{SF}^2 = 2H_{A1}H_E \tag{5.17}$$

one gets, using the above-mentioned value for H_E,

$$H_{A1} = 387 \text{ Oe}, \qquad H_{A2} = 1160 \text{ Oe}, \qquad H_E = 54.6 \text{ KOe}. \tag{5.18}$$

Substituting these values in eq. (5.15) one gets

$$\frac{\kappa_\Delta}{\kappa_{//}} = (0.0283)^{\nu} \epsilon^{-\nu} \tag{5.19}$$

where ν is the critical exponent of the correlation length parallel to the easy-axis. Besides the restriction of the critical slowing-down to the easy-axis below a certain temperature, the magnetic anisotropy also changes the critical point exponents such as ν. In section 2.4.1 we showed however that this change is expected to be rather small. For the theoretical calculations on weakly anisotropic $CuCl_2.2H_2O$ we will use the average value

$$\nu = 0.67 \tag{5.20}$$

This value for ν is about 6 percent differing from the isotropic Heisenberg value. It should be stressed here that our final results for $CuCl_2.2H_2O$ are not very sensitive to a small variation in ν. It will turn out that the cut-off effect in the critical slowing-down is much more drastically influencing the critical relaxation process than the small change of a few percent in ν. Using the above-mentioned value for ν one gets

$$\frac{\kappa_\Delta}{\kappa_{//}} = 0.092 \ \epsilon^{-0.67} \tag{5.21}$$

The only problem left now is to find the value for A, given by eq. (5.8). We will infer it from experiment. Using the relaxation time in the b-axis at ϵ = 0.025 we find

$$A = 5.72\ 10^{-65} \quad \text{c.g.s.u.} \tag{5.22}$$

This adaption is a loss of generality. As however A is only a calibration factor, the temperature dependences and the relative differences between the three axes still allow a thorough confrontation with the theory. Using the values for F given in Fig. 1 and the theoretical relaxation times at high temperatures, we are able to calculate the temperature dependent relaxation times in the three different axes. In the a-axis however some complication arises. At high temperatures we found the relaxation time to be weakly field dependent which implied a small negative undershoot in the memory function $G_a(t)$. When calculating the zero-field relaxation times at lower temperatures one has to count with this effect. As the field dependence is persisting at low temperatures we tentatively suppose now that although the surface under $G_a(t)$ is strongly temperature dependent, the shape itself will be much less so. This may seem a rough approximation but it is justified by the experimental fact (see Fig. 18) that the temperature dependence of the relaxation time is much stronger than the temperature dependence of the relative field effect. Under the above-mentioned assumption one finds the real zero-field relaxation times in the a-axis by multiplying the theoretical zero-field relaxation times by a temperature independent factor. This factor is determined by the relative importance of the negative undershoot in the memory function $G_a(t)$. From our high-temperature measurements in the a-axis we find this factor to be equal to 1.34.
In Fig. 19 the theoretical values for the zero-field relaxation times are plotted together with the experimental results.

In spite of the simplifications in the theory a very good agreement between theory and experiment is found.
Using eq. (2.24a) and the theoretical values for the relaxation times one can also calculate the theoretical values for the full linewidth of the critical EPR line.
Our theoretical results and the experimental results of Zimmerman et al. (43) are plotted together in Fig. 20. Once again a good agreement is found between experiment and theory.

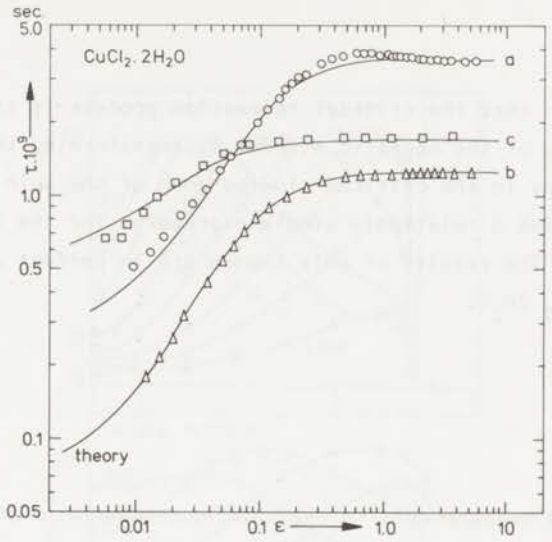

Fig. 19 *Comparison of the theoretical with the experimentally determined zero-field relaxation times in the three magnetic axes of* $CuCl_2.2H_2O$.

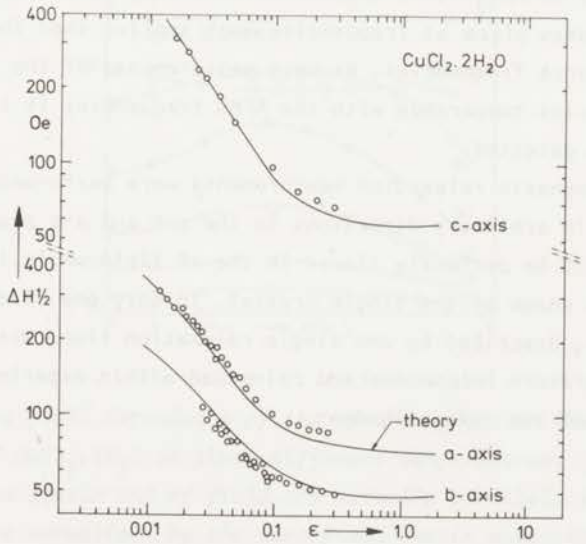

Fig. 20 *Comparison of the theoretical EPR linewidths with the experimental results of Zimmerman et al. (43).*

Conclusion

It has been shown that the critical relaxation process is strongly influenced by the anisotropy of the magnetic system. By transforming the magnetic anisotropy into an anisotropy in the critical slowing-down of the spin fluctuations, we were able to derive a relatively simple expression for the relaxation times in the critical region. The results of this theory are in perfect agreement with experiment in $CuCl_2.2H_2O$.

5.4 *Relaxation measurements in the antiferromagnetic state of* $CuCl_2.2H_2O$

Experimentally it has been found by many authors that if one orients both static and rf field parallel to the easy-axis of an antiferromagnet no absorption will be detected. From our measurements on two copper compounds and those of Verbeek (19) on MnF_2 it is however evident that in the easy-axis a relaxation process takes place at frequencies much smaller than the usual antiferromagnetic resonance frequencies. As most measurements of the past were performed at frequencies comparable with the AFMR frequencies it is clear why no absorption was detected.

Our antiferromagnetic relaxation measurements were performed on several crystals of $CuCl_2.2H_2O$ in arbitrary directions in the a-b and a-c plane. The absorption showed itself to be perfectly linear in the rf field while it was further independent of the shape of the single crystal. In only one direction a pure relaxation character, described by one single relaxation time, was found. This direction was temperature independentand coincided within experimental error with the direction of the spin alignment.

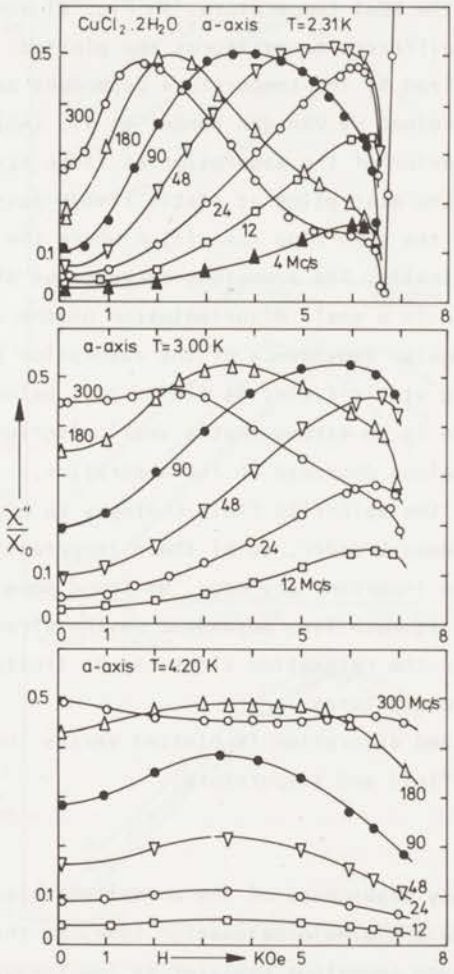

Fig. 21 *The field dependence of the rf absorption in the easy-axis of $CuCl_2.2H_2O$ at three different temperatures. The static and rf field are mutually parallel. The absorptions are normalized by the zero-field static susceptibilities at the corresponding temperatures.*

5.4.1 *Field and frequency dependence of the absorption in the easy-axis*

The rf absorption in the easy-axis of $CuCl_2.2H_2O$ was found to be strongly field dependent below the Néel temperature. In Fig. 21 some of our absorption measurements at three different temperatures are plotted. At all fields the absorptions are normalized by the temperature dependent zero-field static susceptibility as determined by Van den Handel et al. (40). At low temperatures an anomalous behavior of the absorption at large static fields is found. The large increase of the absorption at static fields just below 7 kOe ($T = 2.31$ K) is due to the spin-flop transition where the static susceptibility is increasing drastically. The anomalous decrease at slightly lower fields has probably its origin in a small misorientation of the single crystal. As we will see below, the angular dependence of the absorption sharpens around the easy-axis at increasing static field. At fields just below the spin-flop field this angular dependence is so strong that a small misorientation of less than 0.5° explains the anomalous decrease in the absorption.
At higher temperatures the spin-flop field chainges to higher fields while the angular dependence becomes broader, so at these temperatures the small misorientation will not be important any more. We found some indication that the relaxation time itself is much less dependent on the direction than the absorption, so our values for the relaxation times can be trusted in fields up to about 6.3 kOe at low temperatures.
In Fig. 22 the normalized absorption is plotted versus the frequency at several values for the static field and temperature.

The Lorentzian frequency dependence of the normalized absorption indicates a relaxation process with one single relaxation time. At the lowest temperature the absorption shows some anomalous behavior at low frequencies. This effect, which appears to be field independent, may be due to a second relaxation process at lower frequencies while further the possibility of non-magnetic absorption should not be excluded. If one assumes the anomalous behavior to originate from a low-frequency relaxation process the matched relaxation time would be in the order of $\tau \simeq 10^{-8}$ sec at $T = 2.31$ K.
The field dependence of the relaxation time in the a-axis at different temperatures is given in Fig. 23.

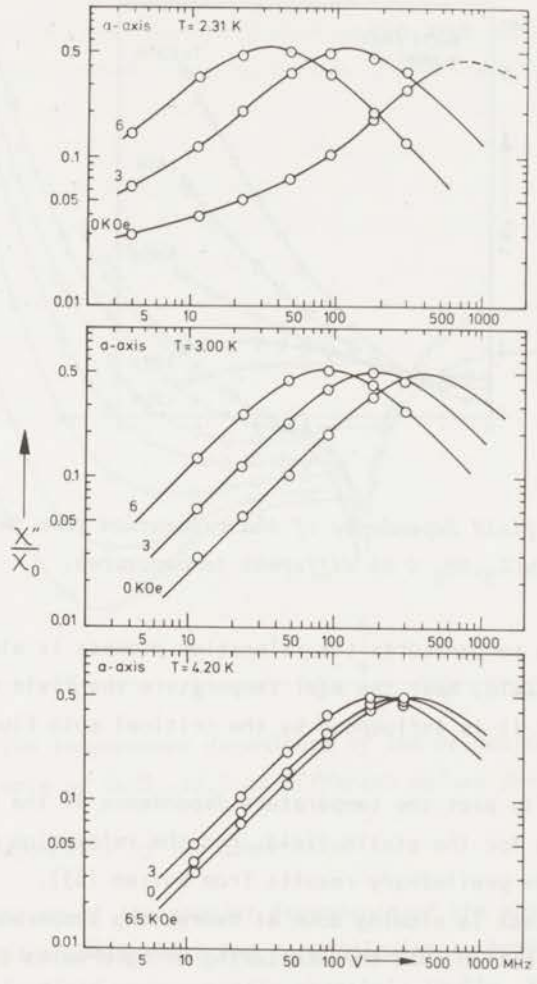

Fig. 22 *The frequency dependence of the normalized absorption in the easy-axis of* $CuCl_2.2H_2O$ *at different values for the static field and temperature.*

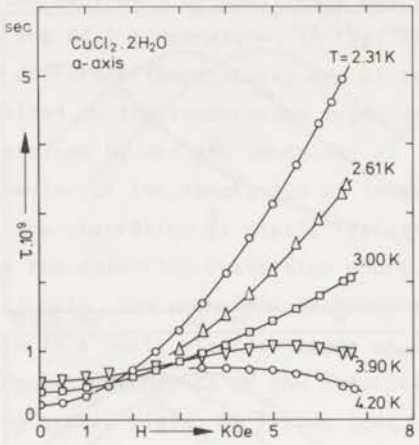

Fig. 23 *The field dependence of the relaxation time in the easy-axis of* $CuCl_2.2H_2O$ *at different temperatures.*

At sufficiently low temperatures the relaxation process is slowing down at increasing static field. Near the Néel temperature the field dependence becomes more complicated as it is influenced by the critical spin fluctuations.

In Fig. 24 we finally plot the temperature dependence of the relaxation time at different values for the static field. For the relaxation times below T = 2 K we used some preliminary results from Rutten (63).
The relaxation process is slowing down at decreasing temperature which is in agreement with the notion that the scattering of spin-waves by thermally excited spin fluctuations decreases at lowering the temperature. Near the Néel temperature a critical speeding up of the relaxation process is seen to occur while the temperature region in which the relaxation process behaves critically, appears to be field dependent.

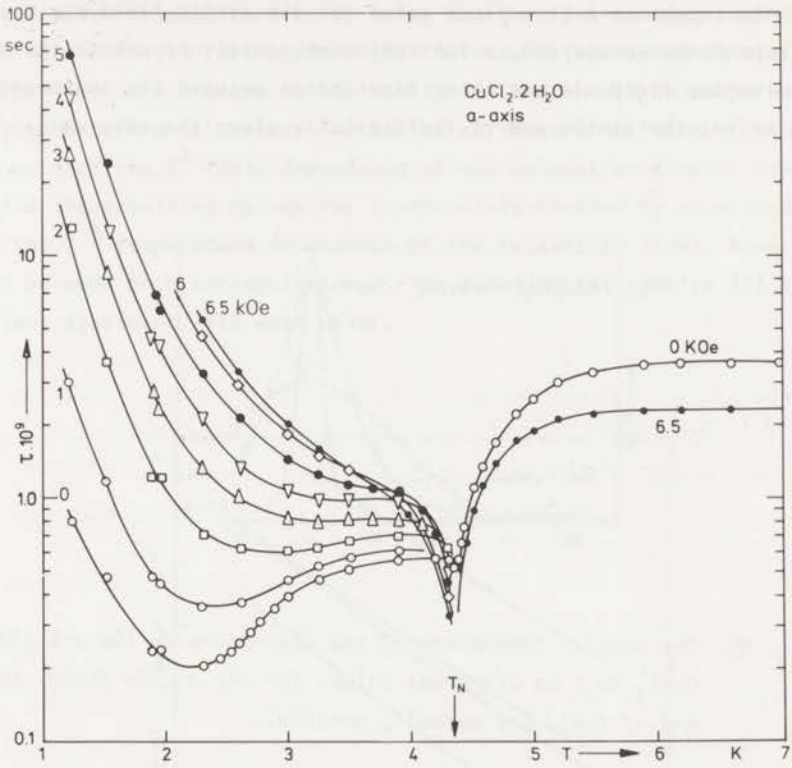

Fig. 24 *The temperature dependence of the relaxation time in the easy-axis of $CuCl_2.2H_2O$ at different values for the static field.*

5.4.2 *Angular dependence of the absorption*

For an investigation of the angular dependence of the absorption the crystal was rotated about an axis which was perpendicular to both rf and static field. The rf and static field were mutually parallel. In Fig. 25 the angular dependence of the absorption in the a-b plane at T = 3.50 K is given.
As the static field increases the angular dependence sharpens around the a-axis. Because of this effect, relaxation measurements at or near the spin-flop field should be regarded with some reserve as a small misorientation completely changes the absorption pattern at those fields. The same sharp angular dependence in $CuCl_2.2H_2O$ has been found by Van Noort (64). The small absorption in the b-axis is the low-frequency tail of an antiferromagnetic resonance line.

The absorption shows, as expected, a tensorial character at zero field. Lowering the temperature at a fixed value for the static field one observes the angular dependence to sharpen, a fact which may partly be due to the decrease of the spin-flop field. In our later experiments we used the sharp angular dependence to orient the static and rf field exactly along the easy-axis.

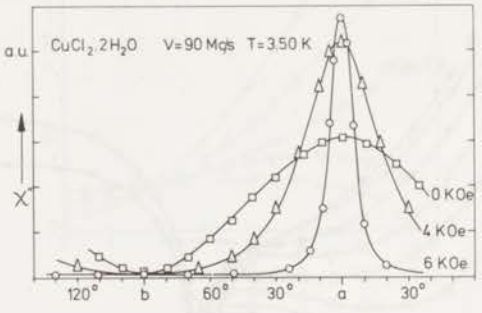

Fig. 25 *The angular dependence of the absorption in the a-b plane of* $CuCl_2.2H_2O$ *at different values for the static field. The static and rf field are mutually parallel.*

5.4.3 *Discussion*

Comparison with other experimental work

Yamazaki and Date (42) observed in $CuCl_2.2H_2O$ the decay of the easy-axis magnetization induced by the low-line antiferromagnetic resonance. In the temperature region from T = 1.4 to 2 K two characteristic times were found, one in the order of 10^{-8} sec and the other of about 10^{-4} sec, the latter being attributed to the lattice-bath energy transfer. These relaxation times were observed at the slightly temperature dependent low-line resonance field of about 5 kOe. The short-time results are plotted as (1) in Fig. 26 and should be compared with the solid line (2) which represents the smoothed values of our relaxation times at the same static field. Although the temperature dependences look similar one still notes an important difference between the two experimental results. An interesting point is that the difference is very near a factor of 2π.

One of the previous authors, Yamazaki (26), determined more recently the k-dependent spin-wave relaxation time by using the parallel pumping technique described in section 2.5.3. His uniform (k = 0) results, measured at static fields of about 6200 Oe, are plotted as (3) in Fig. 26 and should be compared with our extrapolated experimental values (4) at the corresponding field. (For the extrapolation we used the H^2 field dependence of the relaxation time at lower temperatures while the resulting values for τ were cross-checked by an extrapolation based on the T^{-3} temperature dependence of the relaxation times. Good agreement was found between both extrapolations). The experimental results (3) and (4) are in excellent agreement with each other.

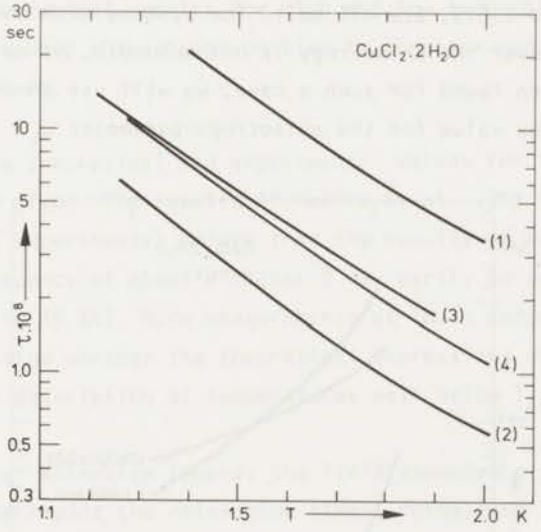

Fig. 26 *Comparison of our experimental low-temperature relaxation times in the easy-axis of $CuCl_2.2H_2O$ with other experimental results.*
(1) The experimental results of ref. (42) at H = 5 kOe
(2) Our results at H = 5 kOe
(3) The experimental results of ref. (26) at H = 6.2 kOe
(4) Our extrapolated experimental results for H = 6.2 kOe
The drawn lines are the smoothed values for the relaxation times.

Naiman and Lawrence (65) determined a characteristic time at the spin-flop field in $CuCl_2.2H_2O$. This relaxation time was found to be temperature independent from 2.3 to 2.5 K with a value of $\tau = 0.7\ 10^{-7}$ sec (H = 7365 Oe). We cannot compare this value with one of ours as we did not perform measurements at the spin-flop field. As was remarked before, these kind of experiments should be regarded with some reserve in view of the enormous anisotropy in the absorption near the spin-flop field. Their value is about 20 times larger than our relaxation time at H = 6 kOe and T = 2.4 K.

Comparison with theory

The theoretical expressions for the k = 0 zero-field relaxation rates, given in table 1 of section 2.5.5, are all valid for systems with uniaxial anisotropy. In $CuCl_2.2H_2O$ however the anisotropy is orthorhombic. As no theoretical expressions have yet been found for such a case, we will use those of table 1 while taking some average value for the anisotropy parameter ω_A.

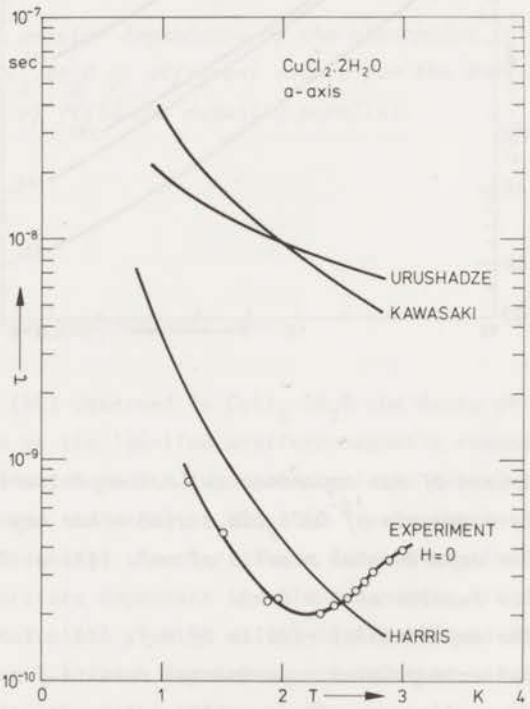

Fig. 27 *Comparison of the theoretical results for the k = 0 spin-wave decay times with our experimental zero-field relaxation times in the easy-axis of* $CuCl_2.2H_2O$.

For $CuCl_2.2H_2O$ one has, see section 5.3.1.,

$$H_{A1} = 387 \text{ Oe}, \qquad H_{A2} = 1160 \text{ Oe}, \qquad H_E = 54.6 \text{ kOe} \tag{5.23}$$

Using the average value

$$H_A = (H_{A1} + H_{A2})/2 = 774 \text{ Oe} \tag{5.24}$$

one gets

$$T_{AE} = g\mu_B k_B^{-1} (2H_A H_E)^{\frac{1}{2}} = 1.35 \text{ K}. \tag{5.25}$$

The theoretical expressions given in table 1 are either valid for $T \ll T_{AE} \ll T_N$ or for $T_{AE} \ll T \ll T_N$. For a theoretical estimate in the region $T \simeq T_{AE}$ we interpolated between the theoretical results for high and low temperatures. For this interpolation we assumed the relaxation time to increase monotonically with decreasing temperature.

In Fig. 27 both the theoretical and experimental values for the zero-field relaxation times are given. The results of Harris et al. (31) are in much better agreement with our experimental values than the results of any of the other authors. The discrepancy of about a factor 2 may partly be due to the approximation made by using (5.24). More measurements at lower temperatures should be necessary to determine whether the theoretical expressions of Harris et al. also give a better description at temperatures well below T_{AE}.

We will now turn our attention towards the field dependence of the relaxation time. In Fig. 28 we replot the relaxation times, normalized by the corresponding zero-field values, versus the square of the static field.
Outside the critical region the field dependence of the relaxation time is very well described by

$$\tau(T,H) = \tau(T,0) + f(T)\, H^2 \tag{5.26}$$

where $f(T)$ is some temperature dependent factor. As all theoretical investigations are restricted to infinitely small static fields, no explanation for this field effect can be given at this moment. At low temperatures $f(T) \propto T^{-3}$.

The temperature dependence of the relaxation time in the critical region is given in Fig. 29. The temperature region where the antiferromagnetic relaxation process shows a critical speeding up becomes larger at increasing static field

along the easy-axis, an effect which does not occur above T_N. The origin of this effect may be found in a field dependent enhancement of the longitudinal cross section of the fluctuations in the staggered magnetization.

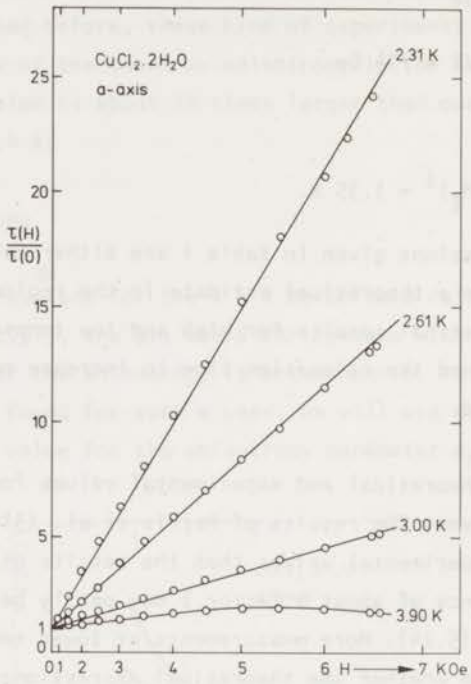

Fig. 28 *The relaxation times in the easy-axis of $CuCl_2.2H_2O$ plotted versus the square of the static field.*

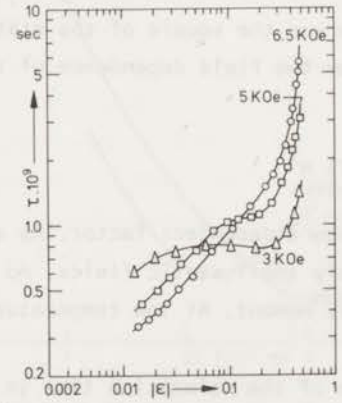

Fig. 29 *The temperature dependence of the relaxation time in the easy-axis of $CuCl_2.2H_2O$ near the Néel point.*

CHAPTER 6

THE DYNAMICAL MAGNETIC BEHAVIOR OF $LiCuCl_3.2H_2O$

6.1 *Introduction*

The static magnetic behavior of $LiCuCl_3.2H_2O$ is less well known than that of $CuCl_2.2H_2O$. The experimental results reported by different authors differ both in fact and in interpretation. The main problem centers on the fact whether the effective spin value is equal to unity or to $\frac{1}{2}$. As the copper ions are distributed as pairs in the chemical unit cell one expects in first instance $S = 1$. It depends however on the interpair interaction whether the magnetic behavior can be described by an effective spin value of 1 or $\frac{1}{2}$.

The heat capacity of $LiCuCl_3.2H_2O$ in the temperature range $T = 2 - 9$ K has been measured by Forstat and McNeely (66). A λ-like anomaly was found at a transition temperature $T_N = 4.40$ K. The magnetic entropy change associated with the transition agreed within 2% with the theoretical value for the $S = \frac{1}{2}$ case. In contrast to this result, heat capacity measurements by Clay and Stavely (54) showed the magnetic entropy change to be very close to the theoretical value for the spin $S = 1$ case.

Vossos et al. (67) reported a preliminary X-ray and susceptibility study on $LiCuCl_3.2H_2O$. The static susceptibility was measured in a temperature range of 2-290 K and was found to be in agreement with a ground state triplet which implies $S = 1$. An extensive neutron diffraction and susceptibility study by Abrahams and Williams (68) showed however that the neutron scattering amplitudes and the susceptibility results were well fitted by an effective spin value of $\frac{1}{2}$.

Although the case is not completely settled, it is our opinion that more credit should be given to the $S = \frac{1}{2}$ case. When $S = 1$ one expects, due to the singlet at higher energy levels, a significant temperature and field dependence of the relaxation time or resonance linewidth at sufficiently high temperatures. Furthermore a complicated angular dependence of the relaxation or resonance absorption can be expected. None of these have been found experimentally. Date and Nagata (69) and Zimmerman et al. (70) found the EPR linewidth to be independent of the temperature from $T = 15$ K up to 300 K. No anomalous angular dependence of the resonance absorption has been found.

Furthermore our relaxation experiments reveal neither field nor temperature dependence of the relaxation time outside the critical region. All this is compatible with S = 1 if one assumes an interaction strength of more than 100 K in the Cu^{2+} pair. This large value for J/k_B is however unrealistic for a Cu-Cl-Cu bond (4.61 Å) which is expected to be the exchange path within the pair. So the most probable value for S equals $\frac{1}{2}$.

6.2 *Crystal structure*

The crystal structure of $LiCuCl_3.2H_2O$ is monoclinic with lattice parameters a = 6.078, b = 11.145, c = 9.145 Å and $\beta = 108^{o}50'$. There are four Cu ions in the chemical unit cell. These Cu ions are distributed as pairs, the centers of the pairs being at positions (0,0,0) and $(0,\frac{1}{2},\frac{1}{2})$. The internuclear dimeric Cu-Cu line lies in good approximation in the a-c plane at $35^{o}30'$ from c and $144^{o}18'$ from a. In Fig. 30 an over-all view of $LiCuCl_3.2H_2O$ along the a-axis is given.

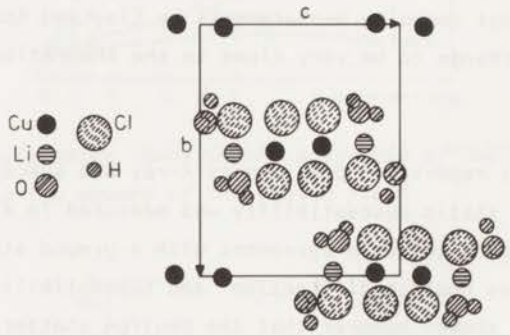

Fig. 30 *Over-all view of $LiCuCl_3.2H_2O$ structure along the a-axis.*

There are stacks of $CuCl_6Li_2O_2$ dimers along the a-axis. The space group of the crystal structure is found to be $P2_1/c$.

The orienting of the single crystal from crystal angles alone is difficult as different combinations of crystal planes lead to nearly the same intersection angles.

This might be the reason why there is so much confusion about the direction of the antiferromagnetic spin alignment. We determined the crystal axes by measuring the intersection angles as accurately as possible while the orientation found was magnetically checked on the g-values given by other authors.

The very deliquescent nature made it necessary to submerse the single crystals in paraffin to avoid surface contamination.

6.3 *Magnetic interactions in $LiCuCu_3.2H_2O$*

The magnetic Hamiltonian of $LiCuCl_3.2H_2O$ is in good approximation given by

$$\mathcal{H} = \mathcal{H}_z + \mathcal{H}_{dd} + \mathcal{H}_{ex} \tag{6.1}$$

$\mathcal{H}_z$ is the Zeeman, $\mathcal{H}_{dd}$ the dipolar and $\mathcal{H}_{ex}$ the exchange part of the spin Hamiltonian. For the exchange Hamiltonian we will assume that, besides an isotropic Heisenberg part, only antisymmetric exchange is important.

$$\mathcal{H}_{ex} = - \sum_{i \neq j} J_{ij} (\vec{S}_i . \vec{S}_j) + \vec{D}_{ij} . (\vec{S}_i \times \vec{S}_j) \tag{6.2}$$

Clay and Stavely (54) determined the magnetic contribution to the heat capacity of $LiCuCl_3.2H_2O$. Using their data, one finds

$$\sum_j (J_{ij}/k_B)^2 = 35.7 \text{ K}^2 \tag{6.3}$$

Metselaar (71) investigated the static antiferromagnetic behavior of $LiCuCl_3.2H_2O$. Several first and second order phase transitions were found of which some could be ascribed to the occurrence of antisymmetric exchange in this compound. The introduction of antisymmetric exchange was partially based on some of our preliminary calculations on the spin-spin relaxation process in $LiCuCl_3.2H_2O$. Metselaar investigated extensively the exchange model which could lead to the supposed antiferromagnetic spin structure. Four different isotropic exchange parameters J_1 - J_4 were introduced. The distribution of these exchange interactions over the chemical unit cell is given in Fig. 31.

Metselaar estimated the exchange parameters from the values for the transition fields and the Néel temperature. It was found that

$$J_1/k_B = 22 \text{ K}, \quad J_2/k_B = -22 \text{ K}, \quad J_3/k_B = -16 \text{ K}, \quad J_4/k_B = 11 \text{ K} \tag{6.4}$$

It is interesting to compare these exchange values with the results from the heat capacity measurements. Using the exchange values of (6.4) one finds

$$\sum_j (J_{ij}/k_B)^2 = 1722\ K^2 \qquad (6.5)$$

Comparing (6.3) with (6.5) one notes a very large difference between both experimental results. In first instance we shall use the exchange model of Metselaar while, when necessary, we shall discuss the consequences of smaller exchange parameters.

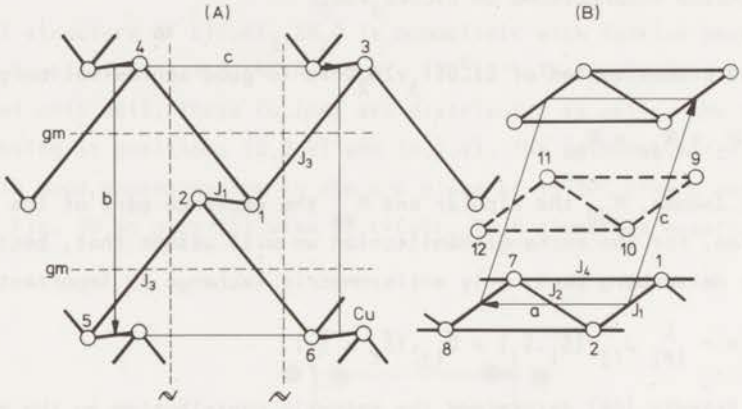

Fig. 31 *The distribution of the exchange interactions, introduced by Metselaar (71), over the chemical unit cell of* $LiCuCl_3.2H_2O$
(A) view along the a-axis, (B) view along the b-axis
gm: glide mirror plane, ~ *: two-fold rotation axis.*

In his further investigations, Metselaar found in $LiCuCl_3.2H_2O$ the flop state-paramagnetic state transition to be rather broad. From this and the occurrence of some additional transitions at lower fields, he concluded that antisymmetric exchange was an important contribution to the spin Hamiltonian in $LiCuCl_3.2H_2O$. It was estimated that $|D/J|$ was in the order of 0.1 which is a very realistic value for such an interaction. At the same time Metselaar performed his experiments on the static properties of $LiCuCl_3.2H_2O$, we started our investigation on the dynamical phenomena. It was known from the measurements of Zimmerman et al. (70) that the EPR linewidths were anomalously broad, a fact which could indicate a large contribution from anisotropic interactions. Some preliminary calculations we performed, showed that antisymmetric exchange interaction was

probably at the origin. A detailed discussion of this interaction in $LiCuCl_3.2H_2O$ will be given in the discussion of the high-temperature relaxation times.

6.4 *Relaxation at high temperatures in $LiCuCl_3.2H_2O$*

We started the experiments at high temperatures by determining the principal magnetic axes. This is possible by measuring the angular dependence of the rf absorption at zero static field. The zero-field rf absorption χ'' has a tensorial angular dependence with as principal axes, by definition, the magnetic axes. In Fig. 32 the absorption in the a-c plane is given.

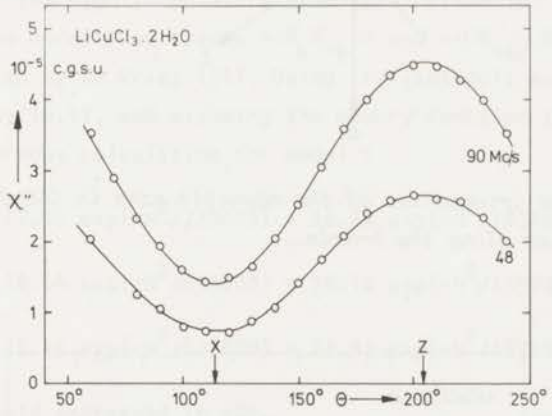

Fig. 32 *The angular dependence of the zero-field rf absorption in the a-c plane of $LiCuCl_3.2H_2O$ at T = 20.4 K. X and Z denote the two magnetic axes in the a-c plane.*

The three magnetic axes will, conformable to the notation of other authors, be denoted as X, Y and Z. The X and Z axes lie in the a-c plane while the Y-axis coincides with the crystallographic b-axis. Furthermore the X-axis was found to coincide, within experimental error, with the internuclear Cu-Cu line of the "pairs" centered around positions (0,0,0) and $(0,\frac{1}{2},\frac{1}{2})$. The orientation of the magnetic axes, visualized in Fig. 33, is in agreement with the results of Zimmerman et al. (70), who determined the magnetic axes from their g-value measurements.

The high-temperature rf absorption in the three magnetic axes of $LiCuCl_3.2H_2O$ was found to be independent of the static field in fields up to 8 kOe. The frequency dependence was found to be perfectly Lorentzian with maxima of 0.5 χ_o which indicates a relaxation process with a single characteristic time. For the normalization of the absorption we used the susceptibility measurements of Abrahams and Williams (68) corrected for the anisotropy in the g-value.

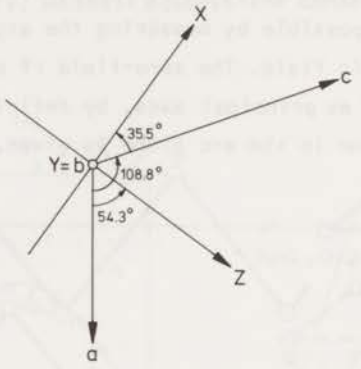

Fig. 33 *The orientation of the magnetic axes in* $LiCuCl_3.2H_2O$. *View along the b-axis.*

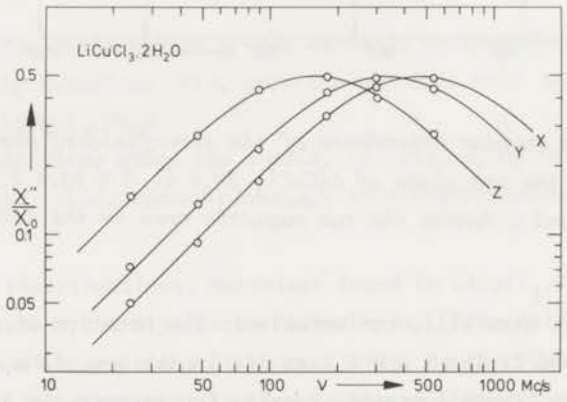

Fig. 34 *The frequency dependence of the zero-field absorption in the three magnetic axes of* $LiCuCl_3.2H_2O$ *at* $T = 20.4$ *K.*

6.4.1 *Discussion*

In analogy to the approach to $CuCl_2.2H_2O$, we will compare the theoretical results of different interaction models with the experimental high-temperature relaxation times. We restrict ourselves to two interaction models.

model 1 The spin Hamiltonian contains only dipolar and isotropic Heisenberg exchange interactions.

model 2 The spin Hamiltonian contains dipolar, isotropic Heisenberg exchange and antisymmetric exchange interactions.

The calculation of the high-temperature spin-spin relaxation times is outlined in section 2.3. The normalized traces $\langle\langle \mathcal{H}_k \mathcal{H}_{-k} \rangle\rangle$ and $\langle\langle [\mathcal{H}_{sec}, \mathcal{H}_k][\mathcal{H}_{-k}, \mathcal{H}_{sec}] \rangle\rangle$ have been calculated by De Vries (72). Using the isotropic exchange values of Metselaar, given by (6.4), and assuming the memory function to be Gaussian, one finds after a laboreous calculation for model 1

$$\tau_X^{-1} = (1+H^2/125000)(2.02 \exp(-H^2/720000) + 10.39 \exp(-H^2/185000))10^6 \text{ sec}$$

$$\tau_Y^{-1} = (1+H^2/125000)(0.64 \exp(-H^2/653000) + 35.10 \exp(-H^2/159000))10^6 \text{ sec}$$

$$\tau_Z^{-1} = (1+H^2/125000)(2.15 \exp(-H^2/800000) + 22.91 \exp(-H^2/182000))10^6 \text{ sec}$$

H is the static field expressed in kOe.

Omitting the negligibly small field dependence at fields up to 8 kOe, one gets for the low-field relaxation times

$$\tau_X = 8.06\ 10^{-8} \text{ sec}, \quad \tau_Y = 2.80\ 10^{-8} \text{ sec}, \quad \tau_Z = 3.99\ 10^{-8} \text{ sec}$$

These theoretical relaxation times should be compared with the experimental values

$$\tau_X = 3.32\ 10^{-10} \text{ sec}, \quad \tau_Y = 4.68\ 10^{-10} \text{ sec}, \quad \tau_Z = 9.95\ 10^{-10} \text{ sec}$$

One notes a very large discrepancy between the experimental and theoretical results. At first sight, there are several possibilities to explain this large difference. First, the exchange values of (6.4) may be too large. Secondly, the Gaussian assumption for the memory spectrum may be wrong. And finally, the spin Hamiltonian may contain another interaction part which, when included in

the Hamiltonian, is speeding up the relaxation process.
The first possibility can be ruled out immediately as an adaption of the exchange values to the experimental relaxation times would lead to unrealistically small exchange parameters. These small exchange values would give rise to a significant field dependence of the relaxation times at small static fields, a fact which is in contradiction to experiment. Moreover, the relative differences of the relaxation times in the three magnetic axes would not be explained in that way.
The second possibility of a non-Gaussian memory spectrum is somewhat more difficult to rule out. As however in the magnetically high-dimensional $LiCuCl_3.2H_2O$ the contributions to the memory functions come from all parts of the Brillouin zone, large deviations from the Gaussian shape are not to be expected.
This leaves us with the third possibility. It will be shown now that the introduction of antisymmetric exchange (model 2) leads to a perfect agreement between theory and experiment.

The inversion centers halfway the Cu ions which are coupled by J_1 and J_2, eliminate antisymmetric components in J_1 and J_2. Using further the two-fold rotation axes, the glide-mirror planes and translational invariance (see Fig. 31), one finally gets

$$\vec{D}_{13} = \vec{D}_{25},\ \vec{D}_{14} = \vec{D}_{26},\ \vec{D}_{17} = \vec{D}_{82},\ \vec{D}_{9\,11} = \vec{D}_{12\,10}$$

$$D_{X13} = D_{X14},\ D_{Y13} = -D_{Y14},\ D_{Z13} = D_{Z14} \qquad (6.6)$$

$$D_{X17} = -D_{X9\,11},\ D_{Y17} = D_{Y9\,11},\ D_{Z17} = -D_{Z9\,11}$$

The indices are taken from Fig. 31 of section 6.3. The indices X, Y and Z denote the three magnetic axes (see Fig. 33).

Both J_3 and J_4 can have an antisymmetric component. Using eq. (2.8) one finds that only the antisymmetric contribution in J_3 leads to a canting of the electron spins in the antiferromagnetic state. We will assume now that the antisymmetric contribution to J_3 is dominant over the contribution in J_4. The justification of this assumption will be given below. Using eqs. (2.9), (2.23), (2.24), (2.40) and (2.41) and the g-values of Zimmerman et al. (70)

$$g_X = 2.050,\ g_Y = 2.136,\ g_Z = 2.224 \qquad (6.7)$$

one calculates, for $\alpha = 0.211$

$$\tau_X = 3.40\ 10^{-10}\ \text{sec},\quad \tau_Y = 4.67\ 10^{-10}\ \text{sec},\quad \tau_Z = 9.65\ 10^{-10}\ \text{sec}$$

These theoretical low-field relaxation times should be compared with the experimental values

$$\tau_X = 3.32\ 10^{-10}\ \text{sec},\quad \tau_Y = 4.68\ 10^{-10}\ \text{sec},\quad \tau_Z = 9.95\ 10^{-10}\ \text{sec}$$

The agreement between theory and experiment is very good. It should be noted that the antisymmetric exchange shifts the relaxation times over about a factor 100 while it also rearranges the relative values.
The value $\alpha = 0.211$ implies $|\vec{D}|/J_3 = 0.056$ which is in agreement with the independent estimate $0.05 \leq |\vec{D}|/J_3 \leq 0.1$ by Metselaar (71) from the spin canting in the antiferromagnetic state.

The fact that the antisymmetric exchange in J_3 alone explains both the values for the relaxation times and the spin canting leads us to the conclusion that the antisymmetric contribution in J_3 is dominant over the contribution in J_4.

There still is an interesting point to be made. One should not interpret the perfect agreement between theory and experiment as absolute credit for the exchange values given by (6.4). Taking for example all exchange values a factor 2 smaller, one gets nearly the same perfect agreement with experiment using the value $\alpha = 0.298$. This value for α leads to $|\vec{D}|/J_3 = 0.079$ which still is in agreement with the independently determined value from Metselaar. So although it is clear that antisymmetric exchange is the mechanism which is speeding up the relaxation process, no absolute information about the isotropic exchange values can be derived for $LiCuCl_3.2H_2O$.

Using eq. (2.24a) and the theoretical relaxation times, derived with antisymmetric exchange included in the spin Hamiltonian, one gets for the field linewidth

$$(\Delta H_{\frac{1}{2}})_X = 176\ \text{Oe},\quad (\Delta H_{\frac{1}{2}})_Y = 212\ \text{Oe},\quad (\Delta H_{\frac{1}{2}})_Z = 260\ \text{Oe}$$

These theoretical low-frequency EPR linewidths can be compared with the experimental results of Zimmerman et al. (70).

$$(\Delta H_{\frac{1}{2}})_X = 186\ \text{Oe},\quad (\Delta H_{\frac{1}{2}})_Y = 234\ \text{Oe},\quad (\Delta H_{\frac{1}{2}})_Z = 308\ \text{Oe}$$

Once again the agreement, although less perfect than in the relaxation case, is good.

Our final conclusion of this section is that antisymmetric exchange is the most dominant source of magnetic anisotropy in $LiCuCl_3.2H_2O$.

6.5 *Relaxation in the critical region of $LiCuCl_3.2H_2O$*

$LiCuCl_3.2H_2O$ has been found to be antiferromagnetic below a Néel temperature of 4.44 K at zero static field. Zimmerman et al. (70) performed some resonance experiments in the critical region and found a critical broadening of the resonance linewidths. EPR linewidth measurements only give information on the average dynamical behavior in the plane perpendicular to the static field.
As in fact critical processes can be strongly anisotropic, it is clear why important information can be masked in the EPR results. Relaxation measurements however yield direct information on the dynamical behavior of the magnetization in one direction. An additional advantage is that relaxation measurements allow one to determine the intrinsic field dependence of this dynamical behavior.

6.5.1 *The direction of the easy-axis*

Much disagreement exists between the easy-axis directions given by different authors. Although the direction of the spin alignment is always found within the a-c plane, the direction reported varies wildly over this plane. In Fig. 35 the relative positions of some of the results are given.
The difference in the results may be due to the difficult orienting of the single crystals. Although at first sight the crystal planes are easily determined, a closer look shows that several combinations of crystal planes lead to nearly the same intersection angles. We determined the easy-axis by measuring the rf absorption below the Néel temperature while rotating the crystal.
As we know already from $CuCl_2.2H_2O$, only in the easy-axis a low-frequency relaxation process occurs. So at low frequencies the easy-axis is easily determined as the direction in which the absorption reaches its maximum. The easy-axis determined in this way coincides with the direction found by Zimmerman et al. (70) and Metselaar (71).
The easy direction does not coincide with a magnetic axis. The angle of the easy-axis with the Z-axis is about 16°. As one expects, when nearing the Néel temperature, some transition in the angular dependence of the zero-field absorption from the magnetic axes to the easy direction, we also performed rotational absorption measurements just above the Néel temperature.

The results, together with the absorption measurements below T_N, are given in Fig. 36.

From these measurements it is clear that at $T - T_N = 0.450$ K ($\in = 0.1$) the high-temperature magnetic axes still act as principal axes for the magnetic rf absorption.

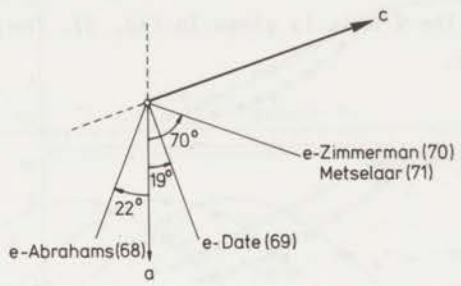

Fig. 35 *The relative orientation of the easy-axis in* $LiCuCl_3.2H_2O$ *as found by different authors. View along the b-axis.*

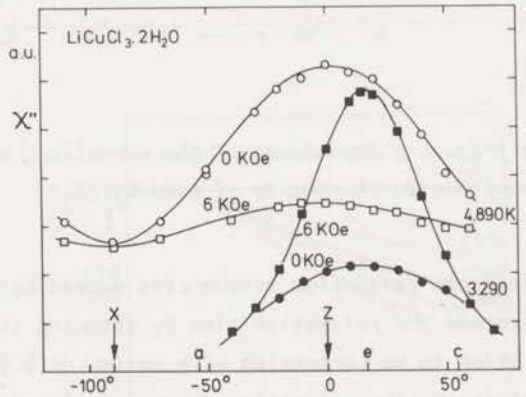

Fig. 36 *The angular dependence of the rf (ν = 180 MHz) relaxation absorption in the a-c plane, above and below the Néel temperature. θ is the angle between the Z-axis and the rf field.*

6.5.2 *Temperature and field dependence of the relaxation process*

Near the Néel temperature a critical speeding-up of the relaxation process is found. This speeding-up is much weaker than in $CuCl_2.2H_2O$. At temperatures where the relaxation frequencies lie well within our frequency region, we find the relaxation process to be very well described by a temperature dependent single relaxation time. As an illustration the frequency dependence of the zero-field absorption in the Z-axis is given in Fig. 37. The Néel temperature at zero-field equals 4.440 K.

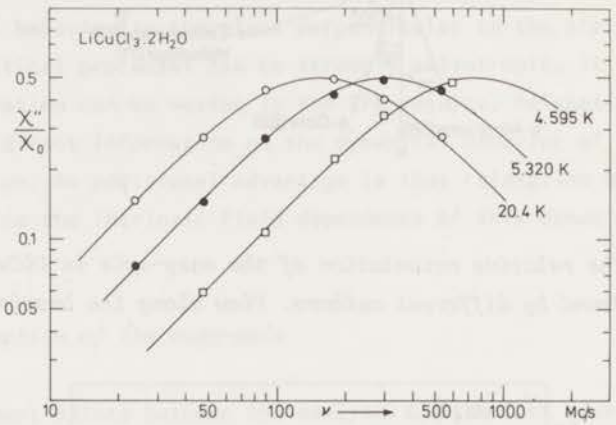

Fig. 37 *The frequency dependence of the normalized zero-field absorption in the Z-axis of* $LiCuCl_3.2H_2O$

At temperatures where the relaxation frequencies exceed our highest measuring frequency, we determined the relaxation time by assuming the frequency dependence of the absorption to be Lorentzian with maxima of $0.5\ \chi_0$.
Near the Néel temperature, the relaxation process is found to be weakly field dependent in the Y and Z axes. The X-axis shows no field dependence outside the experimental error of a few percent. The frequency dependence of the relaxation process at non-zero static fields is equally well described by a single relaxation time as it is at zero field. The relaxation times at a parallel field of 6 kOe are plotted together with the zero-field results in Fig. 38. In the Y and Z axes the relaxation process is speeding-up in increasing static field. Very near the Néel temperature the field dependence appears to decrease somewhat.

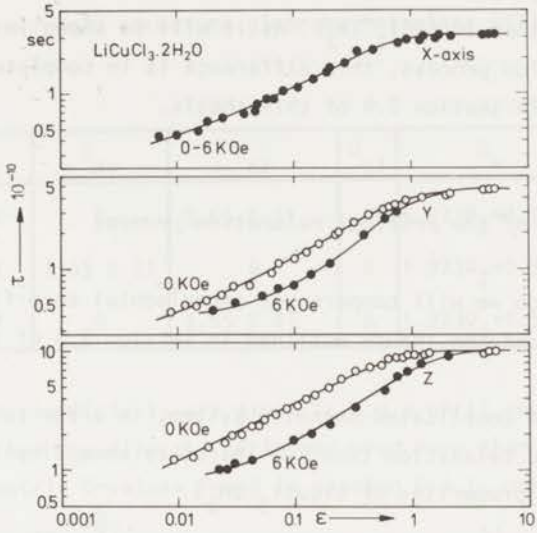

Fig. 38 *The temperature dependence of the relaxation times in the three magnetic axes of $LiCuCl_3.2H_2O$.*
$T_N(H = 0) = 4.440$ K and $T_N(H = 6$ KOe$) = 4.395$ K.
$\epsilon = (T - T_N)/T_N$.

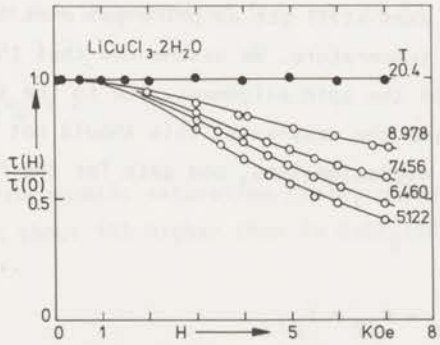

Fig. 39 *The field dependence of the relaxation time in the Z-axis of $LiCuCl_3.2H_2O$ at different temperatures. The relaxation times are normalized by the corresponding zero-field values which can be inferred from Fig. 38.*

Comparison of Fig. 38 with Fig. 16 shows that the critical speeding up is weaker in $LiCuCl_3.2H_2O$ than in $CuCl_2.2H_2O$. As it will be shown in the discussion of the critical relaxation process, this difference is in complete agreement with the theory outlined in section 2.4 of this thesis.

6.5.3 *Discussion of the critical relaxation process*

In this discussion we will compare our experimental zero-field relaxation times with the results of the theory outlined in section 2.4 of this thesis.

$LiCuCl_3.2H_2O$ is a complicated magnetic system. In order to calculate the critical part of the relaxation time, we introduce some simplifying approximations for the magnetic properties of $LiCuCl_3.2H_2O$.

Due to the spin canting by the antisymmetric exchange interaction the antiferromagnetic spin structure consists of four sublattices. As however the canting angle is small (about 6^o), we assume that in the critical region above T_N the antiferromagnetic spin structure is well approximated by a two-sublattice model. Furthermore, the easy direction of the antiferromagnetic spins does not coincide with one of the high-temperature magnetic axes. In Fig. 36 it was shown that these magnetic axes still act as principal axes for the rf absorption just above the Néel temperature. We assume now that the magnetic Z-axis coincides with the direction of the spin alignment. Due to the small angle of about 16^o between the Z-axis and the easy-axis, this should not be an unrealistic approximation. Using these approximations, one gets for the F-functions of eq. (2.75)

$$\begin{aligned} F_{ZZ} &= F_{//\,//} \\ F_{YZ} &= F_{XZ} = F_{ZX} = F_{ZY} = F_{//\perp} \\ F_{YY} &= F_{XX} = F_{XY} = F_{YX} = F_{\perp\perp} \end{aligned} \tag{6.8}$$

The U and D coefficients at the wavevector $\vec{q}_0$, which characterizes the staggered state, are given in table 4. For the calculation of these coefficients we used the antiferromagnetic spin structure given by Metselaar (71).

tabel 4

axis	$U_{xx} - U_{yy}$	U_{xy}	U_{xz}	U_{yz}	D_x	D_y
X	48.6 E 21	0	3.65 E 21	0	$1.923D_Z+0.551D_X$	0
Y	27.5 E 21	3.65 E 21	0	0	$1.923D_Z+0.551D_X$	$1.923D_X+0.551D_Z$
Z	76.1 E 21	0	3.65 E 21	0	$1.923D_X+0.551D_Z$	0

The values for the coefficients are given in c.g.s units and per magnetic ion. The dipolar summation was directly performed over more than 100,000 ions. Using the antisymmetric D-values found in section 6.4.1, one gets

$$(\Delta\frac{1}{\tau})_{crit.X} = A\,\frac{TN}{\chi_o}\,\epsilon^{-\frac{5}{2}\nu}\,(11790\,F_{//\perp} + 0.133\,F_{\perp\perp})\,10^{44}$$

$$(\Delta\frac{1}{\tau})_{crit.Y} = A\,\frac{TN}{\chi_o}\,\epsilon^{-\frac{5}{2}\nu}\,(0.267\,F_{//\,//} + 11780\,F_{//\perp} + 2700\,F_{\perp\perp})10^{44} \qquad (6.9)$$

$$(\Delta\frac{1}{\tau})_{crit.Z} = A\,\frac{TN}{\chi_o}\,\epsilon^{-\frac{5}{2}\nu}\,(2700\,F_{//\perp} + 57.9\,F_{\perp\perp})10^{44}$$

For an explicit calculation of the F-functions we transform the temperature into $\kappa_\Delta/\kappa_{//}$. In section 2.4 we estimated (cf. eq. (2.80))

$$\frac{\kappa_\Delta}{\kappa_{//}} \simeq (\frac{H_{A1} + H_{A2}}{H_E})^{\nu}\epsilon^{-\nu} \qquad (6.10)$$

From the T = 0 antiferromagnetic saturation field, measured by Metselaar (71), we estimate that H_E is about 10% higher than in $CuCl_2.2H_2O$. This yields

$$H_E \simeq 60\ \text{KOe}$$

Using the spin-flop field (H_{SF} = 10.53 kOe at T = 0) measured by Zimmerman et al. (70) one finds from $H_{SF}^2 = 2\,H_{A1}H_E$

$$H_{A1} \simeq 920\ \text{Oe}$$

The orthorhombic anisotropy field H_{A2} can be derived in different ways.

Zimmerman (73) measured the temperature gap between the temperature where the low-branch resonance field is zero and the temperature where the high-branch resonance field is zero. From this temperature gap we derive $H_{A2}/H_{A1} = 3.0$. This value is in reasonable agreement with the value 3.4 derived from the angular dependence of the resonance fields. We suppose the value $H_{A2}/H_{A1} = 1.65$, found by Zimmerman (73) from the resonance field at $\nu = 9.80$ GHz and $T = 0$, to be in error as the accuracy of such a derivation is very small. A few percent deviation in the value for the resonance field would lead to the values quoted above. Using $H_{A2}/H_{A1} = 3.2$ one gets

$$\frac{\kappa_\Delta}{\kappa_{//}} \simeq (0.0644)\epsilon^{-\nu} \qquad (6.11)$$

As the magnetic anisotropy in $LiCuCl_3.2H_2O$ is relatively large and as the critical exponent ν is very sensitive to a small anisotropy (see section 2.4.1) we will take for ν the three-dimensional Ising value $\nu = 0.63$. It should be noted that the final results are only weakly dependent on the choice for ν.
One thus gets

$$\frac{\kappa_\Delta}{\kappa_{//}} \simeq 0.180\,\epsilon^{-0.63} \qquad (6.12)$$

Using the F-values given in Fig. 1 of section 2.4 and

$$A = 1.69\ 10^{-65} \text{ c.g.s.u}$$

inferred from the experimental relaxation time in the Z-axis at $\epsilon = 0.025$, one finally gets the theoretical results plotted in Fig. 40.
It should be noted that the values for A in $CuCl_2.2H_2O$ and $LiCuCl_3.2H_2O$ are of the same order. This gives additional credit to the theory.

In view of the drastic simplifications in the theory and of the complicated nature of magnetic $LiCuCl_3.2H_2O$, it can be said that a very good agreement is found between experiment and theory. Just as in $CuCl_2.2H_2O$, it has been found that two correlation lengths, connected to each other by the anisotropy of the magnetic system, do sufficiently well explain the critical behavior of the relaxation process of the total magnetization $M_z(t)$.

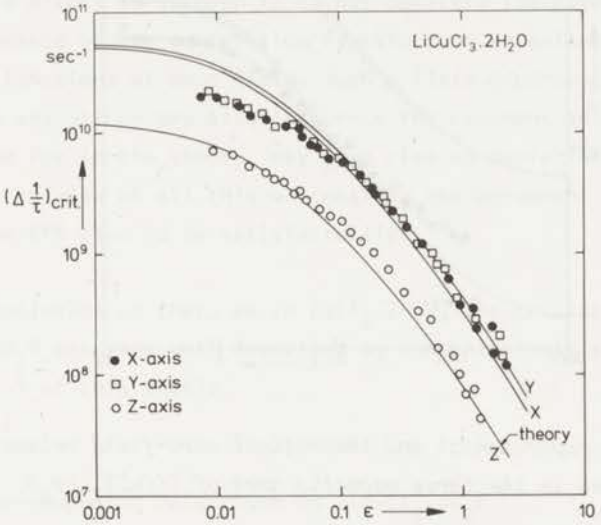

Fig. 40 *The theoretical and experimental critical parts of the relaxation times in the three magnetic axes of* $LiCuCl_3.2H_2O$.

Use of the theoretical high-temperature relaxation times, derived in section 6.4.1, in eq. (2.70)(see also eq. (2.81)) yields the theoretical relaxation times in the whole temperature region above the Néel point.
Both theoretical and experimental results are given in Fig. 41.

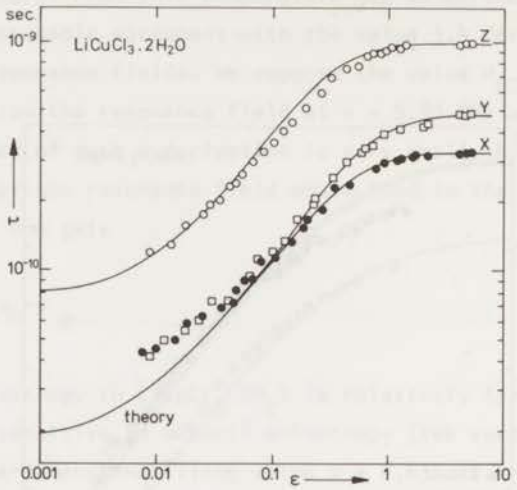

Fig. 41 *The experimental and theoretical zero-field relaxation times in the three magnetic axes of* $LiCuCl_3.2H_2O$.

Using the temperature dependent theoretical relaxation times in eq. (2.24a) one calculates the low-frequency resonance linewidths. The theoretical values together with the experimental results of Zimmerman et al. (70) are plotted in Fig. 42.

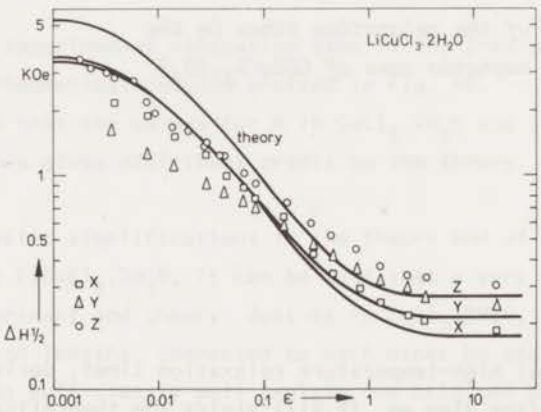

Fig. 42 *Comparison of the theoretical resonance linewidths with the experimental results of Zimmerman et al. (70).*

In the resonance case apparently less perfect agreement between experiment and theory is found than in the relaxation case. This is partly due to the averaging of the discrepancy in the relaxation times in the X and Y axes over all three directions by using eq. (2.24a). Furthermore, as shown in Fig. 39, the relaxation process of $M_z(t)$ is weakly field dependent near the Néel temperature. The origin of this field effect is unknown to us but possibly indicates either an intrinsic field dependence of the correlation functions or an anisotropy in the two-spin correlation functions at zero field. Such a field dependence at relatively small fields or an ansiotropy may also influence the resonant absorption and, as it is not accounted for in the theory, may give rise to deviations from the theoretical predictions. In view of all this we consider the agreement between experiment and theory in the EPR case to be satisfactorily.

Our final conclusion is that, as in $CuCl_2.2H_2O$, the critical dynamical phenomena of $LiCuCl_3.2H_2O$ are very well described by the relatively simple theory outlined in section 2.4 of this thesis.

6.6 *Antiferromagnetic relaxation in $LiCuCl_3.2H_2O$*

In $CuCl_2.2H_2O$ we saw that in the easy-axis (both rf and static field parallel to this axis) a low-frequency relaxation process occurs. In $LiCuCl_3.2H_2O$ essentially the same phenomenon is found.
In Fig. 43 the rf absorptions in the easy-axis are plotted at three different temperatures. The absorptions are normalized by the zero-field uniform susceptibility as determined by Metselaar (71). The maxima at certain fields indicate the shifting of the top of the absorption curves through our frequency region. At low temperatures the field dependence of the absorption and thus of the relaxation process, is much stronger than at temperatures nearer the Néel temperature (but outside the critical region). This has also been found in $CuCl_2.2H_2O$. The frequency dependence of the absorption is given in Fig. 44. Lorentzian curves with maxima of 0.5 are found at all static fields parallel to the easy-axis. These frequency dependences indicate that the relaxation process can be described by a single relaxation time. At low temperatures the relaxation process is slowing down at increasing static field. Near the Néel temperature a strongly field dependent critical speeding-up is found. All this is analog to the dynamical behavior of $CuCl_2.2H_2O$. The angular dependence of the absorption is given in Fig. 36 of section 6.5.1.

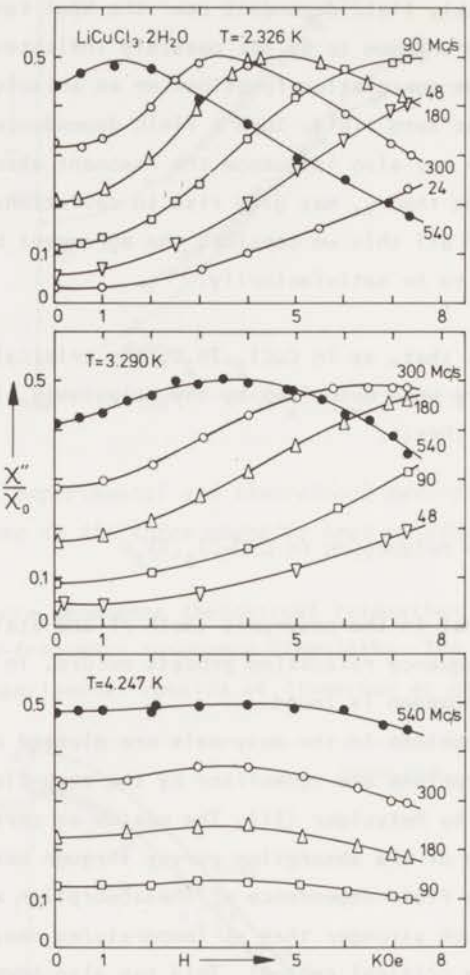

Fig. 43 *The field dependence of the normalized rf absorption in the easy-axis of $LiCuCl_3.2H_2O$. Both rf and static field are parallel to the easy-axis.*

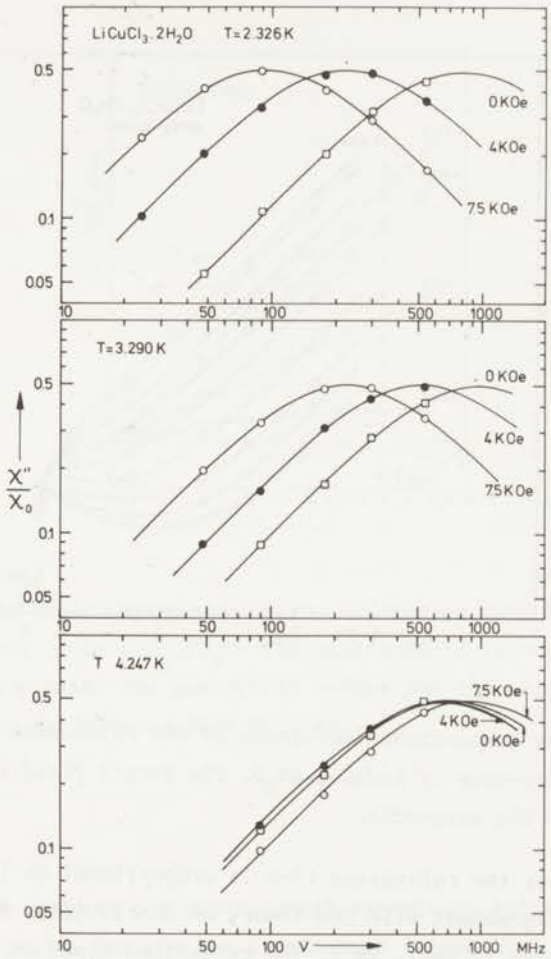

Fig. 44 *The frequency dependence of the rf absorption in the easy-axis of $LiCuCl_3.2H_2O$. Both rf and static field are parallel to the easy-axis.*

We performed some relaxation time measurements below the λ-transition of the He-bath (T = 2.172 K). These measurements are difficult to perform with our calorimetric method as the small pressure of the calorimeter He-gas, necessary to get a reasonably ideal gas, limits both the sensitivity and the accuracy. From Fig. 45 it is clear however that, if special care is taken, these measurements can be sufficiently accurate.

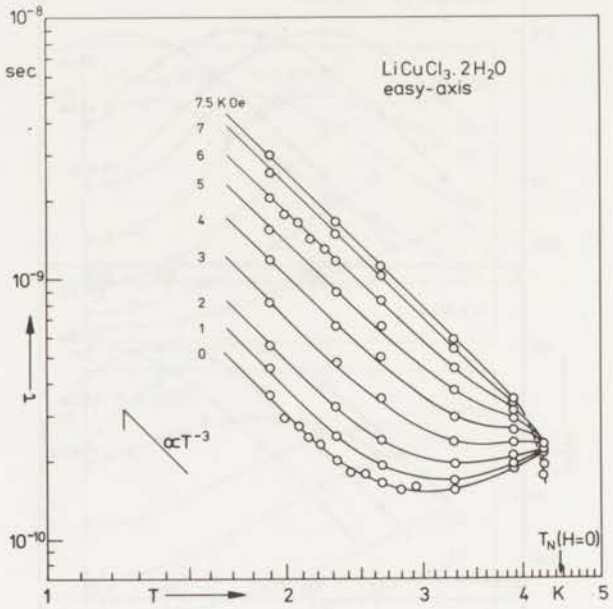

Fig. 45 *The temperature dependence of the relaxation time in the easy-axis of $LiCuCl_3.2H_2O$. The static field is parallel to the easy-axis.*

At low temperatures the relaxation time is proportional to T^{-3}. This temperature dependence is in agreement with the theory of Harris (31). The same temperature dependence was found in $CuCl_2.2H_2O$. The relaxation times in $LiCuCl_3.2H_2O$ are smaller than in $CuCl_2.2H_2O$. As it will be shown in the discussion, this experimental result is consistent with the larger magnetic anisotropy in the Li compound.

In Fig. 46 the field dependent relaxation time is plotted versus the square of the static field. As in $CuCl_2.2H_2O$, the low-temperature relaxation times are well described by

$$\tau(T,H) = \tau(T,0) + f(T)\ H^2 \qquad (6.13)$$

where f(T) is some temperature dependent factor.

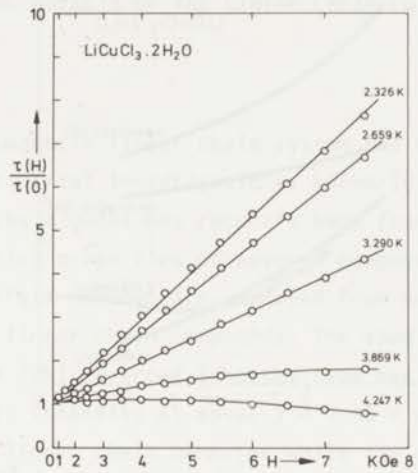

Fig. 46 *The field dependence of the relaxation time in the easy-axis of $LiCuCl_3.2H_2O$. The static field is parallel to the easy-axis. The zero-field values for the relaxation times can be inferred from Fig. 45.*

6.6.1 *Discussion*

In this section we compare our experimental zero-field relaxation times with the theoretical results for the k = 0 spin-wave relaxation.
Using the orthorhombic anisotropy values H_{A1} = 920 Oe and H_{A2} = 2950 Oe and $H_A = (H_{A1} + H_{A2})/2$, one gets

$$\omega_A = 3.75\ 10^{10}\text{Hz}, \qquad \omega_E = 1.17\ 10^{10}\ \text{Hz}, \qquad T_{AE} = 2.26\ \text{K}$$

The symbols ω_A, ω_E and T_{AE} are defined in section 2.5.5. The theoretical expressions for the relaxation rates, given in table 1, are either valid for $T \ll T_{AE}$ or for $T \gg T_{AE}$. For the theoretical relaxation rates near T_{AE} we interpolate between both limit situations. As the expressions for high and low temperatures lead, around T_{AE}, to relaxation rates of about the same absolute magnitude, we do not believe that this interpolation introduces important errors.

The experimental and theoretical k = 0 relaxation times are given in Fig. 47.

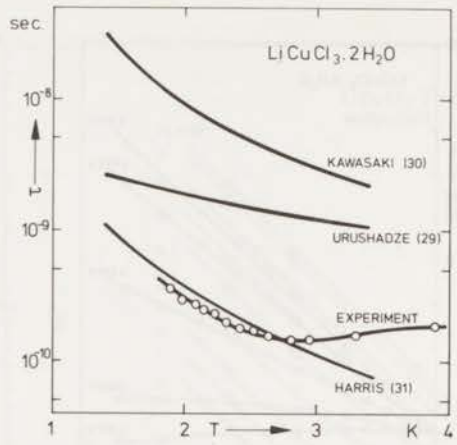

Fig. 47 *Comparison of the experimental zero-field relaxation times with the theoretical k = 0 spin-wave relaxation results.*

Both absolute magnitude and temperature dependence of the zero-field relaxation time are in near perfect agreement with the theory of Harris (31).
As in $CuCl_2.2H_2O$, the relaxation measurements show that at zero field the spin-wave approach is valid for temperatures below about 0.5 T_N.
Further theoretical investigation is necessary to explain the dynamical behavior at non-zero static fields. An interesting experimental result is that, apart from the simple H^2 field dependence, the temperature dependence of the relaxation times appears to be independent of the static field at sufficiently low temperatures (see Fig. 45). This implies that at low temperatures, as in $CuCl_2.2H_2O$, $f(T) \propto T^{-3}$.

CHAPTER 7

DYNAMICAL ASPECTS OF THE LINEAR CHAIN $Cu(NH_3)_4SO_4.H_2O$

7.1 *Introduction*

In recent years the magnetic linear chain system has been the subject of many theoretical and experimental investigations. Formerly of academic interest only, the magnetic linear chain model has recently been found to describe satisfactorily the (mostly static) properties of several compounds.
Copper tetrammine sulfate monohydrate, denoted from now on as CTS, was one of the first known magnetic linear chain compounds. The specific heat has been measured by Haseda and Miedema (74). A broad Schottky type maximum near T = 3 K and a sharp maximum of small intensity at about T = 0.40 K were found. The broad maximum pointed to a linear chain behavior while the sharp peak at lower temperatures indicated the occurrence of three-dimensional long-range order. As an ideal linear chain does not exhibit such a three-dimensional transition, the sharp peak at about 0.40 K implies a certain amount of interchain coupling. Using a two-time temperature dependent Green function technique, Oguchi (75) estimated from the value for the Néel temperature the ratio of interchain and intrachain interaction. Denoting the (supposedly isotropic) interchain and intrachain interactions as J' and J respectively, Oguchi found $J'/J \simeq 0.01$. Watanabe and Haseda (76) measured the static susceptibility in the principal magnetic axes of CTS. Here also broad maxima at about T = 3 K were found. Using the exact computer calculations of Bonner and Fisher (77), Griffiths (78) showed that the broad maxima in both specific heat and magnetic susceptibility could be explained by an isotropic antiferromagnetic exchange interaction between neighboring spins in a linear chain of Cu ions. The intrachain exchange, $|J|/k_B$, was found to be equal to 3.15 K.

From these experiments it is evident that although the small interchain exchange J' has a significant effect in ultimately producing three-dimensional order, it does not alter the static magnetic behavior at temperatures well above T_N. The same holds for a small anisotropic component in the intrachain exchange J.

The dynamical behavior of nearly perfect linear chain systems is governed by the long-time persistence of the spin correlations. This persistence, which is due to the slow rate of diffusion in one-dimensional systems, implies a long-

time tail to the memory function as defined by eq. (1.19) of section 1.1.2. Such a long-time tail corresponds to a strong anomaly (divergency) at $\omega = 0$ in the memory spectrum. Hennessy et al. (79) have shown that, in contrast to the static properties, the long-time behavior of the spin correlation functions is drastically influenced by a relatively small interchain interaction. As a consequence, interchain coupling can be very effective in limiting the one-dimensional divergencies at $\omega = 0$ in the memory spectrum. A short survey of the theory will be given in the discussion of the high-temperature relaxation times.

The exact long-time behavior of the correlation functions is usually difficultly visualized from experiment. In practice, one assumes a certain long-time behavior for the correlation functions and calculates its influence on the dynamical phenomena. One might however look for a possibility to extract the real long-time behavior straightforwardly from some relatively transparant experiments. Paramagnetic resonance has been shown (80)(81) to be a valuable tool in testing theories on the long-time persistence of the correlations. The disadvantage however is that in resonance experiments important information may be masked, as in fact the resonance line shape stems from the average dynamical behavior in the plane perpendicular to the static field. A better approach may be found in paramagnetic relaxation time measurements. In these experiments, where static and rf field are mutually parallel, the long-time behavior of the memory function is relatively easily determined from the field dependence of the relaxation times or the frequency dependence of the rf absorption.

At high temperatures we shall use the relaxation time measurements of Van der Molen (10) and Lieffering (82). We remeasured some of their results and found an agreement within the experimental error of a few percent. At low temperatures, down to about T = 2 K, we performed both relaxation and resonance experiments. At these temperatures an anisotropic speeding-up of the relaxation process has been found.

7.2 *Crystal structure of* $Cu(NH_3)_4SO_4.H_2O$

The crystal structure of CTS has been determined by Mazzi (83). The crystal is found to be orthorhombic with a tetramolecular unit cell of dimensions

$$a = 7.08\ \text{Å}, \qquad b = 12.14\ \text{Å}, \qquad c = 10.68\ \text{Å}$$

The space group is P_{mcn}. The crystal is composed of $Cu(NH_3)_4$,SO_4 and H_2O elements. The $Cu(NH_3)_4$ group is planar and square with the distance Cu-N equal to 2.05 Å. Each copper ion has two water neighbors at different distances, 2.59 and 3.37 Å. The crystal structure is visualized in Fig. 48.

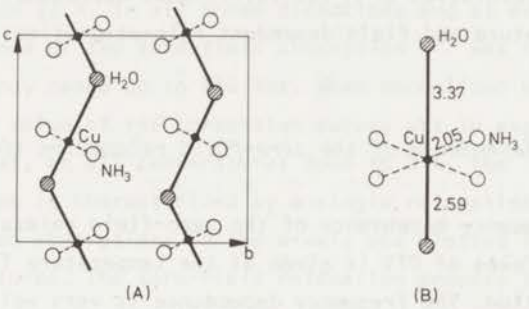

Fig. 48 *(A) Projection of the unit cell of CTS on its b-c plane.*
(B) Atomic configuration surrounding a Cu ion in CTS.

From the crystal structure it is probable that the intrachain exchange path is through the -Cu-H_2O-Cu- bonds. The chains of Cu ions are parallel to the c-axis.

For our experiments we used several single crystals of about 0.5 gram. The dark violet crystals were oriented by measuring the intersection angles of the different crystal planes. To prevent decomposition, the single crystals were submersed in paraffin (hexadecane). It was found that a thin film of paraffin on the crystal surface was already sufficient to prevent such a decomposition.

7.3 *Relaxation and resonance experiments in $Cu(NH_3)_4SO_4.H_2O$*

For a single relaxation process the memory spectrum should be reasonably constant over a sufficiently large frequency region around $\omega = 0$. This is easily seen from section 1.1.2 as such a constant part implies a narrow memory function. As in near-perfect linear chain compounds the memory spectrum shows a strong anomaly around $\omega = 0$, the relaxation process of the total magnetization $M_z(t)$ is not expected to be described by a single relaxation time. In CTS however, the frequency dependence of the relaxation absorption is very well Lorentzian, even at frequencies far beyond the top frequency (see Fig. 49).

This experimental result indicates a relatively large interchain coupling as such a coupling removes the divergency at $\omega = 0$ in the memory spectrum. This is in agreement with the resonance experiments of Hennessy et al. (79) who found the EPR lines to be Lorentzian, even at fields far from the resonance field. Consequently, the description of the dynamical behavior of CTS is simplified by the fact that the time evolution of $M_z(t)$ is, in good approximation, characterized by a single temperature and field dependent relaxation time.

7.3.1 *Temperature dependence of the zero-field relaxation times*

In Fig. 49 the frequency dependence of the zero-field relaxation absorption in the three magnetic axes of CTS is given at the temperature T = 20.4 K. The c-axis is the chain direction. The frequency dependence is very well described by the Lorentzian form

$$\frac{\chi''}{\chi_o} = \frac{\omega\tau}{1+\omega^2\tau^2} \qquad (7.1)$$

For the normalization of χ'' we used the static susceptibility results of Watanabe and Haseda (76).

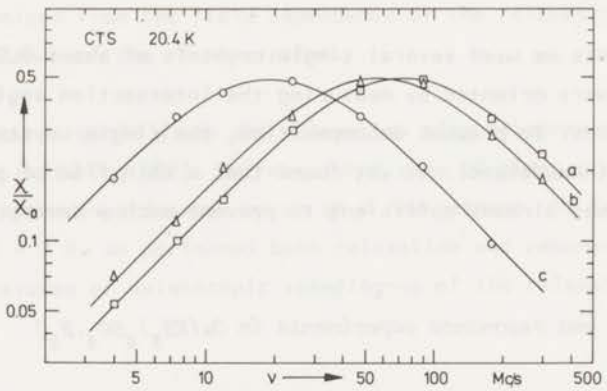

Fig. 49 *The frequency dependence of the normalized zero-field absorption in the three magnetic axes of CTS at 20.4 K*

Our zero-field relaxation times at T = 20.4 K.

$$\tau_a = 2.15, \quad \tau_b = 2.72, \quad \tau_c = 8.25 \quad 10^{-9} \text{ sec}$$

are in good agreement with the experimental results of Van der Molen (10) at the same temperature

$$\tau_a = 2.12, \quad \tau_b = 2.78, \quad \tau_c = 7.90 \quad 10^{-9} \text{ sec}$$

We performed absorption measurements, such as given in Fig. 49, at temperatures from 2 K upwards to 77 K. In all three directions and at every temperature the frequency dependence of the zero-field absorption χ'' was found to be Lorentzian within our frequency range up to 540 MHz. When normalized by the static susceptibility, the top value of the Lorentzian curves was in every case equal to 0.5. This indicates that, at all temperatures down to 2 K, the long-time decay of the total magnetization is characterized by a single relaxation time. As an illustration the normalized absorptions in the a-axis are plotted in Fig. 50 at three different temperatures. The zero-field relaxation process in the a-axis is speeding up when lowering the temperature.

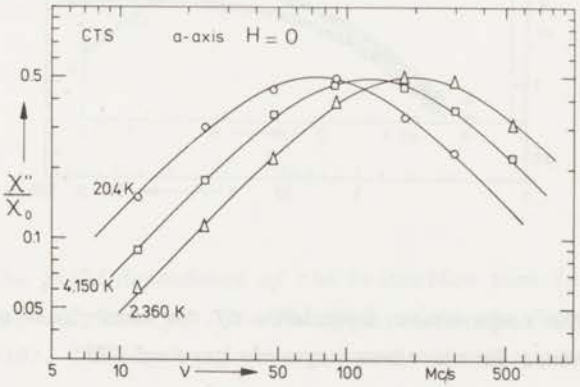

Fig. 50 *The frequency dependence of the normalized absorption in the a-axis of CTS at three different temperatures.*

The speeding-up of the relaxation process at lower temperatures is found to be anisotropic. The relaxation times in the a and b axes show nearly the same temperature dependence while in the c-axis (the chain axis) no relevant temperature dependence was detected at all. In Fig. 51 the temperature dependence of the relaxation times in the three magnetic axes of CTS is given. The measurements at temperatures between 4 and 15 K were performed by heating the sample adiabatically using its own rf absorption.

Every relaxation time given in Fig. 51 has been determined by fitting eq. (7.1) to the frequency dependence of the absorption at the given temperature. As one sees from Fig. 50, very good fits are obtained with only a few percent scatter. Some confusion may exist about the definition of the magnetic axes a, b and c as the crystallographic axes have been defined by some authors in different ways. We used the definition of Mazzi (83) throughout. For further information, the a-axis is the magnetic axis with the smallest g-value (g_a = 2.050) while the values in the b and c axes are equal to 2.123 and 2.184 respectively.

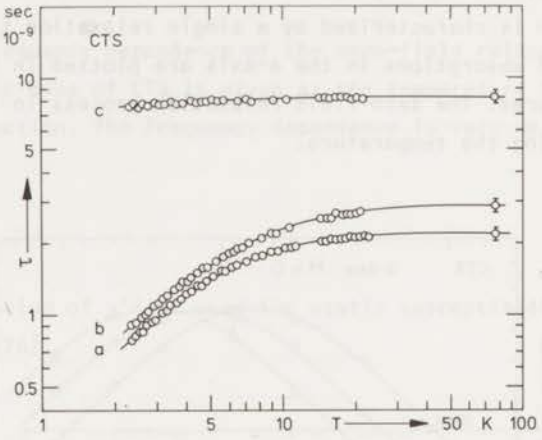

Fig. 51 *The temperature dependence of the zero-field relaxation times in the three magnetic axes of CTS.*

7.3.2 *Field dependence of the relaxation process*

The field dependence of the relaxation times at H_2 temperatures (15-20 K) has been measured by Van der Molen (10). We remeasured some of his results and found a good agreement within the experimental error of a few percent. The field dependence of the relaxation times gives us very important information as in fact it reflects the low-frequency dependence of the memory spectrum. As already stated before, it is exactly in this low-frequency region that the typical linear chain anomalies occur. It should once again be stressed that in a near-perfect linear chain it cannot be expected that the relaxation process can be described by a single relaxation time.

Even in that case, however, the frequency dependence of the absorption χ'' would give us all the relevant information on the long-time persistence of the spin correlations. In CTS the problem is simplified by the relatively large inter-chain coupling.
The field dependences of the relaxation times at T = 20.4 K are given in Fig. 52.

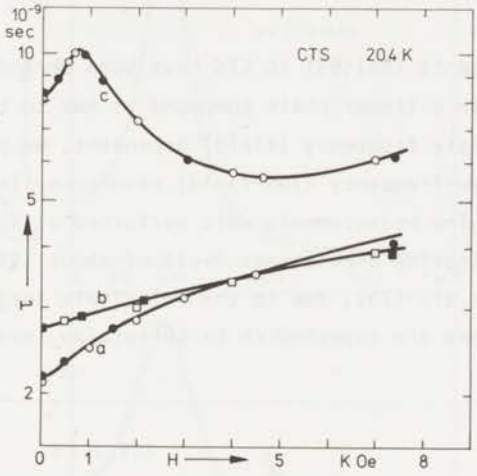

Fig. 52 *The field dependence of the relaxation time in the three magnetic axes of CTS. The open points are from Van der Molen (10). The black points represent our own measurements.*

At lower temperatures down to 2 K the field dependences remain roughly the same, although at small fields some minor changes occur. In the c-axis the maximum at small fields becomes less pronounced while in the a and b axes the field dependences become slightly stronger. These changes are however small and not too much attention should be paid to it.

Careful inspection of the field dependence of the relaxation times shows now why the frequency dependence of the rf absorption χ'' was so well described by a Lorentzian. In field ranges of about 200 Oe around every, arbitrary value for the static field, the relaxation times are nearly field independent. Assuming the well-known weak-coupling feature of rigid line shape for the memory

spectrum to hold (the four lines of the memory spectrum shift rigidly with the static field) one finds that the memory spectrum is nearly constant from $\nu = 0$ up to at least $\nu = 600$ MHz. This, on its turn, implies that the frequency dependence of χ'' should be Lorentzian up to at least 600 MHz, a value far above the relaxation frequencies.

7.3.3. *Resonance experiments in CTS*

Most resonance experiments (84)(85) in CTS have been performed at relatively high frequencies. As in a linear chain compound it has to be expected (86) that the linewidth is strongly frequency (field) dependent, we performed extensive measurements of the low-frequency (low-field) resonance linewidth in the three magnetic axes of CTS. The measurements were performed at a measuring frequency of $\nu = 300$ Mcs which implies a resonance field of about 100 Oe. As already pointed out by Hennessy et al. (79), due to the relatively large interchain coupling the resonance lines are expected to be Lorentzian, even at fields far from the resonance field.

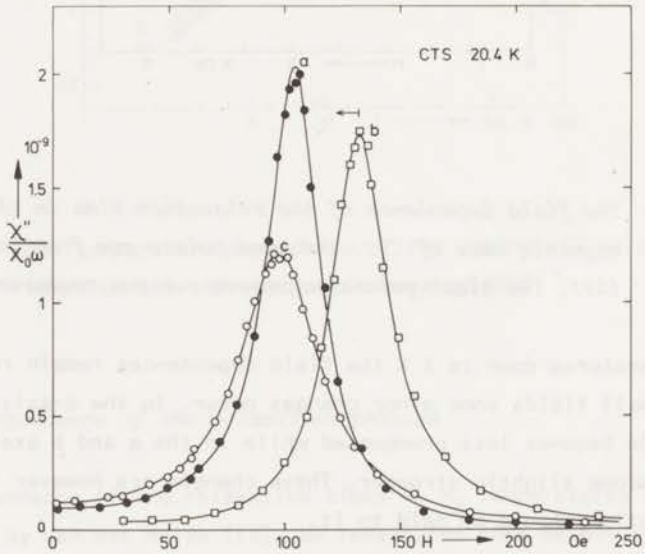

Fig. 53 *The paramagnetic resonance lines in the three magnetic axes of CTS. For clarity the line in the b-axis has been shifted over 30 Oe to the right. The solid lines represent least-square fits of eq. (7.2). In the a-axis the rf field is parallel to the b-axis, in the b-axis parallel to the c-axis and in the c-axis parallel to the a-axis.*

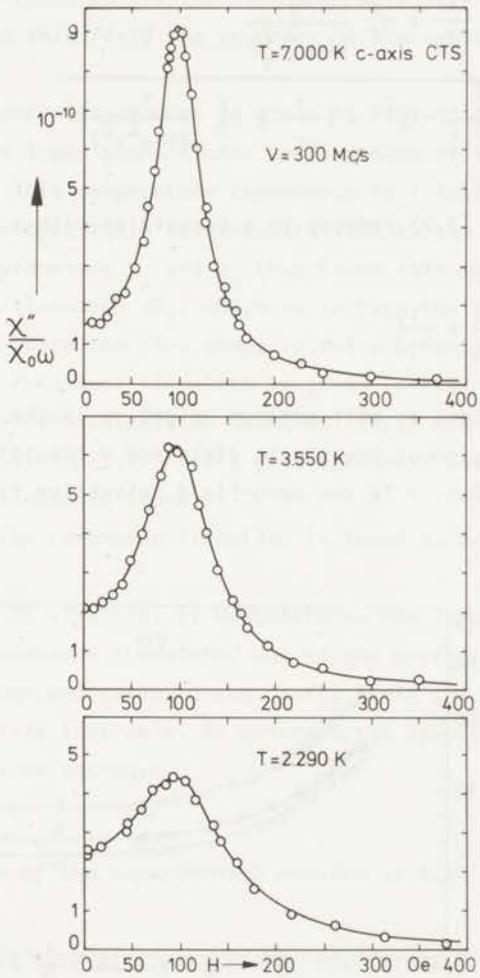

Fig. 54 *The resonance lines in the c-axis of CTS at three different temperatures. The rf field is parallel to the a-axis. The solid lines are least-square fits of eq. (7.2).*

At zero static field the resonance absorption is determined by the relaxation rate in the direction of the rf field. At increasing static field the relaxation rate of the third direction (perpendicular to both rf and static field) will also play a role. The resulting lineshape has been given by Verbeek et al. (19) (cf. eq. (5.3))

$$\left(\frac{\chi''}{\chi_o}\right)_\alpha = \frac{\frac{1}{\omega\tau_\alpha} + \eta_\beta^2 \frac{\tau_\gamma}{(1+\omega^2\tau_\gamma^2)}}{\left[\eta_\beta^2 \frac{\tau_\gamma^2}{1+\omega^2\tau_\gamma^2} - 1\right]^2 + \left[\frac{1}{\omega\tau_\alpha} + \eta_\beta^2 \frac{\tau_\gamma}{\omega(1+\omega^2\tau_\gamma^2)}\right]^2} \qquad (7.2)$$

At higher frequencies (7.2) reduces to a Lorentzian with a field linewidth given by

$$(\Delta H_{\frac{1}{2}})_\beta = \frac{\hbar}{g_\beta \mu_B} \left(\frac{1}{\tau_\alpha} + \frac{1}{\tau_\gamma}\right) \qquad (7.3)$$

$\Delta H_{\frac{1}{2}}$ is the full linewidth at half maximum height. α is the direction of the rf field, β the direction of the static field and γ the third direction perpendicular to the other two. τ is the zero-field relaxation time.

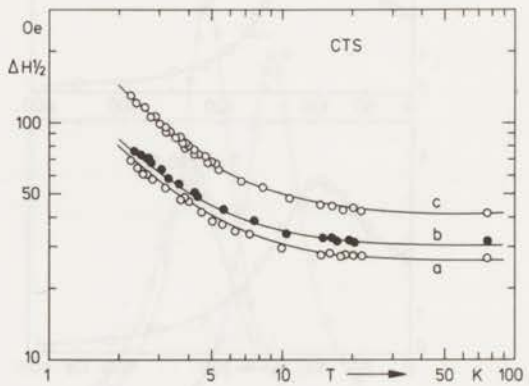

Fig. 55 *The temperature dependence of the resonance linewidths in the three magnetic axes of CTS. $\Delta H_{\frac{1}{2}}$ denotes the full linewidth at half maximum. The linewidths were measured at ν = 300 MHz. The solid lines are derived from our experimental relaxation times, see Fig. 51, using eq. (7.3).*

In Fig. 53 the resonance lines in the three magnetic axes of CTS are plotted at a temperature T = 20.4 K. The solid lines are least-square fits of eq. (7.2) to the data. The parameters τ_α and τ_γ are found to be equal, within experimental error, to the zero-field relaxation times given in section 7.3.1.
Eq. (7.2) has been found to fit the resonance data very well at fields up to about 8 $\Delta H_{\frac{1}{2}}$. Beyond this field the accuracy is too small to allow any conclusion.

We performed the same measurements as given in Fig. 53 at temperatures from 2 K upwards to 77 K. At lower temperatures a broadening of the linewidth was found in all directions. This temperature dependence is illustrated in Fig. 54.
The solid lines are once again least-square fits to the absorption data. Substituting the parameters τ_α and τ_γ thus found into eq. (7.3) we were able to calculate the full linewidth $\Delta H_{\frac{1}{2}}$, which is in fact the linewidth at slightly higher frequencies where the line shape is fully Lorentzian. The temperature dependence of this resonance linewidth is given in Fig. 55. The solid lines represent the linewidths calculated using eq. (7.3) and the experimental relaxation times from section 7.3.1. A very good agreement between both relaxation and resonance experiment is found.
The broadening of the resonance linewidth is found to be more or less isotropic.

Comparison of Fig. 55 with Fig. 51 demonstrates how important information can be masked in the resonance linewidth. Due to the averaging of the dynamical process in the plane perpendicular to the static field the broadening of the linewidths is more or less isotropic. In contrast, the speeding-up of the relaxation process is strongly anisotropic.

7.4 *Confrontation of the experimental results at high temperatures with theory*

As already mentioned several times before, the interesting dynamical property of magnetic linear chain systems is the long-time persistence of the spin correlations. It has been shown by many authors, see e.g. refs. (87) and (88), that in the ideal linear Heisenberg chain these long-time tails lead to divergencies at $\omega = 0$ in the Fourier transforms of the correlation functions. Such anomalies were clearly demonstrated by the computer calculations of Carboni and Richards (86). In their basic work these authors calculated straightforwardly the time evolution of the two-spin correlation functions in closed and open Heisenberg linear chains of up to 10 spins. Using the same extrapolation procedure as Bonner and Fisher (77) they were able to give reliable estimates for infinite

linear chains.

In this discussion we will compare our experimental high-temperature results with an adapted version of the theory of Hennessy et al. (79) for CTS.

In the DRPA, defined by eq. (2.54), the zero-field high-temperature memory function of the relaxation process of $M_z(t)$ is given by (cf. eq. (2.55))

$$G_z(t) = \frac{3g^4\mu_B^4}{\hbar^2 S(S+1)N} \sum_q |C(q)|^2 \, \langle\langle S_{-q} S_q(t) \rangle\rangle^2 \qquad (7.4)$$

$C(q)$ is a wavevector dependent weight factor which arises from dipolar and other non-secular interactions. This factor is taken per magnetic ion. In (7.4) use has been made of the high temperature approximation

$$\langle\langle S^{\alpha}_{-q} \, S^{\alpha}_{q}(t) \rangle\rangle \equiv \frac{\mathrm{Tr}\, S^{\alpha}_{-q} \, S^{\alpha}_{q}(t)}{\mathrm{Tr}\, 1} = k_B T \, (S^{\alpha}_{-q}, \, S^{\alpha}_{q}(t)) \qquad (7.5)$$

while further it has been assumed that the two-spin correlation functions are isotropic

$$(S^{x}_{-q}, \, S^{x}_{q}(t)) = (S^{y}_{-q}, \, S^{y}_{q}(t)) = (S^{z}_{-q}, \, S^{z}_{q}(t)) \equiv \frac{1}{k_B T} \langle\langle S_{-q} \, S_q(t) \rangle\rangle \qquad (7.6)$$

From eq. (7.4) it is evident that, if all assumptions about DRPA and isotropy are correct, the memory function is positive semi-definite for all times.

Assuming now, in the spirit of the theory of Hennessy et al., that the two-spin correlation functions can be approximated by a simple product of the unperturbed linear chain correlation function and a function $\phi_q(t)$ which depends on the interchain coupling, one gets for sufficiently long times

$$\langle\langle S_{-q} \, S_q(t) \rangle\rangle = \tfrac{1}{3} S(S+1) \, e^{-D^{*} q_c^2 \, t} \, \phi_q(t) \qquad (7.7)$$

D^{*} is the diffusion constant along the chain axis, the symbol $*$ being introduced to eliminate any possible confusion with the antisymmetric exchange D. In eq. (7.7) it has been supposed that the time evolution of the unperturbed linear chain correlation function is completely governed by the isotropic intrachain Heisenberg exchange only. In ref. (79) it has been shown that in the case of Heisenberg interchain coupling, $\phi_q(t)$ is given by

$$\frac{\partial \phi_q(t)}{\partial t} = - \int_0^t \psi_q(\tau) \, \phi_q(t-\tau) d\tau \qquad (7.8)$$

with

$$\psi_q(t) = \frac{4S(S+1)}{3N\hbar^2} \sum_{q'} e^{-2D^* q_c'^2 t} \left| J^{nc}_{q'} - J^{nc}_{q'-q} \right|^2 \qquad (7.9)$$

where J^{nc} denotes the interchain exchange interaction.

For the explicit calculation of the q'-sum we will take a look at the crystal structure of CTS.
Each copper ion in CTS has, within the a-b plane, six neighbors at approximative the same distance. See Fig. 56.

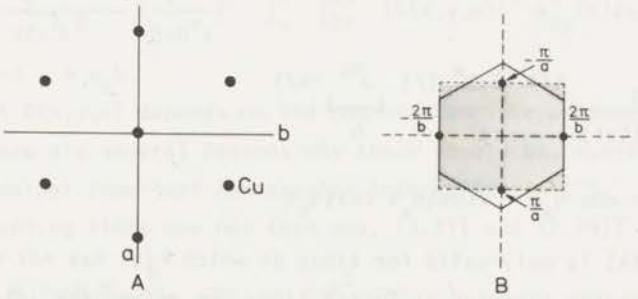

Fig. 56 *(A) Positions of the nearest neighbors in the a-b plane.*
(B) The first magnetic Brillouin zone of CTS. For symmetry reasons the contributions from the rectangle are the same as from the real Brillouin zone.

For symmetry reasons the exchange interactions between corner and base-center ions are equal. Although the exchange interactions along the a-axis may be different we suppose the coupling to be equally strong ($J^{nc}_{ij} = J^{nc}$) in all six directions. Using

$$J^{nc}_q = \sum_j J^{nc}_{ij} e^{i \vec{q}.\vec{r}_{ij}} \qquad (7.10)$$

one then gets

$$J^{nc}_q = 2 J^{nc} (\cos q_a a + 2 \cos \tfrac{1}{2} q_a a \cos \tfrac{1}{2} q_b b) \qquad (7.11)$$

Substituting eq. (7.11) in (7.9) and transforming the q'-sum into an integral, one finds for sufficiently long times

$$\psi_q(t) = \frac{8}{3} S(S+1) \left(\frac{c^2}{8\pi D^* t}\right)^{\frac{1}{2}} \frac{J^{nc}}{\hbar^2} \quad (3 - \cos q_a a - 2 \cos \tfrac{1}{2} q_a a \cos \tfrac{1}{2} q_b b) \qquad (7.12)$$

At times which are short compared with the characteristic decay time(s) of $\phi_q(t)$, the integro-differential equality (7.8) may be approximated by

$$\phi_q(t) = e^{-\int_0^t \psi_q(\tau) d\tau \, dt} = e^{-\int_0^t (t-\tau) \psi_q(\tau) d\tau} \qquad (7.13)$$

Substituting (7.12) in eq. (7.13) one finds

$$\phi_q(t) = e^{-\left(\frac{t}{t_o}\right)^{3/2} F(q)} \qquad (7.14)$$

with

$$t_o = \left(\frac{9}{32 S(S+1)}\right)^{2/3} \left(\frac{8\pi D^*}{c^2}\right)^{1/3} \left(\frac{J^{nc}}{\hbar}\right)^{-4/3} \qquad (7.15)$$

$$F(q) = 3 - \cos q_a a - 2 \cos \tfrac{1}{2} q_a a \cos \tfrac{1}{2} q_b b \qquad (7.16)$$

Expression (7.14) is only valid for times at which $\phi_q(t)$ has not decayed significantly. To get the behavior at larger times, we solved the integro-differential equality (7.8) numerically. A typical result is shown in Fig. 57.

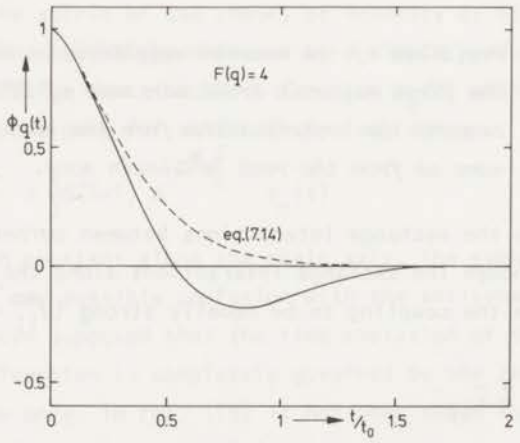

Fig. 57 *The solution $\phi_q(t)$ of integro-differential equality (7.8) using kernel (7.12) limited at very short times by convolution with a Gaussian. $\phi_q(t)$ is given for the set of q-values for which F(q) = 4.*

From these computer calculations we found that, at times of interest, $\phi_q(t)$ is very well described by

$$\phi_q(t) = e^{-(\frac{t}{t_o})^{3/2}F(q)} \left[1 - (\tfrac{3}{4}F(q))^{7/3}(\frac{t}{t_o})^{7/2}\right] \qquad (7.17)$$

Use of eq. (7.7) in (7.4) leads to the memory function

$$G_z(t) = \frac{g^4\mu_B^4\, S(S+1)}{3\hbar^2 N} \sum_q |C(q)|^2\, e^{-2D^*q_c^2 t}\, \phi_q^2(t) \qquad (7.18)$$

By further transforming the q-sum into an integral one gets, under the assumption that C(q) shows no singularity at or near $\vec{q} = 0$, the long-time expression

$$G_z(t) = \frac{g^4\mu_B^4\, S(S+1)}{48\pi^2\hbar^2} \left(\frac{c^2}{8\pi D^* t}\right)^{\frac{1}{2}} \int_{-\pi}^{\pi}\int_{-2\pi}^{2\pi} |C(x,y,o)|^2\, \phi_{xy}^2(t)\,dx\,dy \qquad (7.19)$$

with $x = q_a a$ and $y = q_b b$.

The coefficient C(x,y,o) depends on the non-secular interactions in the magnetic system. There are several reasons why there should be, apart from dipolar interaction, another important non-secular interaction in CTS.

In the weak-coupling limit one has (see eqs. (2.21) and (2.24))

$$\frac{\langle\langle \mathcal{H}_1 \mathcal{H}_{-1}\rangle\rangle + 2\langle\langle \mathcal{H}_2 \mathcal{H}_{-2}\rangle\rangle}{\hbar\, \langle\langle S_z^2\rangle\rangle} = \frac{g\mu_B}{\pi} \int_0^{\infty} \frac{\langle\langle \mathcal{H}_{sec}^2\rangle\rangle}{\langle\langle \mathcal{H}^2\rangle\rangle} \frac{1}{\tau(H)}\, dH \qquad (7.20)$$

The double brackets denote normalized traces. As all factors are positive, the left-hand side should be larger than the right-hand side when the integral is only extented from zero field to a finite maximum field. Theoretical calculation of the normalized traces, taking only non-secular dipolar contributions into account, yields in the a-axis for the left-hand side $9.46\ 10^{18}$ c.g.s.u. From the relaxation time measurements, given in Fig. 52, we find for fields up to 7 kOe for the right-hand side $13.4\ 10^{18}$ c.g.s.u. The right-hand side being larger than the left-hand side implies that in CTS another non-secular interaction occurs which increases the surface of the memory spectrum. As it has been shown in this thesis that several copper compounds exhibit antisymmetric exchange, we suppose this interaction, as it is allowed by crystal symmetry, to be at the origin of the surface increase in CTS.

Additional credit for this assumption is that the antisymmetric exchange in CTS leads to a small canting of the electron spins in the antiferromagnetic state, which may be in agreement with the susceptibility data reported by Saito (89). To be of any importance here the antisymmetric contribution should be found in

the intrachain exchange J. Assuming that the memory spectrum is Gaussian for large ω (which is equivalent with a Gaussian behavior of the memory function at short times) we can estimate the antisymmetric exchange parameter from our relaxation measurements. Using eqs. (2.9), (2.40), (2.41) and the symmetry elements of CTS we find $\alpha \simeq 0.1$.

This value is small but not unrealistic. It can be shown now that the antisymmetric contribution to the normalized traces in eq. (7.20) is an order larger than that of the dipolar interaction. We will adopt now an interaction model for CTS which contains, besides the intrachain and interchain exchange interactions, an antisymmetric contribution in the intrachain exchange J.

As the antisymmetric exchange occurs between copper ions along the c-axis, one has

$$C(x,y,0) = C(0,0,0) \tag{7.21}$$

Substitution of eq. (7.21) in (7.19) yields

$$G_z(t) = \frac{g^4 \mu_B^4 S(S+1)}{48\pi^2\hbar^2} \left(\frac{c^2}{8\pi D^*}\right)^{\frac{1}{2}} |C(0)|^2 t^{-\frac{1}{2}} \int_{-\pi}^{\pi} \int_{-2\pi}^{2\pi} \phi_{xy}^2(t)\, dx\, dy \tag{7.22}$$

From eq. (7.22) it follows that the functional time dependence of the memory function is the same in all directions while the intensity of the long-time tail is proportional to $|C(0)|^2$. These theoretical predictions, embodied in eq. (7.22), will be confronted with the memory functions as derived from our relaxation experiments. One has

$$G_z(t) = 4 \int_0^{\infty} \{\tilde{G}_{z1}(\omega) + \tilde{G}_{z2}(\omega)\} \cos \omega t\, d\omega \tag{7.23}$$

Our model with only antisymmetric interaction as non-secular contribution, implies that the memory spectrum is completely dominated by $\tilde{G}_{z1}(\omega)$ (see section 2.3).

For that case one has

$$\tilde{G}_{z1}(\omega) + \tilde{G}_{z2}(\omega) \simeq \tilde{G}_{z1}(\omega) = \left\{\frac{1}{2\pi\tau(H)} \frac{\langle\langle \mathcal{H}_{sec}^2 \rangle\rangle}{\langle\langle \mathcal{H}^2 \rangle\rangle}\right\} \quad H = \frac{\hbar\omega}{g\mu_B} \tag{7.24}$$

Using the experimental relaxation times in eq. (7.24) and substituting the result in (7.23), one easily calculates the memory function in the corresponding direction. Pathological frequency dependences of the memory spectrum at high frequencies are excluded by the Gaussian cut-off assumed above.

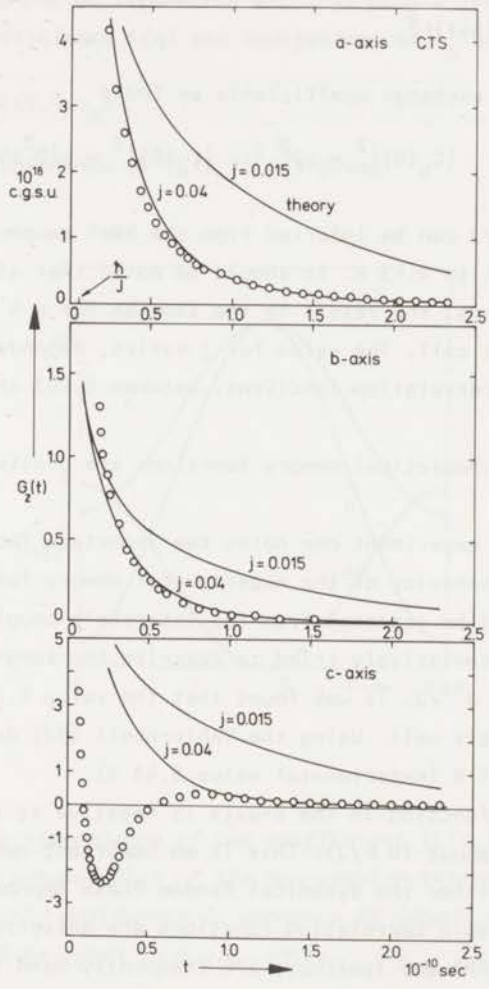

Fig. 58 *The experimental and theoretical long-time behavior of the memory function in the three magnetic axes of CTS. The solid lines represent the theoretical results for two different values for* $j = J^{nc}/J$. *The open points are calculated from our experimental relaxation times.*

For the calculation of the theoretical $G_z(t)$ from eq. (7.22) we use the diffusion constant (90)

$$D^* = 1.38 \frac{c^2 J}{4\hbar} [S(S+1)]^{\frac{1}{2}} \qquad (7.25)$$

For the antisymmetric exchange coefficients we found

$$|C_a(0)|^2 = pD_b^2, \quad |C_b(0)|^2 = pD_a^2, \quad |C_c(0)|^2 = p(D_a^2+D_b^2), \quad p = \frac{16}{g^4 \mu_B^4} \qquad (7.26)$$

The value for $j = J^{nc}/J$ can be inferred from the Néel temperature which has been found (91) to be equal to 0.43 K. It should be noted that although we included 6 next-nearest neighbors, the result is the same as for a 4 next-nearest neighbors orthorhombic unit cell. The value for j varies, dependent on the decoupling method in the static correlation functions, between 0.007 and 0.015 (79).

The experimental and theoretical memory functions are plotted together in Fig.58.

Comparing theory with experiment one notes two important facts.
First, the long-time behavior of the experimental memory functions is much less pronounced than should be expected from the interchain coupling derived from the Néel temperature. We tentatively tried to describe the long-time behavior with another value for $j = J^{nc}/J$. It was found that the value 0.04 fitted the long-time behavior reasonably well. Using the Tahir-Kheli (92) decoupling method, this value yields $T_N = 0.75$ K (experimental value 0.43 K).
Secondly, the memory function in the c-axis is negative at intermediate times (the minimum lies at about 10 $\hbar/J$). This is an important result as it implies that at those times either the dynamical Random Phase Approximation is inaccurate or that the two-spin correlation functions are anisotropic, even at high temperatures. Both, DRPA and isotropy, are frequently used in theories on the high-temperature dynamical behavior of weakly anisotropic magnetic systems.

In $CuCl_2.2H_2O$ the memory function in the a-axis also showed a negative undershoot at intermediate times (see section 5.1.2). It was found that in the directions where the memory functions were positive at all times, most contributions to the q-sum in the theoretical expression of $G_z(t)$ (cf. eq. (2.55)) came from the center (intermediate q-values) of the Brillouin zone. In contrast, in the a-axis the contributions from the center were small and most contributions came from small q-values and from the border of the Brillouin zone. In the case of anisotropy of the two-spin correlation functions at certain q-values, this different sampling could very well explain why only the a-axis showed the anoma-

lous behavior at intermediate times. We will now investigate if the same difference in sampling also occurs in CTS.
Due to the fact that the antisymmetric exchange occurs between copper ions along the c-axis, the coefficients C(q) are independent of q_a and q_b.

$$C(q_a,q_b,q_c) = C(0,0,q_c) \tag{7.27}$$

In Fig. 59 the q_c-dependence of $|C(q_c)|^2$ is given

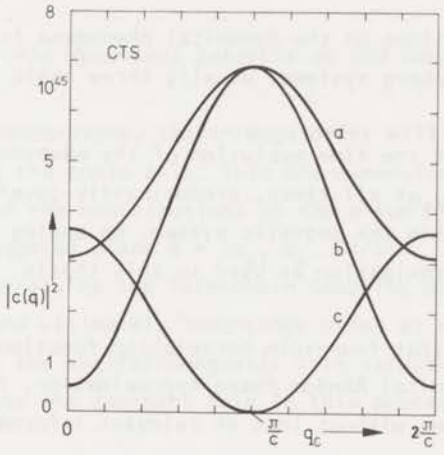

Fig. 59 *The q_c-dependence of the coefficient $|C(q_c)|^2$. It has been assumed that of the non-secular interactions in CTS only antisymmetric exchange is important. The coefficient is given in c.g.s. units.*

Just as in $CuCl_2.2H_2O$, one notes that the direction (c-axis) in which the negative shoulder in the memory function occurs, shows a strong tendency for contributions from large and small q-values. Again, in contrast, in the other two directions most contributions come from intermediate q-values. All this gives credit for anisotropy in the two-spin correlation functions at either large or small q-values. The origin of the anisotropy is not clear but may probably be found in the antisymmetric exchange (and to a lesser extent in dipolar interaction) itself.
However, in spite of all this the possibility of inaccuracy in the DRPA should not be ruled out.

It may very well be possible that, due to the peculiar character of antisymmetric exchange, cross correlations such as $(S^x_{-q}, S^y_q(t))$ are unequal to zero (and negative) at intermediate times. As both DRPA and isotropy have been used in the theory exposed in this chapter, deviations from it may very well occur. One can only hope that, due to the time dependent sampling over the Brillouin zone, anisotropy and inaccuracy in the DRPA only play a minor role at really long times.

Some final remarks

In theoretical investigations on the dynamical phenomena in low-dimensional weakly anisotropic Heisenberg systems, usually three basic assumptions are made.

First, it is assumed that the time evolution of the wavevector dependent two-spin correlation functions is, at all times, predominantly governed by the secular interactions within the magnetic system. An analog assumption is found in the weak-coupling approximation as used in this thesis.

Secondly, it is assumed that four-spin correlation functions can be decoupled, using the so-called dynamical Random Phase Approximation, into products of two-spin correlation functions without loss of relevant information.

Thirdly, it is assumed that at high temperatures the two-spin correlation functions are isotropic at all values for q and t.

Confrontation of experiment with the theory of Hennessy et al. (79) in which these three basic assumptions are embodied, shows that the experimental memory functions decay to zero in unexpectedly short times. Although the relative "intensities" of the long-time tails of the memory functions in the different directions are in good agreement with the theory, a description of the behavior at really long times requires a ratio interchain-intrachain coupling which is nearly a factor 3 larger than the largest estimate for this ratio from the Néel temperature.
This important discrepancy between experiment and theory can be due to a brake down of the validity of each of the assumptions mentioned abcve.

In the case that the first assumption does not hold, not only the theoretical predictions but also our derivation of the memory functions from experiment may be in error as, in that case, the lines in the memory spectrum cannot

be expected to shift rigidly with the static field

If the weak-coupling approximation is sufficiently accurate, we find strong indication for either anisotropy in the two-spin correlation functions or gross inaccuracy in the dynamical Random Phase Approximation at intermediate times. Whether these facts, anisotropy and inaccuracy in the DRPA, fully explain the deviation from the expected theoretical time behavior at really long times is unknown.

7.5 *Discussion of the dynamical behavior at low temperatures*

When lowering the temperature, short-range order will progressively develop between spins along the chain axis. This one-dimensional short-range order leads to an enhancement of the contributions to the q-sum of eq. (2.55) from q-values near and at the staggered plane $\vec{q} = (q_a, q_b, 2\pi/c)$.
At still lower temperatures the interchain coupling produces three-dimensional short-range order and ultimately long-range order at a temperature unequal to zero. It depends on the antiferromagnetic spin structure which part of the staggered plane plays the dominant role in this process.

In first instance, the effects of three-dimensional short-range order are expected to be only important very near the Néel temperature ($\in \lesssim 1$). As the experimental speeding-up of the relaxation process in CTS starts at about $T = 10$ K ($\in \simeq 20$), one should expect that this speeding-up arises from the development of one-dimensional short-range order along the chain.

In CTS the memory functions decay to zero at times sufficiently short to describe the relaxation process of $M_z(t)$ by a single relaxation time. In that case, we may use an approach similar to that in section 2.4 with some adaptions to the linear chain case. The anisotropy of the magnetic interactions will be neglected as it is small and probably only plays a role very near the Néel temperature.
For the near-perfect linear chain compound one gets for the region of one-dimensional short rage order

$$\Delta\frac{1}{\tau} = \frac{1}{\tau(T)} - \frac{1}{\tau(\infty)} \propto \frac{T}{\chi_o}\,\kappa^{-4.5} \qquad (7.28)$$

where κ is the inverse correlation length along the chain axis. For the linear chain it has been found (93) that, at sufficiently low temperatures, κ is proportional to the temperature

$$\kappa \propto T \tag{7.29}$$

Substitution of eq. (7.29) in (7.28) yields

$$\frac{\chi_o}{T}\left(\Delta\frac{1}{\tau}\right) \propto T^{-4.5} \tag{7.30}$$

In Fig. 60 the experimental values for the left-hand side of (7.30) have been plotted versus the temperature.

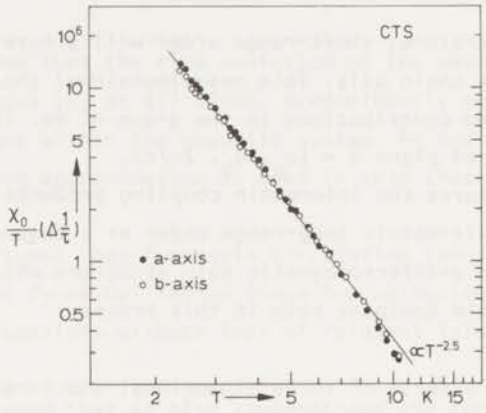

Fig. 60 *The experimental, normalized critical parts of the relaxation rates in the a and b axes of CTS. The solid line corresponds to the theoretical results using a linear dependence of the inverse correlation length on the temperature (see text).*

One notes that the experimental temperature dependence does not support, as far as the dynamical properties are concerned, a purely one-dimensional short-range ordering along the chain, even at temperatures reasonably far from the Néel temperature. A possible explanation of this unexpected result will be given below.

At high temperatures we found the experimental memory functions to decay to zero in unexpectedly short times. This discrepancy between theoretical and experimental time dependence of the memory function may indicate that in the theory, in which several approximations are embodied (see the final remarks of section 7.4), the interchain coupling, secular and non-secular, is not properly taken into account. In fact, the experimental results possibly indicate a more important role of this interchain coupling. There is no reason now why this should not equally hold at lower temperatures. As, due to the critical slowing-down of the spin fluctuations, the relevant correlation functions are extending to longer times, one expects the interchain coupling to be even more important at lower temperatures. This then leads to a decay rate of the correlation functions (see eq. (2.57)) which is not only dependent on q_c, as it is in an ideal linear chain compound, but also on q_a and q_b. It should be stressed that the dependence on q_a and q_b does not automatically imply a regular three-dimensional short-range ordering. The static and equal-time staggered susceptibility (see eq. (2.66)) may even, in very good approximation, show the normal ideal linear chain behavior. The only point made here is that the time evolution of the spin correlations is strongly influenced by the interchain coupling.

A calculation analog to that of section 2.4 leads then to

$$\Delta\frac{1}{\tau} \propto \frac{T}{\chi_o}\kappa^{-2.5} \tag{7.31}$$

Substitution of (7.29) in (7.31) yields

$$\frac{\chi_o}{T}\left(\Delta\frac{1}{\tau}\right) \propto T^{-2.5} \tag{7.32}$$

As is shown in Fig. 60, this result is in very good agreement with experiment.

In spite of this agreement the explanation above is only tentative as in the derivation (7.31) some of the approximations have been used of which we questioned the validity at higher temperatures. In the critical region, however, other parts of the Brillouin zone play the dominant role in the dynamical process, so these approximations may be better at lower than at higher temperatures.
For further investigations on the dynamical properties of non-ideal linear chain compounds, more experiments should be performed in CTS at lower temperatures. Especially, neutron scattering experiments should be performed to reveal the possible q_a and q_b dependence of the relaxation rates of the wavevector dependent two-spin correlation functions.

REFERENCIES

(1) R. Kubo, J.Phys.Soc.Japan 12(1957)570

(2) D.L.Huber, Phys.Rev.B 6(1972)3180

(3) E.K.Riedel, J.Appl.Phys.42(1971)1383

(4) I.Dzialoshinsky, J.Phys.Chem.Solids 4(1958)241

(5) T.Moriya, Phys.Rev.120(1960)91

(6) W.Rutten, m.sc. thesis Leiden 1974

(7) J.A.Tjon, Physica 30(1964)1,1341

(8) R.H.Terwiel and P.Mazur, Physica 32(1966)1813

(9) M.Blume and J.Hubbard, Phys.Rev.B 1(1970)3815

(10) K.van der Molen, Ph.D. thesis Leiden 1969

(11) J.G.A.Hillaert, Ph.D. thesis Leiden 1973

(12) D.L.Huber, M.S.Seehra and P.W.Verbeek, Phys.Rev.B 9(1974)4988

(13) B.I.Halperin and P.C.Hohenberg, Phys.Rev.177(1969)952

(14) B.Widom. J. Chem.Phys.43(1965)3898

(15) L.Kadanoff, Physics 2(1966)263

(16) M.P.Schulhof, P.Heller, R.Nathans and A.Linz, Phys.Rev.B 1(1970)2304

(17) D.S.Ritchie and M.E.Fisher, Phys.Rev.B 5(1972)2668

(18) E.Toyota and K.Hirakawa, J.Phys.Soc.Japan 30(1971)692

(19) P.W.Verbeek, J.C.Verstelle and J.A.Tjon, Physica 66(1973)545

(19a) P.W.Verbeek, Ph.D. thesis Leiden 1973

(20) G.A.Baker, H.E.Gilbert, J.Eve and G.S.Rushbrooke, Phys.Rev.164(1967)800

(21) G.Paul and H.E.Stanley, Phys.Rev.B 5(1972)2578

(22) D.Jasnow and M.Wortis, Phys.Rev. 176(1968)739

(23) N.W.Dalton and D.W.Wood, Proc.Phys.Soc.(London) 90(1967)459

(24) H.Y.Lau,L.M.Corliss,A.Delapalme,A.Tucciarone,Phys.Rev.Lett.23(1969)1225

(25) E.Schlömann, J.J.Green and U.Milano, J.Appl.Phys. 31(1960)386S

(26) H.Yamazaki, J. Phys.Soc.Japan 32(1972)1227

(27) A.B.Harris, D.Kumar, B.I.Halparin, P.C.Hohenberg, Phys.Rev.B 3(1971)961

(28) V.N.Genkin and V.M.Fain, Sov.Phys.JETP 14(1962)1086

(29) G.I.Urushadze, Sov.Phys.JETP 12(1961)476

(30) T.Kawasaki, Progr.Theor.Phys. 34(1965)357

(31) A.B.Harris, J.Appl.Phys.37(1966)1128

(32) J.C.Verstelle, Ph.D. thesis Leiden 1962
see also N.J.Poulis, Physica 17(1951)392

(34) N.J.Poulis and G.E.G.Hardeman, Physica 18(1952)201

(35) L.Néel, Ann.Physique 18(1932)5,5(1936)232,3(1948)137

(35a)C.J.Gorter and J.Haantjes, Physica 18(1952)285
(36) J.Ubbink, Physica 19(1953)919
(37) T.Nagamiya, Progr.Theor.Phys.11(1954)309
(38) K.Yosida, Progr.Theor.Phys. 7(1952)425
(39) S.A.Friedberg, Physica 18(1952)714
(40) J.van den Handel, H.M.Gijsman and N.J.Poulis, Physica 18(1952)862
(41) L.C.van der Marel, J.van den Broek, J.D.Wasscher, C.J.Gorter, Physica 21(1955)685
(42) H.Yamazaki and M.Date, J.Phys.Soc.Japan 23(1967)737
(43) N.J.Zimmerman,F.P.van der Mark and J.van den Handel,Physica 46(1970)204
(43a)J.J.Eggermont, private communication
(44) G.Shirane, B.C.Frazer and S.A.Friedberg, Phys.Letters 17(1965)95
(45) P.van Dalen, Ph.D. thesis Eindhoven 1966
(46) T.Moriya and K.Yosida, Progr.Theor.Phys.9(1953)663
(47) J.H.van Vleck, Phys.Rev.52(1937)1178
(48) J.H.van Vleck, J. Phys.Radium 12(1951)262
(49) H.Umebayashi, B.C.Frazer, D.E.Cox and G.Shirane, Phys.Rev.167(1968)519
(50) T.Oguchi, Progr.Theor.Phys.13(1955)148
(51) W.Marshall, Phys.Chem.Solids 7(1958)159
(52) O.Nagai, J. Phys.Soc.Japan 18(1963)510
(53) A.C.Hewson, D.ter Haar and M.E.Lines, Phys.Rev.137(1965)A1465
(54) R.M.Clay and L.A.Stavely, Ann.Acad.Sci.Fennicae (A6 210)194
(55) L.J.de Jongh and A.R.Miedema, Adv.Phys.23(1974)1
(56) G.M.Ryabchenko and L.A.Shul'man, Sov.Phys.Solid State 8(1967)1757
(57) E.Buluggiu, A.Dall'Olio and V.Varacca, Phys.Stat.Sol.32(1969)745
(58) R.J.Joenk, Phys.Rev.126(1962)565
(59) H.L.van Noort, private communication
(60) J.Itoh, M.Fujimoto and H.Ibamoto, Phys.Rev.83(1951)852
(61) H.L.van Noort, private communication
(62) N.J. Poulis and G.E.G.Hardeman, Physica 18(1952)429
(63) W.Rutten, private communication
(64) H.L.van Noort, private communication
(65) C.S.Naiman and T.R.Lawrence, J.Appl.Phys.36(1965)1161
(66) H.Forstat and D.R.McNeely, J. Chem.Phys.35(1961)1594
(67) P.H.Vossos, L.D.Jennings and R.E.Rundle, J. Chem.Phys.32(1960)1590
(68) S.C.Abrahams and H.J.Williams, J. Chem.Phys.39(1963)2923
(69) M.Date and K.Nagata, J. Appl.Phys.34(1963)1038
(70) N.J.Zimmerman,J.D.Bastmeyer and J.van den Handel,Phys.Lett. 40A(1972)259

(71) J.W.Metselaar, Ph.D. thesis Leiden 1973
(72) E.de Vries, m.sc. thesis Leiden 1973
(73) N.J.Zimmerman, Ph.D. thesis Leiden 1974
(74) T.Haseda and A.R.Miedema, Physica 27(1961)1102
(75) T.Oguchi, Phys.Rev.133(1964)A1098
(76) T.Watanabe and T.Haseda, J. Chem.Phys.29(1958)1429
(77) J.C.Bonner and M.E.Fisher, Phys.Rev.135(1964)A640
(78) R.B.Griffiths, Phys.Rev.135(1964)A659
(79) M.J.Hennessy, C.D.McElwee and P.M.Richards, Phys.Rev.B 7(1973)930
(80) R.N.Rogers, F.Carboni and P.M.Richards, Phys.Rev.Letters 19(1967)1016
(81) R.E.Dietz, F.R.Merritt, R.Dingle, D.Hone, B.Silbernagle and P.M.Richards Phys.Rev.Letters 26(1971)1186
(82) H.Lieffering, m.sc. thesis Leiden 1965
(83) F.Mazzi, Acta Cryst.8(1955)137
(84) M.Date, J. Phys.Soc.Japan 11(1956)1016
(85) M.J.Hennessy and P.M.Richards, Phys.Rev.B 7(1973)4084
(86) F.Carboni and P.M.Richards, Phys.Rev.177(1969)889
(87) J.F.Fernandez and H.A.Gersch, Phys.Rev.172(1968)341
(88) F.A.Malinoski, Int.J. Magnetism 4(1973)245
(89) S.Saito, J. Phys.Soc.Japan 26(1969)1388
(90) F.B.McLean and M.Blume, Phys.Rev.B 7(1973)1149
(91) S.Saito and E.Kanda, J. Phys.Soc.Japan 22(1967)1241
(92) R.A.Tahir-Kheli, Phys.Rev.132(1963)689
(93) H.Tomita and H.Mashiyama, Progr.Theor.Phys.48(1972)1133

In dit proefschrift is, zowel experimenteel als theoretisch, het dynamische gedrag van enkele zwak anisotrope magnetische systemen onderzocht. Het onderzoek was in het bijzonder gericht op de tijdsevolutie van de totale magnetisatie van het geïsoleerde elektron spin systeem. Hiervoor werden relaxatie en resonantie metingen verricht in de paramagnetische, kritische en antiferromagnetische toestand van drie verschillende koper verbindingen. Van twee van de verbindingen $CuCl_2.2H_2O$ en $LiCuCl_3.2H_2O$ is bekend dat ze magnetisch drie-dimensionaal zijn terwijl de derde, $Cu(NH_3)_4SO_4.H_2O$, één van de eerst bekende magnetische lineaire keten systemen is.

In de hoge temperatuur limiet is de invloed van antisymmetrische Dzialoshinsky-Moriya exchange interactie op relaxatie en resonantie onderzocht. Introductie van deze antisymmetrische interactie in de koperverbindingen leidde tot een perfecte overeenkomst tussen experiment en theorie. Het interactie model, dat slechts één aanpasbare exchange parameter bevat, is getest op de onafhankelijke experimentele resultaten verkregen in de kritische en antiferromagnetische toestand. Het model bleek volledig consistent te zijn.

In het kritische gebied dichtbij de Néel temperatuur werd een anisotrope speeding-up van het relaxatie proces gevonden. Gebruik makend van Random Phase Approximation, ruimtelijk Fourier transforms en dynamical scaling is een theorie ontwikkeld over kritische relaxatie en resonantie in zwak anisotrope magnetische systemen. Hierin werd aangetoond dat de dynamische kritische verschijnselen van een magnetisch systeem sterk kunnen worden beïnvloed door de magnetische anisotropie. Door deze anisotropie te transformeren in een anisotropie in de kritische slowing-down van de spin fluctuaties, werd een relatief eenvoudige uitdrukking voor de relaxatie tijden (en dus ook voor de resonantie lijnbreedten) gevonden. De resultaten van deze theorie die een generalisatie is van de theorie van Huber (2)(12), zijn in goede overeenstemming met het experiment in zowel $CuCl_2.2H_2O$ als $LiCuCl_3.2H_2O$. Dezelfde theorie op de lineaire keten $Cu(NH_3)_4SO_4.H_2O$ toegepast, geeft als experimenteel resultaat dat de correlatie lengte omgekeerd evenredig is met de temperatuur.

Beneden de Néel temperatuur is in de easy-axis van de orthorhombische antiferromagneten een laag-frequente relaxatie gevonden. Er is aangetoond dat deze relaxatie metingen een bruikbare test vormen voor spin-golf verstrooiings theorieën.

Goede overeenkomst is gevonden met de theoretische voorspellingen van Harris (31).

In de lineaire keten CTS is speciale aandacht besteed aan het lange-tijd gedrag van de tijdsafhankelijke correlatie functies. De lange-tijd staarten van de relaxatie geheugen functies zijn direct berekend uit de relaxatie metingen. De resultaten van deze berekeningen zijn vergeleken met een aangepaste versie van de theorie van Hennessy et al. (79). Alhoewel de meeste verschijnselen kwalitatief konden worden verklaard, werd gevonden dat de geheugen functies minder uitgesproken lange-tijd gedrag vertonen dan theoretisch kon worden verwacht. Uit de metingen volgt een indicatie voor óf belangrijke onnauwkeurigheid in de Random Phase Approximation óf een anisotropie in de golfvector afhankelijke tweespin correlatie functies.

Op verzoek van de faculteit der Wiskunde en Natuurwetenschappen volgt hier een overzicht van mijn studie.

Na de middelbare schoolopleiding aan het Johannes Calvijn Lyceum te Rotterdam, waar mijn interesse voor de exacte vakken werd vergroot door de zeer persoonlijke wijze van lesgeven van de heer W. Kors, en na de militaire diensttijd begon ik eind 1962 mijn studie in Leiden. Interesse voor niet-natuurkundige activiteiten bracht met zich mee dat ik, naast de voorbereiding van de natuurkunde tentamens, een groot gedeelte van mijn tijd doorbracht in het land van Marianne.

In 1967 legde ik het kandidaatsexamen (D') af, waarna ik mij in april 1967 bij de relaxatiegroep van Dr. J.C. Verstelle voegde. In het eerste half jaar assisteerde ik Dr. K. van der Molen en Dr. J.J. Eggermont waarbij de experimentele feeling en nauwkeurigheid waarmee eerstgenoemde werkte op mij een diepe indruk heeft achtergelaten. Na deze eerste maanden van initiatie begon ik mijn eigen metingen waarbij ik na zekere tijd geassisteerd werd door Drs. E. de Vries en later de heer A.J. Bijlsma. Vanaf 1968 assisteerde ik op het elektronisch praktikum.

In november 1971 legde ik het doktoraal examen natuurkunde af waarna ik, eind 1972, werd benoemd tot wetenschappelijk medewerker.

De goede sfeer in de werkgroep werd voor mij bepaald door de zeer goede samenwerking met, naast bovengenoemden, Dr. P.W. Verbeek en Drs. H.L. van Noort terwijl Dr. J.G.A. Hillaert voor een vrolijke noot zorgde door af en toe guitig een zwaar metalen voorwerp door de lucht te laten vliegen. De hechte samenwerking met Dr. P.W. Verbeek culmineerde in 1972 in de ontdekking van een nieuw effect, het zgn. Kvanndal effect.

De heer L.J. de Haas assisteerde mij bij het verrichten van enige numerieke berekeningen vermeld in dit proefschrift.

De tekeningen in dit proefschrift werden op vlotte wijze vervaardigd door de heer W. Rijnsburger. Het technische gedeelte van het onderzoek werd op sympathieke wijze verzorgd door de heer J. Turenhout en zijn medewerkers. De heren C.J. van Klink en L. van As fabriceerden met veel deskundigheid de kwarts capillairen.

STELLINGEN

behorende bij het proefschrift van

W.M. DE JONG

10 september 1975

1.

De bewering van Joshua dat hij op groepentheoretische gronden heeft aangetoond dat $CuCl_2.2H_2O$ een gekantelde spinstructuur heeft, is onjuist.

S.J. Joshua, Phys.Stat.Sol. 38(1970)643

2.

Bij de confrontatie van de experimentele temperatuurafhankelijkheid van AFMR lijnbreedtes met theoretische verwachtingen wordt vaak ten onrechte geen rekening gehouden met de intrinsieke veldafhankelijkheid van deze lijnbreedtes.

J.P. Kotthaus en V.J. Jaccarino, Phys.Lett. 42A(1973)361

3.

De wijze waarop Hennessy en Richards bij hun analyse van de temperatuurafhankelijkheid van de paramagnetische resonantielijnbreedte in $Cu(NH_3)_4SO_4.H_2O$ gebruik maken van de lineaire-keten berekeningen van Carboni en Richards, is aanvechtbaar.

M.J. Hennessy en P.M. Richards, Phys.Rev.B 7(1973)4086
F.Carboni en P.M.Richards, Phys.Rev. 177(1969)889

4.

De bij ministeriëel besluit geregelde promotie van het Franse wijnkasteel "Mouton Rothschild" tot premier cru du Médoc is, zelfs uit propagandistisch oogpunt, zinloos.

Arrêté du Ministre de l'Agriculture - juin 1973 - France

5.

Voor meer inzicht in het dynamische gedrag van niet-ideale lineaire-keten systemen bij lage temperatuur, dient met neutronenverstrooiing de afhankelijkheid te worden onderzocht van $(S_q, S_{-q}(t))$ van de golfvektor loodrecht op de ketenrichting.

Dit proefschrift, sectie 7.5

6.

Bij de interpretatie van de meetresultaten verkregen met de door Rollins et al. voorgestelde nieuwe methode voor het bepalen van de fluxdichtheidsgradiënt in irreversibele type II supergeleiders, wordt onvoldoende rekening gehouden met de beweeglijkheid van de fluxdraden in de pincentra.

R.W. Rollins, H. Küpfer en W.Gey, J.Appl.Phys. 45(1974)5392

7.

Bij de voor de bergsport gebruikelijke indeling van bergpassages in moeilijkheidsgraden, dient men te bedenken dat de moeilijkheidsgraad van sommige van deze passages een functie is van de afmetingen van de bergbeklimmer.

Guide du Massif des Ecrins - Arthaud - Paris

8.

De bewering van Månson en Sjölander dat boven het overgangspunt Random Phase Approximation in Heisenberg systemen geen zinvolle resultaten geeft voor de dynamische verschijnselen, is in zijn algemeenheid onjuist.

M. Månson en A. Sjölander, Phys.Rev.B 11(1975)4639

9.

Uit de in het temperatuurgebied van 14 tot 20 K geconstateerde discrepantie tussen de IPTS - 68 temperatuurschaal en de magnetische temperatuurschalen volgt dat de IPTS - 68 schaal niet voldoende nauwkeurig is en gecorrigeerd dient te worden.

" The International Practical Temperature Scale of 1968 ",
Metrologica 5(1969)35

10.

De grafische voorstelling van een Chebyshev polynoom is een Lissajous figuur.

" Theory and problems of numerical analyses ", Francis Scheid,
McGraw-Hill Book Company, New York

11.

Recente onderzoekingen waarbij gebleken is dat voor de mens carcinogene stoffen in bepaalde bacteriestammen (Salmonella typhimurium) over het algemeen veel meer mutaties veroorzaken dan niet-carcinogene stoffen, moeten ook in Nederland aanleiding zijn, mede gezien het feit dat een stof in twee dagen kan worden onderzocht, het wettelijk te verplichten elke in ons milieu kunstmatig geïntroduceerde stof op mutagene eigenschappen te laten onderzoeken en de lozing en het verwerken in voedsel van sterk mutagene stoffen te verbieden.

B. Commoner, Report to the Environmental Protection Agency (USA), juli 1975

Zie ook de publikaties van de ter gelegenheid van het 400-jarig bestaan van de Leidse universiteit tot eredoctor bevorderde Dr. Charlotte Auerbach.

ISBN 90 6231 002 8